Dissertation

submitted to the

Combined Faculties for the Natural Sciences and for Mathematics
of the Ruperto-Carola University of Heidelberg, Germany

for the degree of

Doctor of Natural Sciences

presented by
Julia Ritterhoff
M.Sc. Molecular Medicine
born in Twistringen

Oral examination:…….

S100A1 acts positive inotropic and prevents Ca^{2+} triggered after-contractions in a model of Engineered Heart Tissue

Referees: PD. Dr. rer. Nat. Martin Müller
Prof. Dr. med. Patrick Most

I. Statement of independent work

I hereby declare that this submission is my own work and that it contains no material previously published or written by another person and that no additional assistance was provided except where the acknowledgment has been made in the text.

…… …….

Place and date Signature

II. Table of content

III. List of figures

IV. Abbreviations

$[Ca^{2+}]_i$	intracellular Ca^{2+} concentrations
$[K^+]_i$	reduces intracellular potassium concentrations
$[Na^+]_i$	intracellular sodium concentrations
aa	amino acid
AC	adenylatecyclase
ACM	adult rat cardiomyocytes
ANOVA	analysis of variance
ANT	adenosine nucleotide translocator
AP	action potential
apoCaM	Ca^{2+}-free CaM
Ca^{2+}	calcium
CaM	calmodulin
CamKII	calcium/calmodulin-dependent protein kinase II
cAMP	cyclic adenosine monophosphate
cDNA	complementary deoxyribonucleic acid
CICR	Ca^{2+} induced Ca^{2+} release
CM	cardiomyocyte
CsCl	cesium chloride
CSQ	calsequestrin
CTGF	connective tissue growth factor
Cx43	Connexin43
DAD	delayed after-depolarization
E1/E3	Early 1/3 genes
EC	excitation-contraction
ECG	electrocardiography
EHT	Engineered Heart Tissue
ET-1	endothelin-1
FCMs	failing rat ventricular cardiomyocytes
FCS	Fetal calf serum
FKBP12.6	FK506 binding protein 12.6
GAPDH	glyceraldehyde 3-phosphate dehydrogenase
GFP	green fluorescent protein
Hek293A	human embryonic kidney carcinoma 293A cells
HF	heart failure
I_{ca}	Ca^{2+} influx

ICAM-1	intercellular adhesion molecule 1
IF	immunofluorescence
I_{K1}	inward rectified potassium current
IL-6	interleukin 6
IP	immunoprecipitation
Iso	isoproterenerol
K^+	potassium
LAD	left anterior descending
LTCC	L-type Ca^{2+} channel
MOIs	multiplicities of infections
Na^+	sodium
Na^+K^+-ATPase	sodium-potassium-ATPase
NCF	neonatal rat cardiac fibroblasts
NCM	neonatal rat cardiomyocytes
NCX	sodium-calcium-exchanger
ON	over night
PCR	polymerase chain reaction
PKA	cAMP-dependent kinase
PKG	Protein kinase G
PLA	proximity ligation assay
PLB	phospholamban
P_o	open probability
PP1, PP2a	protein phosphatases 1 and 2a
PTMs	post-translational modifications
RNA	ribonucleic acid
ROS	reactive oxygen species
Rpm	revolutions per minute
RT	room temperature/ reverse transcription
RyR2	SR Ca^{2+} release channel/ryanodine receptor
SDS page	sodium dodecyl sulfate polyacrylamide gel electrophoresis
SEM	standard error of mean
Ser	serine
SERCA2a	sarco/endoplasmic reticulum calcium-ATPase
SMA	smooth muscle actin
SNO	s-nitrosylation
SOICR	store overload-induced Ca^{2+} release
sorcin	soluble resistance-related calcium-binding protein

SR	sarcoplasmic reticulum
TGF-β	transforming growth factor β
Thr	threonine
TNF-α	tumor necrosis factor α
TnI	Troponin I
TT	twitch tension
TTP	time to peak
TUNEL	TdT-mediated dUTP-biotin nick end labeling
WB	western blot
β-AR	β-adrenergic receptor

Physical units

A	ampere
°C	degree Celsius
g	gram/ acceleration of gravity on earth
h	hour
L	liter
m	meter
M	molar (mol/L)
min	minute
pH	negative common logarithm of the proton concentration
sec	second
V	volt

Prefixes

k	kilo- 10^{3}
c	centi- 10^{-2}
m	mili- 10^{-3}
µ	micro- 10^{-6}
n	nano- 10^{-9}

0. Abstract

The small calcium (Ca^{2+}) binding protein S100A1 is as a critical regulator of cardiomyocyte Ca^{2+} handling thereby enhancing cardiac performance *in vivo* and *in vitro*. Our previous studies demonstrated that the positive inotropic effects of S100A1 are due to enhanced Ca^{2+} transients and sarcoplasmic reticulum (SR) Ca^{2+} load in isolated adult cardiomyocytes. These effects are independent of and in addition to cAMP-dependent positive inotropic mechanisms. However, inotropic interventions come at the risk of arrhythmogenic diastolic Ca^{2+} leakage when the SR Ca^{2+} content exceeds the threshold for spontaneous diastolic Ca^{2+} release. In a more recent study we could demonstrate that enhanced Ca^{2+} transients after S100A1 overexpression are associated with a reduced incidence of diastolic Ca^{2+} sparks and Ca^{2+} waves. These results favor the assumption that S100A1 might reduce the diastolic RyR2 leak, thereby impeding the development of pro-arrhythmogenic events.

Thus, the aim of this work was to investigate the effect of S100A1 on diastolic Ca^{2+} handling and on the impact of Ca^{2+}-triggered arrhythmias in a multicellular system. For this reason, the 3-dimensional tissue culture model of Engineered Heart Tissue (EHT) was chosen. Due to its syncytial architecture, EHT closely mimics functional alterations, intercellular communication and reverse remodeling of whole hearts *in vivo* despite eased handling and pharmacological as well as therapeutic manipulations.

Pharmacological stimulation of EHT with endothelin-1 resulted in a heart failure-like phenotype with strong impairment of contractile performance. Adenoviral-mediated S100A1 overexpression was able to rescue failing EHT and resulted in superior contractility in normal EHT. Triggered contraction abnormalities, referred to as after-contractions, were induced by Ca^{2+} and β-AR stimulation and served as a surrogate of SOICR (store-overload-induced-Ca^{2+}-release). S100A1 overexpression significantly protected against Ca^{2+} and β-adrenergic receptor (β-AR) triggered after-contractions in normal and failing EHT. Despite persistent abnormal phosphorylation-dependent changes at the RyR2 and altered complex formation with accessory proteins, S100A1 overexpression enhanced S100A1/RyR2 stoichiometry, which seems to be key for S100A1's effects, combining inotropic and anti-arrhythmic potency.

1. Zusammenfassung

Das kleine Kalzium (Ca^{2+}) bindende Protein S100A1 ist ein wichtiger Regulator der Ca^{2+}-Homöostase in Kardiomyozyten, welches die kardiale Leistungsfähigkeit *in vivo* und *in vitro* steigert. Unsere bisherigen Untersuchungen zeigten, dass die positive inotrope Wirkung von S100A1 auf erhöhte Ca^{2+}-Transienten und einem erhöhten sarkoplasmatischen Retikulum (SR) Ca^{2+} Gehalt in isolierten adulten Kardiomyozyten zurückzuführen ist. Diese Effekte sind unabhängig von und zusätzlich zu den cAMP-abhängigen positiven inotropen Mechanismen. Allerdings können inotrope Interventionen zu einem pro-arrhythmogenen diastolischen Ca^{2+}-Leck führen, wenn der SR Ca^{2+}-Gehalt die kritische Schwelle für die spontane diastolische Ca^{2+}-Freisetzung übersteigt. In einer aktuellen Studie konnten wir zeigen, dass die erhöhten Ca^{2+}-Transienten nach S100A1 Überexpression mit einer verringerten Inzidenz für diastolische Ca^{2+}-Sparks und Ca^{2+}-Wellen einhergehen. Diese Ergebnisse unterstützen die Hypothese, dass S100A1 das diastolische Leck am RyR2 reduzieren und somit die Entwicklung von pro-arrhythmogenen Ereignissen entgegenwirken kann.

Daher war das Ziel dieser Arbeit, den Effekt von S100A1 auf die Ca^{2+}-Homöostase und den Einfluss auf Ca^{2+}-induzierte ventrikuläre Arrhythmien in einem multizellulären System zu untersuchen. Aus diesem Grund wurde das 3-dimensionale Gewebekulturmodell des Engineered Heart Tissue (EHT) verwendet. Das EHT hat eine gewebeähnliche Architektur und eignet sich daher, funktionelle und molekulare Veränderungen *in vitro* zu simulieren. Außerdem ist es leicht zu kultivieren und pharmakologische und therapeutische Manipulationen sind einfach durchzuführen.

Die pharmakologische Stimulation der EHT mit Endothelin-1 resultierte in einem Herzinsuffizienz-ähnlichen Phänotyp mit starker Beeinträchtigung der kontraktilen Funktion. Die adenovirale Überexpression von S100A1 konnte die insuffizienten EHTs rescuen und führte zu einer verbesserten Kontraktilität in normalen EHTs. Kontraktionsanomalien, die so genannten After-contractions, wurden durch Ca^{2+} und β-Adrenorezeptor (β-AR) Stimulation induziert und dienten als Surrogat der Ca^{2+}-Überladung des SRs und des so genannten SOICR (store-overload-induced-Ca^{2+}-release). Die adenovirale Überexpression von S100A1 schützte normale und insuffiziente EHT vor Ca^{2+} und β-AR-induzierten After-contractions. Diese Effekte waren trotz bestehenden abnormalen Veränderungen des Phosphorylierungsmusters und einer unveränderten Komplexbildung mit akzessorischen Proteinen am RyR2 zu sehen. Die S100A1-Überexpression erhöhte die S100A1/RyR2 Stöchiometrie, die sich als Schlüssel für die S100A1-vermittelten Effekte darstellt und damit die inotrope und antiarrhythmische Potenz zu kombinieren scheint.

2. Introduction

2.1 Epidemiology of heart failure

Heart failure (HF) belongs to the main causes of deaths worldwide, showing an increasing prevalence particularly in Western civilizations.[1, 2] It is a multifaceted syndrome, which manifests itself when the heart is unable to supply the whole body adequately with blood.[3] Major symptoms include reduced contractile performance, reduced energy utilization, chronic neurohumoral stimulation and an increased incidence of tachyarrhythmias.[1, 2, 4]

Current therapeutic strategies for the treatment of HF are limited to the deceleration of disease progression and the attempt to improve cardiac output by reducing neurohumoral activation, increasing contractile performance or reducing the incidence of tachyarrhythmias.[1, 2, 4] However, in the majority of cases, these measures are unable to reverse the disease progression and might even become contraindicative in the long-term.[1, 2, 4] Thus, there is a great need for the development of novel innovative therapeutic approaches that are able to stop and reverse HF. Yet, before dealing with novel therapeutic concepts, one needs to understand the underlying basic mechanisms controlling cardiovascular function in the physiological and pathophysiological state.

2.2 Calcium – the main factor controlling cardiomyocyte contractility

2.2.1 Calcium – an intracellular signaling molecule

Calcium (Ca^{2+}) is involved in the control of almost all cellular processes: Gene transcription, proliferation, muscle contraction and cell death - the small ion seems to be a universal second messenger controlling a diverse range of cellular processes.[5, 6] To transmit information, Ca^{2+} needs to be accumulated in the cytosol, where it is precisely controlled by different Ca^{2+} signaling toolkits, coordinating the above mentioned functions.[7-11] Each cell type has its own components of the toolkit, comprising a variety of signaling, homeostasis and sensory machineries that enables it to regulate Ca^{2+} signals to its physiology.[6, 12] This allows spatial, temporal and quantitative Ca^{2+} sensing and sets the basis for its versatility.[5, 6, 8]

In the cytosol, Ca^{2+} acts by binding to specific targets, the calcium-binding proteins (to which also S100A1 belongs, see 2.6).[13] These are mainly homologous proteins containing EF-hand motifs (helix-loop-helix structural domains in which the Ca^{2+} ions are coordinated), which either have a very high binding affinity for Ca^{2+} and act as Ca^{2+} buffers or show Ca^{2+}-dependent target protein interaction and act as Ca^{2+} sensors.[7, 14-16] Despite the great number of known calcium-binding proteins, their exact mechanism often remains elusive.

2.2.2 Regulation of cardiomyocyte function: Cardiac excitation contraction coupling

Ca^{2+} is also the main factor controlling cardiomyocyte (CM) function, including excitation-contraction coupling (EC) and contractile response.[17, 18] Oscillations in intracellular Ca^{2+} concentrations ($[Ca^{2+}]_i$) that link cardiomyocyte excitation to myocyte contraction in the whole heart are the basis for each heartbeat. The sarcoplasmic reticulum (SR) is the Ca^{2+} store within the CM and Ca^{2+} release from this internal store activates the contractile machinery.

EC coupling is initiated with the depolarization of the plasma membrane that activates voltage gated L-type Ca^{2+} channels (LTCC) which are located in the t-tubules and plasma membrane (Fig. 1.1). [19, 20] This causes Ca^{2+} influx, however the amount is not sufficient to induce contraction.[21] This rather small increase in local $[Ca^{2+}]_i$ triggers opening of the ryanodine receptor 2 (RyR2), which are located in the SR membrane and the so called Ca^{2+} induced Ca^{2+} release (CICR) leads to extrusion of Ca^{2+} from the SR into the cytoplasm (Fig. 1.2).[22-24] Due to the ultrastructure of cardiomyocytes, t-tubules and junctional SR form dyads, where 10–25 LTCCs and 100–200 RyR2 are clustered to one couplon.[18, 21, 25] Hence, LTCC-induced Ca^{2+} influx stimulates Ca^{2+} release from adjacent RyR2, that manifest as Ca^{2+} spark and can further synchronize neighboring RyR2 across the whole couplon (coupled gating).[17, 18, 26, 27] Synchronous activation of all couplons rises $[Ca^{2+}]_i$ from about 100nM to 1µM and finally activates contraction by the binding of Ca^{2+} to Troponin C, which induces conformational changes at the myofilaments and initiates action-myosin crossbridge (Fig. 1.3).[6, 17, 18, 21, 28]

This systolic Ca^{2+} rise and following contraction is terminated by the rapid inactivation of LTCC and RyR2 by rising $[Ca^{2+}]_i$.[29] Furthermore, the sodium-calcium-exchanger (NCX) and the SR Ca^{2+}-ATPase 2 (Serca2), which are located in the plasma membrane and in the SR membrane, respectively, are activated by rising $[Ca^{2+}]_i$.[18] During diastole, both extrude Ca^{2+} from the cytoplasm into the cytosol or back into the SR (Fig. 1.4, 1.5). Thereby, systolic Ca^{2+} influx through the LTCC matches diastolic Ca^{2+} extrusion through the NCX and systolic SR Ca^{2+} extrusion through the RyR2 matches diastolic Ca^{2+} uptake through Serca2.[18, 30-32] Importantly, Ca^{2+} flux is always balanced, providing the basis for constant Ca^{2+} cycling during EC coupling.[18, 33] Serca2 activity is further regulated by phospholamban (PLB), a pentameric protein that inhibits Serca2 activity by reversible interaction (Fig. 1.5).[20, 31, 34]

In diastole, the RyR2 is normally inactive. However, stochastic diastolic Ca^{2+} release can occur. These resting sparks are normally rare and spatial isolated, so that they do not trigger Ca^{2+} release from other couplons and are not able to initiate contraction.[26, 35]

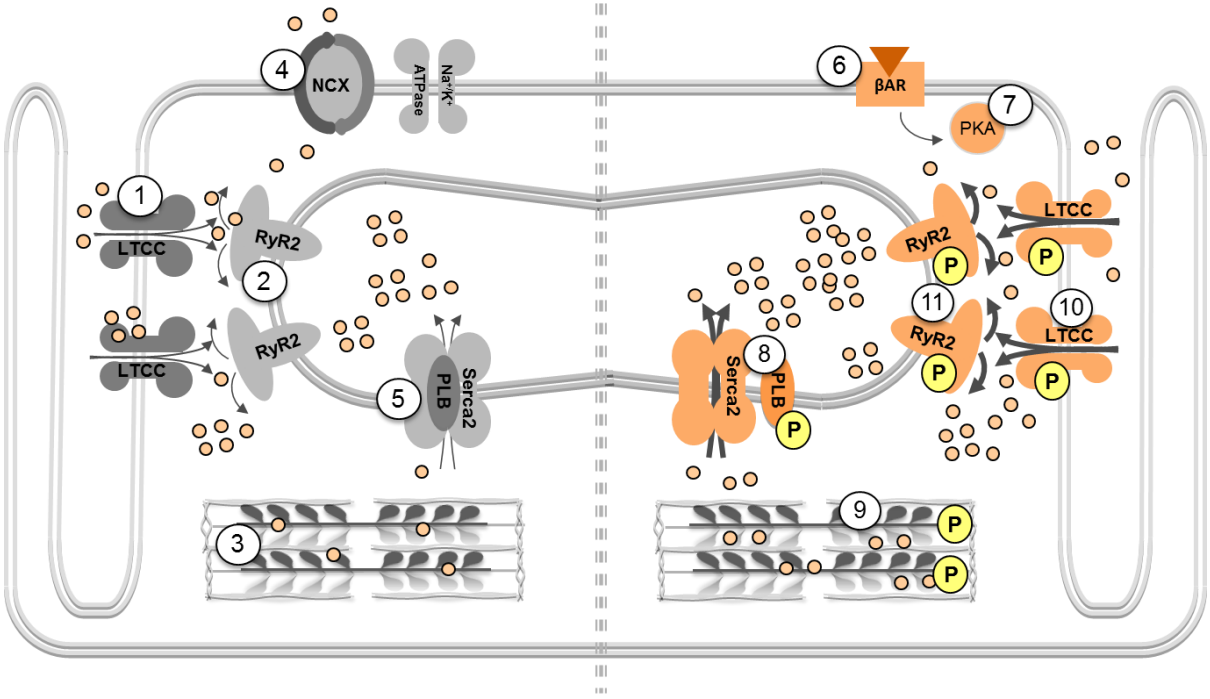

Figure 1: Cardiac EC coupling
Left: Basal EC coupling in normal CM: During systole, action potential-dependent opening of the LTCC enables Ca^{2+} entry (1), triggering Ca^{2+} induced Ca^{2+} release from the SR via RyR2 (2) that activates myofilament crossbridge and mechanical contraction (3). During diastole, SR Ca^{2+} resequestration occurs through NCX (4) and Serca2 (5), allowing Ca^{2+} dissociation from the myofilaments and initiation of relaxation. To maintain EC coupling, Ca^{2+} extrusion always balances Ca^{2+} entry.
Right: EC coupling during β-AR stimulation: β-AR stimulation (6) activates PKA (7), which increases phosphorylation of PLB (8), TnI (9), LTCC (10) and RyR2 (11). This increases Ca^{2+} flux during EC coupling and acts positive inotropic (=increased force) and positive lusitropic (=facilitated relaxation). Adapted from [36-38]

2.2.3 Fine-tuning contractile force: Modulation of calcium signaling

β-adrenergic receptor (β-AR) stimulation is one way of the body to adjust cardiac output to the needs of increasing oxygen consumption. On the cellular level, β-AR stimulation modulates amplitude and duration of Ca^{2+} transients, resulting in positive inotropic (=increased force) and positive lusitropic (=facilitated relaxation) actions.[39, 40]

Agonist binding to β-ARs activates the adenylate cyclase (AC) (Fig. 1.6), which increases cyclic adenosine monophosphate production (cAMP).[41] cAMP in turns activates protein kinase A (PKA) (Fig. 1.7) that phosphorylates its downstream target as LTCC, PLB, RyR2 and Troponin I (TnI) (Fig. 1 right).[21, 42-44] Phosphorylation of PLB releases Serca2 which increases the activity of the ATPase and facilitates SR Ca^{2+} uptake (Fig. 1.8).[31, 34] This seems to be the major reason for increased lusitropy.[18, 21] Furthermore, phosphorylation of TnI facilitates Ca^{2+} dissociation from the myofilaments, increasing relaxation (Fig. 1.9).[18] Increased Serca2 activity also leads to increased SR load. Besides, phosphorylation of LTCC increases systolic Ca^{2+} influx (I_{ca}) and RyR2 phosphorylation results in enhanced open probability (P_o) of the channel pore (Fig. 1.10 and 1.11). All together, the effects increase systolic $[Ca^{2+}]_i$ and Ca^{2+} transients that act positive inotropic.[39, 40, 42, 45] Increased $[Ca^{2+}]_i$ furthermore enhance Ca^{2+}/calmodulin-dependent protein kinase (CamKII) activity, which also

phosphorylates LTCC, PLB and RyR2. Although phosphorylation sites are distinct from the PKA site, CamKII phosphorylation also operates positive inotropic and lusitropic.

Lusitropy and inotropy are further regulated at the myofilaments. Upon cardiomyocyte stretch, on the one hand, sarcomere overlapping becomes more efficient and results in stronger contraction; on the other hand Ca^{2+} sensitivity increases, facilitating relaxation.[21, 46]

2.3 Heart failure – from deranged calcium handling to ventricular arrhythmias

Abnormal Ca^{2+} handling has been identified as a hallmark of failing cardiomyocytes and is held responsible for the progression towards HF.[42, 47] This leads to defective EC coupling, which is mainly characterized by reduced SR Ca^{2+} load, reduced systolic Ca^{2+} transient amplitudes, increased Ca^{2+} decay and increased diastolic $[Ca^{2+}]_i$.[9, 48-50] It is the result of altered expression, function and interplay of proteins required for Ca^{2+} homeostasis, however, deducing cause and effect is often difficult if not impossible.[51, 52]

Despite maintained LTCC activity, reduced Serca2 expression and enhanced suppression by PLB (by either increased phosphorylation or reduced Serca/PLB ratio) together lead to reduced SR Ca^{2+} load (Fig. 2.1).[9, 48, 52, 53] Reinforcing this effect, increased expression of NCX results in an improved competition of NCX with Serca2 for diastolic Ca^{2+} extrusion (Fig. 2.2).[54] Systolic RyR2 Ca^{2+} release is also reduced (possibly by RyR2 hyperphosphorylation, see 2.5.1), supporting negative impact on Ca^{2+} transient amplitude (Fig. 2.3).[55] To maintain contractile response, β-AR activity might be able to compensate for defective EC coupling at the beginning; however, chronic sympathetic overdrive results in desensitization of β-ARs, further contributing to contractile deterioration (Fig. 2.4).[56] On the other hand, RyR2 function is also compromised in diastole, as its proper closure is impaired (Fig. 2.5). This increases the diastolic leak, which manifests itself in an increased frequency of Ca^{2+} sparks.[50, 57] When Ca^{2+} sparks get more pronounced, these normally exclusive stochastic events become more frequent and synchronized.[58-62] Due to residual β-AR activity, the SR Ca^{2+} load can exceed the threshold for spontaneous diastolic Ca^{2+} leakage (Fig. 2.6).[59] This can lead to Ca^{2+} waves that propagate across the whole cell.[21]

As NCX expression is increased, the increased diastolic Ca^{2+} is mainly extruded in exchange with sodium (Na^+). In addition, the sodium-potassium-ATPase (Na^+K^+-ATPase) activity is reduced, as well as the inward rectified potassium current (I_{K1}), which leads to reduced intracellular potassium concentrations ($[K^+]_i$) (Fig. 2.7).[63, 64] In combination, increased intracellular sodium concentrations ($[Na^+]_i$) and reduced $[K^+]_i$ destabilize the resting potential, so that Ca^{2+} waves can trigger delayed after-polarizations (DADs) (Fig. 2.8).[26, 58, 59] When these depolarisations exceed the threshold for action potential (AP) generation, they can trigger mature APs, leading to extra-contractions that can results in

ventricular arrhythmias.[65] Aggravating this mechanism, prolonged AP duration also occurs in failing CM. [21, 66-68]

Clinically, it is assumed that about 50% of ventricular tachyarrhythmias in ischemic and non-ischemic cardiomyopathies originate from non-reentrant mechanisms such as DADs.[69] This phenomenon also explains the contraindication of positive inotropic agents for the treatment of heart failure, as they indeed improve inotropy in the short term, but might trigger ventricular arrhythmias in the long term.

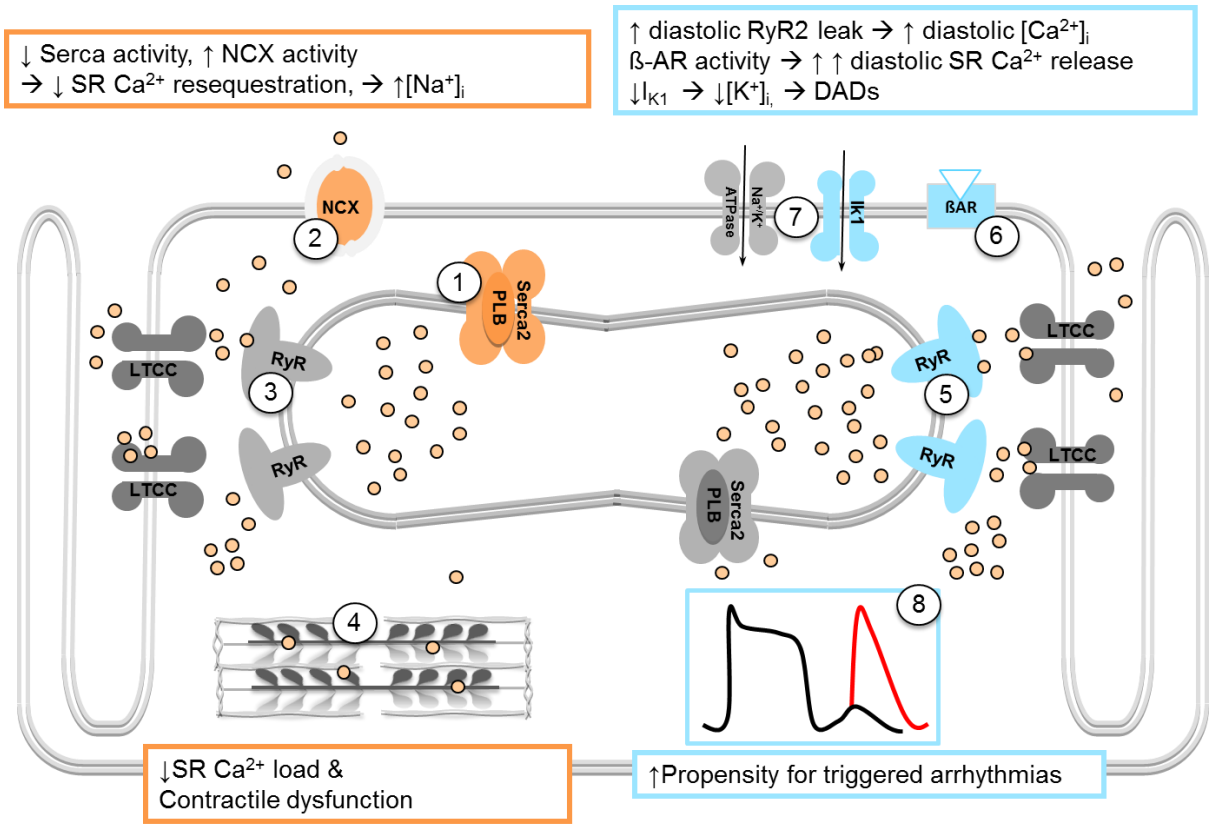

Figure 2: EC coupling in failing CMs
Left: Reduced Serca2 activity impairs SR Ca^{2+} resequestration and diminishes SR Ca^{2+} load that results in contractile dysfunction (1). Additionally, increased NCX activity (2) and reduced Na^+K^+-ATPase (7) activity lead to increased $[Na^+]_i$. **Right**: Furthermore, the resting potential is destabilized, reducing $[K^+]_i$ (7). As the RyR2 is leaky in diastole (5), residual β-AR activity, which increases the diastolic Ca^{2+} leak (5), can trigger DADs (blue inlet, 8), which might result in mature action potential generation and finally lead to ventricular arrhythmias. Adapted from [37]

2.4 Special focus on the RyR2: SR Ca^{2+} release channel and scaffolding protein

RyR are homotetrameric receptors with high molecular weight. They have a large cytosolic N-terminal domain, which serves as scaffold for the binding of regulatory proteins and the intramembrane C-terminal domain which forms the channel pore.[70]

RyR2 are important regulators of systolic and diastolic Ca^{2+} flux. In systole, they promote SR Ca^{2+} release and form the basis for myocyte contraction, whereas in diastole they are supposed to be sealed

to maintain relaxation. Thus, RyR2 activity needs to be tightly yet flexibly regulated in order to sustain cellular function.[5] Therefore, RyR2 opening is not only controlled by cytosolic and luminal [Ca^{2+}] but also by phosphorylation and other post-translational modifications (PTMs) as well as by the binding of accessory proteins such as calmodulin (CaM), FK506 binding protein 12.6 (FKBP12.6), soluble resistance-related calcium-binding protein (sorcin) and also S100A1.[71]

2.4.1 Regulation of RyR2 by phosphorylation

RyR2 is targeted both by PKA and CamKII at the N-terminal domain. Both enzymes interact with the RyR2 in cardiomyocytes and phosphorylate it under physiological conditions.[21, 43]

Upon β-AR stimulation, increased PKA activity enhances phosphorylation at serine 2808.[72, 73] This activates the RyR2 and increases systolic Ca^{2+} release, but also the incidence of diastolic Ca^{2+} sparks.[44, 74, 75] Furthermore, PKA also phosphorylates RyR2 at serine 2030, which is reported to increase RyR2 activity as well.[44, 76, 77] However, this phosphorylation site is not well analyzed so far.

Upon increased $[Ca^{2+}]_i$ and CaM activation, CamKII phosphorylation occurs at serine 2814. CamKII-mediated RyR2 phosphorylation also activates RyR2 and increases P_o in systole.[21] Similarly, it also increases Ca^{2+} sparks frequency in diastole.[78, 79]

To maintain cellular equilibrium, dephosphorylation is sustained by the protein phosphatases PP1 (serine 2808) and PP2a (serine 2814), which are also associated to the RyR2.[77]

In heart failure, general phosphatase activity is enhanced, but local activity of PP1 and PP2a at the RyR2 is reduced.[53] Despite generally maintained PKA activity, this reduced phosphatase activity in combination with increased cAMP levels can lead to hyperphosphorylation of RyR2 at serine 2808.[44, 80] This phosphorylation may be responsible for the increased diastolic Ca^{2+} leak in failing cardiomyocytes; however, this effect is discussed quite controversially at presence.[74, 75, 81-83]

CamKII activity is also increased in failing cardiomyocytes, which leads to increased serine 2814 phosphorylation.[84, 85] Recent work suggests that this phosphorylation is the major reason for the increased diastolic Ca^{2+} leak and that PKA-mediated phosphorylation at serine 2808 has only minor impact on RyR2 regulation.[39, 40, 86-88]

2.4.2 Regulation of RyR2 by accessory proteins

At their large N-terminal cytosolic domain, RyR2 tetramers are occupied by different accessory proteins, which also modulate channel gating properties in the pore region. But also the C-terminal domain of RyR2 is occupied by accessory proteins.

In the SR, junctin and triadin bind to the C-terminal part of RyR2. These proteins are associated with calsequestrin (CSQ), the primary Ca^{2+}-binding protein of the SR.[89] Triadin establishes a functional connection between RyR2 and CSQ, enabling adjustment of SR Ca^{2+} release to SR Ca^{2+} load.[71, 90]

On the N-terminal domain, proteins like CaM, FKBP12.6 and sorcin bind to the RyR2.

CaM is a small Ca^{2+} binding protein that interacts with the RyR2 in a Ca^{2+} dependent manner.[71, 91, 92] CaM:RyR2 stoichiometry is reported to be 1:1, whereas apo-CaM and Ca^{2+} bound CaM can bind with equal affinity.[92] Planar lipid bilayer recordings of RyR2 demonstrated that CaM inhibits RyR2 P_o at low as well as at high cytosolic and luminal [Ca^{2+}].[30, 91] Contrary, overexpression of CaM in intact cardiomyocytes increased Ca^{2+} transient amplitude and decay, however these effect were mainly due to enhanced CamKII activity.[25] In HF, CaM shows reduced affinity for RyR2.[93] However, it is assumed that beat-to-beat variability in CaM binding or dissociation do not account for increased RyR2 activity under e.g. β-AR stimulation.[71, 92]

FKBP12.6, also known as calstabin2, is supposed to have a major role on RyR2 coupled gating.[27] Four molecules are reported to bind per RyR2 tetramer under physiological conditions, however latest research indicated that this number is overestimated and corrected it to 20-30% of RyR2 that are occupied by FKB12.6.[94] FKBP12.6 functionally couples RyR2 clusters, stabilizing the receptor and inhibiting subconductance state.[27] In failing cardiomyocytes, RyR2 hyperphosphorylation is supposed to mediate FKBP12.6 dissociation, thereby prompting the diastolic Ca^{2+} leak.[44, 95] However, the so called "Marks paradigm in HF" is still discussed controversially and current data also suggests that FKBP12.6 has not such a strong impact on RyR2 function.[44]

Additionally, **sorcin** also binds to the RyR2 already to resting [Ca^{2+}].[96, 97] In saponin-skinned cardiomyocytes, addition of sorcin reduced Ca^{2+} transients and Ca^{2+} decay rate but also decreased Ca^{2+} spark frequency.[97-99] This reduces the EC coupling gain and might be a negative feedback mechanism to quench CICR. Furthermore, sorcin is supposed to translocate quickly upon increasing $[Ca^{2+}]_i$, indicating that sorcin might be able to change its location during EC coupling [Ca^{2+}].[97] However, the exact consequences of this translocation remain unclear.

2.4.3 Regulation of RyR2 by redox-modification

Additionally to alterations in phosphorylation status, other PTMs of the RyR2, such as oxidation, nitrosylation or glutathionylation, can affect its function. RyR2s contain 80–100 cysteines per monomer with approximately 25–50 in the reduced state. An additional six to eight are considered hyperreactive, making them suitable for redox modification.[100, 101] Current research focuses on the activation of RyR2 by cysteine nitrosylation (SNO): On the one hand, previous work demonstrated that enhanced RyR2-SNO increased mean P_o in lipid bilayer recordings of RyR2 preparations.[101] On the other hand, inhibition of NOS1-mediated RyR2-SNO increased Ca^{2+} spark frequency and Ca^{2+} wave in isolated cardiomyocytes.[102, 103] In general, protein-nitrosylation is supposed to be cardioprotective.

In HF, increased oxidative stress results from the formation of reactive oxygen species (ROS) (e.g. superoxide anion, hydrogen peroxide, and hydroxyl radical). These compounds are capable of interacting with the reactive cysteines, causing RyR2 oxidation.[85, 103-109] This can change RyR2 function and increase the diastolic Ca^{2+} leak; however, there is still a lot of research ongoing and the exact interplay of different redox-modifications needs to be understand in greater detail.

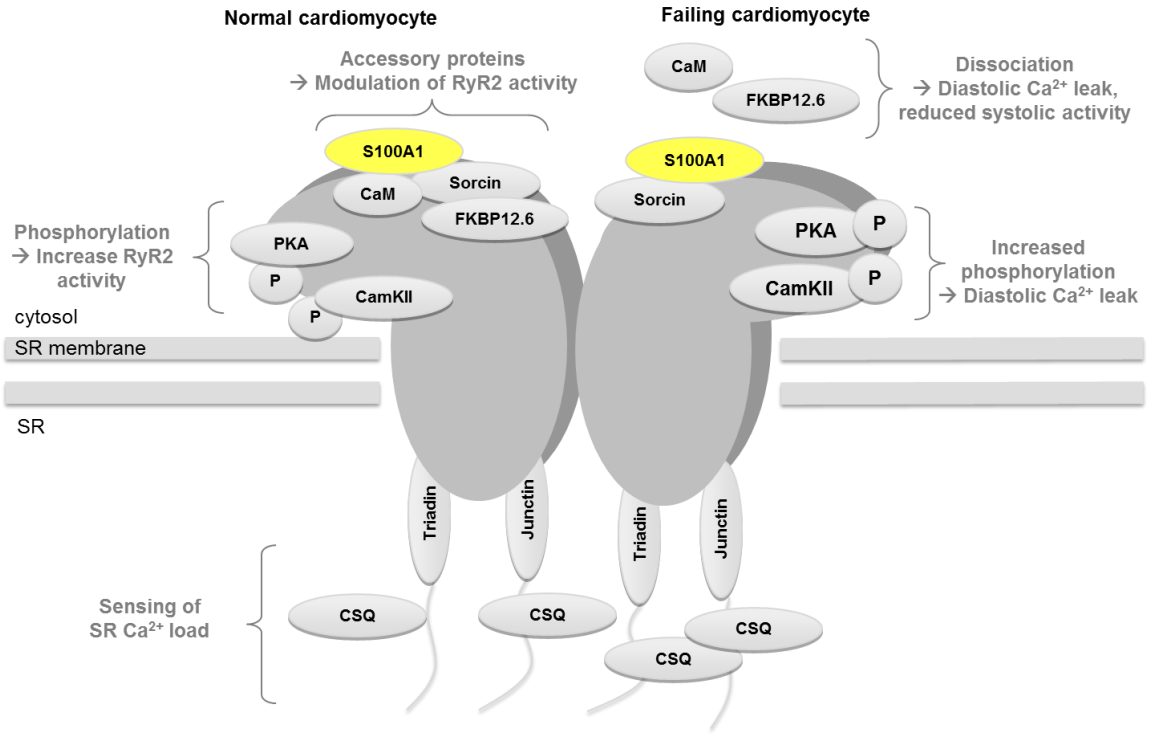

Figure 3: The RyR2 macrocomplex: Ca^{2+} release channel and scaffolding protein
Left: On the N-terminal domain, RyR2 is subjected to phosphorylation by PKA and CamKII, which increases RyR2 activity. Further regulation occurs from the binding of accessory proteins that modulate RyR2 activity. On the luminal side, SR Ca^{2+} load and RyR2 opening is also controlled by accessory proteins.
Right: In heart failure, hyperphosphorylation by PKA or CamKII might mediate the diastolic Ca^{2+} leak. Potential dissociation of CaM and FKBP12.6 support this effect. Modified from [110, 111]

2.5 S100A1 - function and fiction

2.5.1 S100A1 structure and expression pattern

S100A1 belongs to the family of S100 proteins, a group of small Ca^{2+} binding proteins exclusively expressed in vertebrates. S100 proteins control numerous cellular and molecular functions including proliferation, differentiation, cell survival and motility as well as protein phosphorylation, NO homeostasis and Ca^{2+} handling.[112, 113]

In general, S100 proteins reside as dimers, whereas their tertiary structure compromises two EF hand motifs that recognize Ca^{2+} and change their 3-dimensional structure, enabling target protein recognition.[112-115]

In special, S100A1 has a high Ca^{2+} affinity, which is further enhanced by PTMs such as s-nitrosylation or s-glutathionylation. [116-119] Nevertheless, it has low Ca^{2+} binding capacity, which makes it an optimal intracellular Ca^{2+} sensor.

S100A1 shows highest abundance in cardiac muscle and it is expressed to lower levels in skeletal muscle, the brain and the kidneys. It shows highest expression levels in the left ventricle and lower abundance in the right ventricle and the atria. In the heart, S100A1 mainly resides in CM, with no

evidence for expression in cardiac fibroblasts. To a small extent, S100A1 is also expressed in endothelial cells and the vasculature.[120-124]

2.5.2 S100A1 action in cardiomyocytes

S100A1 has been identified as a major regulator of cardiovascular function, controlling the Ca^{2+} driven networks in cardiomyocytes. S100A1 was shown to interact with structures in the mitochondria, at the myofilaments and at the SR (Fig. 4).

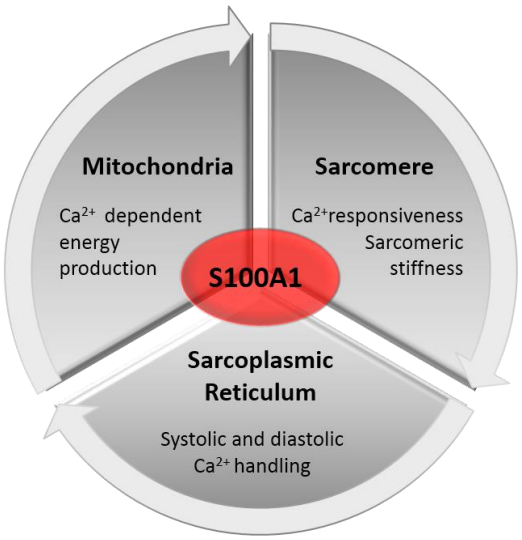

Figure 4 : Conceptual framework of S100A1 target structures in CM.
S100A1 regulates the Ca^{2+} driven key compartments in CM: the sarcoplasmic reticulum, the sarcomere and the mitochondria. Modified from [125]

At the mitochondria, S100A1 increases energy generation and utilization, as it interacts with key factors from the ATP-producing machinery e.g. with the F1-ATPase of complex V and the adenosine nucleotide translocator (ANT) (Fig. 5.4).[126, 127]

At the myofilaments at the I-Band, S100A1 interacts with the PEVK-domain of the giant protein titin.[128, 129] Titin normally contributes to the passive tension of the myofilaments, as actin binding to the PEVK-domain is supposed to inhibit action/myosin crossbridge and increase diastolic stiffness.[28, 130-132] S100A1/titin interaction therefore might liberate actin before active contraction, thereby reducing pre-contractile passive tension and facilitating contraction. Furthermore, S100A1 might decrease the Ca^{2+} sensitivity of the myofilaments (Fig. 5.3).[133] However, the mechanism for this effect is still unclear.

At the SR, S100A1 facilitates Ca^{2+} cycling by regulating Serca2 and RyR2 activity. In diastole, S100A1/Serca2 interaction enhances Serca2 activity, augmenting SR Ca^{2+} load and facilitating relaxation (Fig. 5.1). In systole, S100A1 ameliorates RyR2 activity and improves Ca^{2+} extrusion (Fig. 5.2).[134, 135] In combination with the increased SR Ca^{2+} load, enhanced systolic Ca^{2+} transients manifest in positive inotropy and increased EC coupling gain.[136] As enhanced SR and myofilament

ATPase activity rise energy demands, S100A1 might be able to meet this demand by increasing ATP generation and availability.

In general, S100A1 effects are similar to β-AR stimulation; however, S100A1 acts independent of known cAMP/ PKC pathways, enhancing target protein activity by direct interaction.[137]

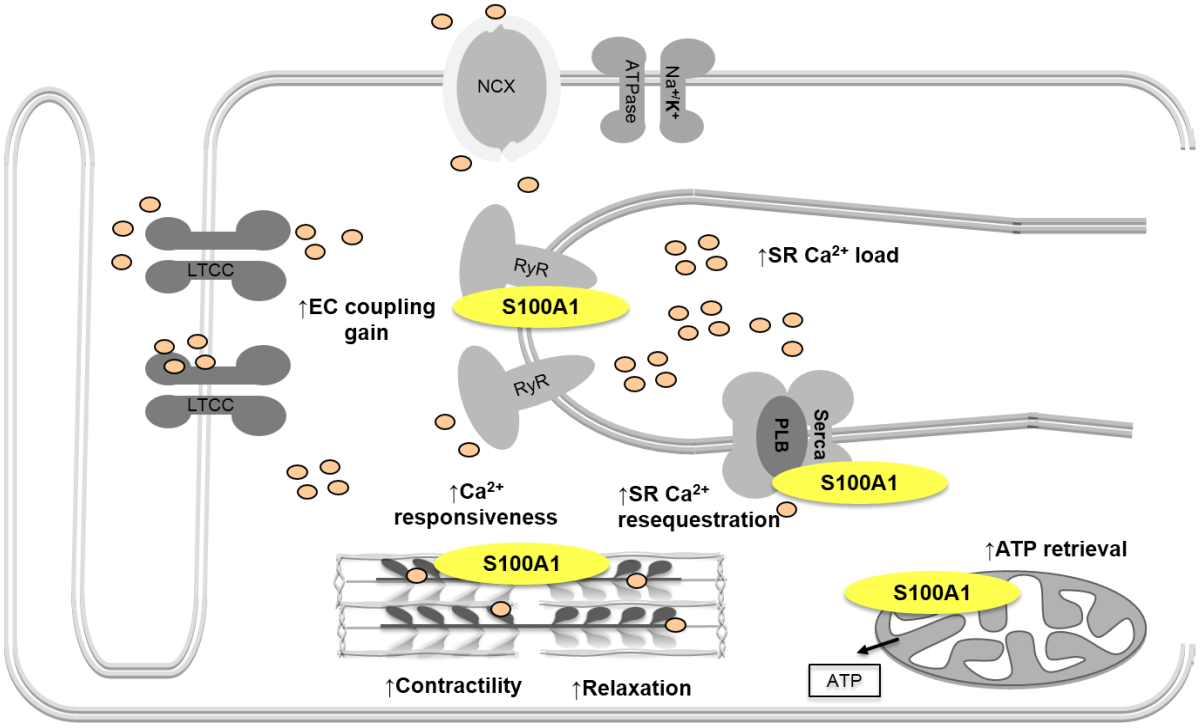

Figure 5: S100A1 actions in cardiomyocytes
Enhanced Serca2 activity increases SR Ca^{2+} resequestration and SR Ca^{2+} load (1), facilitating relaxation and systolic Ca^{2+} release via RyR2 (2). Together, this results in improved EC coupling gain and mechanical force generation. Additionally, myofilament stiffness is decreased alleviating relaxation (3). Finally, enhanced mitochondrial ATP production and retrieval matches increased energy demands (4). Modified from [36, 125]

2.5.3 S100A1 in heart failure: Development of S100A1 gene therapy

Different studies revealed diminished S100A1 expression in failing human hearts which could be confirmed *in vitro* and in various HF animal models *in vivo*.[134, 135, 138-140]

However, the actual rationale for S100A1 genetically targeted therapy originated from comprehensive studies in S100A1 transgenic and knockout mice, which showed opposite phenotypes when subjected to cardiac stress and underlined the importance of S100A1 for proper cardiomyocytes function.[138, 141, 142] First experiments with adenoviral-mediated S100A1 overexpression in normal and failing isolated rat and human cardiomyocytes confirmed increased Ca^{2+} transients and SR Ca^{2+} load.[134, 143-145] Further *in vivo* experiments with experimental HF in mice and rats using AAV-vectors with cardiomyocyte-specific S100A1 expression confirmed success and feasibility of S100A1 re-expression, resulting in beneficial long-term inotropic, anti-hypertrophic and anti-apoptotic therapeutic effects and restored energy homeostasis in the failing myocardium.[135, 139, 146] Although not all effects of S100A1 in cardiomyocytes and in the heart have been clarified, these studies clearly demonstrate

efficacy of viral-mediated S100A1 gene therapy and foster the development of positive inotropic S100A1 gene therapy for chronic heart failure.

2.5.4 S100A1 positive inotropic *and* anti-arrhythmic potential?

As described above, in failing cardiomyocytes, the reload of unstable SR (e.g. under β-AR stimulation) with Ca^{2+} can trigger diastolic SR Ca^{2+} leakage, as the SR load exceeds the critical threshold for spontaneous diastolic Ca^{2+} release (Fig. 6 right).[26, 37, 58, 59] This can induce delayed after-depolarizations which can result in lethal ventricular arrhythmias.

S100A1 enhances the SR Ca^{2+} load in a similar way than β-AR stimulation (Fig. 6 left). Raising concerns about this potential pro-arrhythmogenic potential of positive inotropic S100A1 gene therapy prompted most recent studies in isolated CMs. Surprisingly, these studies indicated that adenoviral-mediated S100A1 overexpression in quiescent normal CMs and failing CMs decreased SR Ca^{2+}-spark frequency and prevented β-AR-triggered compound Ca^{2+}-sparks and Ca^{2+} waves (Fig. 6 left, right) (unpublished data).[147, 148] These effects were independent of PKA-mediated RyR2 phosphorylation. Thus, despite persistent changes in RyR2 phosphorylation, S100A1 overexpression rather seems to prevent diastolic Ca^{2+} leakage and therefore might act positive inotropic and anti-arrhythmic.

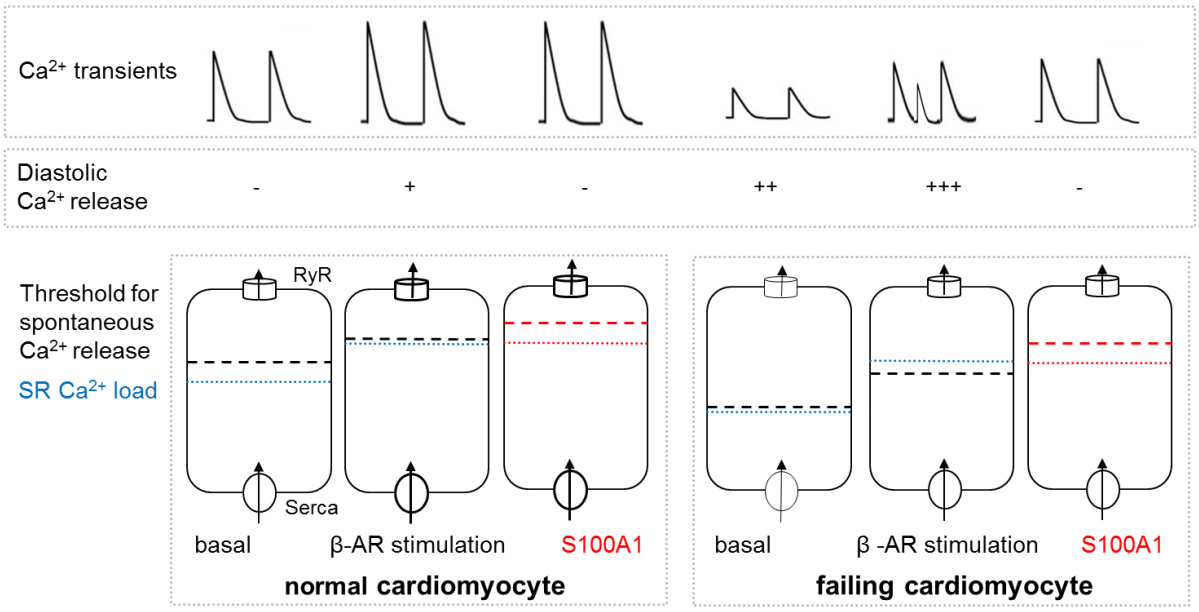

Figure 6: Schema of S100A1 effects on Ca^{2+} transients, SR Ca^{2+} load and the development of the diastolic Ca^{2+} leak in isolated CM

Left: In normal CMs, β-AR stimulation increases SR Ca^{2+} load and Ca^{2+} transient amplitudes, as well as diastolic Ca^{2+} release. S100A1 has similar effects on SR Ca^{2+} load and Ca^{2+} transient amplitudes; however it does not trigger diastolic Ca^{2+} release.

Right: In failing CMs, the threshold for spontaneous Ca^{2+} release is reduced, so that diastolic Ca^{2+} release already occur under basal conditions. β-AR stimulation aggravates the diastolic Ca^{2+} leak, further increasing diastolic Ca^{2+} release, which manifests as Ca^{2+} waves. However, S100A1 inhibits the diastolic Ca^{2+} leak despite maintained increased SR Ca^{2+} load. Modified from [149, 150]

2.6 Aim of the study

The investigation of the potential anti-arrhythmic mechanism of S100A1 has only been performed in single cells so far but Ca^{2+} regulation in the multicellular heart is far more complex. So it remained unclear, if the inhibition of the diastolic Ca^{2+} leak also impedes mature arrhythmogenic contractions. Furthermore, the exact mechanism and effects of S100A1 on RyR2 modifications remained unclear, as most studies propose normalized RyR2 phosphorylation and restored binding of accessory proteins as prerequisite for proper RyR2 function. Although a most recent study demonstrated that S100A1 effects are irrespective of PKA-mediated RyR2 phosphorylation, CamKII-mediated RyR2 phosphorylation has not been analyzed so far.

Thus, the aim of this work was to investigate the effect of S100A1 on Ca^{2+}-and β-AR-triggered cellular arrhythmias in a multicellular system and to determine changes in RyR2 phosphorylation or complex formation.

For that reason, I chose the model of Engineered Heart Tissue, which represents a 3-dimensional tissue culture model composed of neonatal rat heart cells. EHT outmatches conventional 2-dimensional cell culture, as neonatal rat cells (whole heart isolates) are cultivated in a collagen matrix under cyclic stretch (referred to as loaded conditions). After almost two weeks of maturation, this cell culture model resembles adult myocardium and forms a functional syncytium.[151, 152] Still, cellular or pharmacological manipulations as well as biochemical analysis are as easy to conduct as in conventional 2-dimensional cultures. Furthermore, functional force analyses are carried out under isometric conditions, which is an improvement over conventional cell shortening analysis in adult rat cardiomyocytes. Still, it is not as complex as a whole body, as compensatory mechanisms or secondary effects do not bias outcomes in this model.

Accordingly, the first goal of this study was to induce a HF-like phenotype in EHT and to develop a stimulation protocol, where potential arrhythmogenic events can be analyzed on a contractile level. The second part aimed to confirm the inotropic effects of 100A1 gene transfer in normal and HF-like EHT before investigating S100A1's potential anti-arrhythmic effects. The last part focused on the underlying mechanisms that might mediate S100A1 anti-arrhythmic effects.

3. Materials and Methods

3.1 Materials

3.1.1 Equipment

Device	Purchased from
37°C water bath	Karlheinz Dosch
Aspirator for cell culture	Neolab
Centrifuge Rotina 420 R	Hettich Zentrifugen
Custom-designed organ bath equipment	Föhr Medical Instruments
EHT casting molds	Self-made
Electrical stimulator STI-08	Föhr Medical Instruments
Force transducer	Ing. Büro Jäckel, Hanau
Heating block	Neolab
Hera Safe Laminar Flow	Thermo Electron cooperation
Incubator Hera cell 150	Thermo Electron cooperation
McILWAIN Tissue Chopper	The mickle laboratory engineering co. Hd
Microscope for cell culture	Leica
My iQ Single Color Real-Time PCR Detection System	Bio Rad
NanoDrop Spectrophotometer ND-1000	Peqlab Biotechnologie GmbH
Neubauer counting chamber	Brand
Odyssey Infrared Imaging System +Software	LI-COR Biosciences
Organ bath solution (custom design)	FMI
pH meter	WTW
Pipetboy accu	IBS Integra Biosciences
Pipettes	Eppendorf
Power Pac 300	Bio Rad
Precellys Homogeniser	Peqlab
Recording System (Powerlab, Measuring Amplifier)	ADI Instruments
Rotor for ultracentrifuge SW41 Ti	Beckman
Rotor wheel	Neolab
Shaker	Hermed SW, Neolab
Stretching device	Precision engineering workshop University of Heidelberg
Table top centrifuge	Roth
Tank blot	University Heidelberg
Thermomixer 5436	Eppendorf
U-2000 Spectrophotometer	Hitachi
Ultracentrifuge WXUltra 80	Thermo Electron cooperation
Vortex	Bender und Hobein AG
X cell Sure Lock Mini-cell	Invitrogen

3.1.2 Consumables

Item	Purchased from
0.5, 1.5, 2.0 ml tubes	Sarstedt
5ml, 15ml, 50 ml tubes	Greiner Bio-One GmbH
Balance paper	VWR
Cell culture plates and dishes	Greiner Bio-One GmbH, Nunc

Cell scraper	Greiner Bio-One GmbH
Cell strainer	BD
Detachable needles	BD
Dialysis cassette 10000 MWCO	Thermo Scientific
Disposable scalpel	Feather
Filter paper 0.5mm for western blot	Neolab
Immobilon-FL PVDF membrane	Millipore
Magnetic stir bar	Neolab
Microscope cover glasses	Marienfeld GmbH&Co.KG
Microscope slides	Thermo Scientific
Pipette tips with filters	Sarstedt
Serological pipettes	Greiner Bio-One GmbH
Sterile syringes	BD
Ultracentrifugation tubes	Herolab

3.1.3 Chemicals and reagents

Common chemicals were obtained from AppliChem, CARL ROTH GmbH, Merck, Serva and Sigma-Aldrich. Some selected chemicals, reagents and enzymes are listed below:

Chemical/ Reagent	**Purchased from**
$CaCl_2$	Sigma-Aldrich
Chick embryo extract	Seralab biologicals
Collagen Type I, rat tail	Promocell
Collagenase	Cellsystems
DEPC water	Roth
DMEM high glucose	PAA
DMEM low glucose	PAA
DNAse I (4.1 mg/ml)	Roche
Dulbecco's PBS (Ca^{2+}-free and Mg^{2+}-free)	PAA
Duolink In Situ Detection Reagents Red	Olink
Duolink In Situ PLA probe anti-Mouse PLUS	Olink
Duolink In Situ PLA probe anti-Rabbit MINUS	Olink
Fetal Calf Serum (FCS) gold EU approved	PAA
Heparin-Natrium 25 000 (25000 I.E.)	ratiopharm
Horse serum	PAA
I-block blocking buffer	LI-COR Biosciences
In situ cell death detection kit TRD	Roche
Insulin Insuman Rapid 40 I.E./ml	Sanofi Aventis
iQ SYBR Green Supermix	Bio Rad
iScript cDNA Synthesis Kit	Bio Rad
Isoproterenol bistitrate salt	Sigma-Aldrich
Laminin	Sigma-Aldrich
L-glutamine, 200 nM	PAA
Matrigel	BD
Medium 199	Sigma-Aldrich
Penicillin-Streptomycin (10 000 U/ 10 mg/ml)	PAA
Phosphatase inhibitor 1,2,3	Sigma-Aldrich
Protease inhibitor tablets	Roche
Protein A/G PLUS-Agarose	Santa Cruz
Protein standard for SDS-PAGE	New England Biolabs

Thiopental Inresa (5 mg/10 ml)	Inresa Arzneimittel GmbH
Tris-glycine gels (4-20 %)	ANAMED
Trizol reagent	Invitrogen
Tropix I-Block	Applied Bioscience
Trypsin-EDTA (0.05 %/ 0.02 %)	PAA
Vectashield Mounting Medium with DAPI	LINARIS

3.1.4 Primers

All primers were obtained from Eurofins MWG Operon and annealing temperature optimized by a temperature gradient PCR. Collagen-1 primer was obtained from Life Technologies, which do not give information about primer sequences.

Name	Gene name	Primer forward	Primer reverse	Size (bp)	Annealing Temp
18s	Rn18s	5´- TCA AGA ACG AAA GTC GG – 3´	5´- GTG ATG CCC TTA GAT GTC C – 3´	488	57-63.5
ANP	Nppa	5`-TGC CGG TAG AAG ATG AGG TC -3`	5`-TGC TTT TCA AGA GGG CAG AT -3`	205	63.5
Collagen-1	Col1A	-	-	-	60
CTGF	Ctgf	5`-GAG GAA AAC ATT AAG AAG GGC AAA -3`	5`- CGG CAC AGG TCT TGA TGA -3`	235	63.5
GFP	Egfp	5`- TGA CCT ACG GCG TGC AGT GC -3`	5`- TGC TGG TAG TGG TCG GCG AG -3`	361	63.5
ICAM-1	Icam1	5’- CTG TCG GTG CTC AGG TAT CC -3’	5’- CCA ACT TCT CAG TCA CCT CC -3’	620	63.5
IL-6	Il6	5´- CTT CCA GCC AGT TGC CTT CT -3`	5´- GAG AGC ATT GGA AGT TGG GG -3`	496	57
NCX	Slc8a1	5´- GCT CAT ATT ACT GTA AGA AAG GGG TG -3`	5´- GGC GGC GCT TCC CAC AAT GG -3`	377	57
RyR2	Ryr2	TAA CCT ACC AGG CCG TGG AT -3`	GCT GCG ATC TGG ATA AGT TCA A -3`	114	57
S100A1	S100a1	5`-CCA TGG AGA CCC TCA TCA AT -3`	5`-TTG AAG TCC ACT TCC CCA TC -3`	210	63.5
Serca2a	Atp2a2	5`- TGA GAC GCT CAA GTT TGT GG -3`	5`-ATG CAG AGG GCT GGT AGA TG -3`	189	63.5
SMA	Acta2	5´- TGC TGG ACT CTG GAG ATG -3`	5´- GTG ATC ACC TGC CCA TC -3`	292	63.5
TGF-β1	Tgfb1	5`-ACC TGC AAG ACC ATC GAC ATG -3`	5`- CGA GCC TTA GTT TGG ACA GGA T -3`	85	63.5

3.1.5 Antibodies

Primary Antibody	Clonality	Host	Application	Molecular weight (kDa)	Dilution	Obtained from
Calmodulin	Monoclonal EPR5028	Rabbit	Duolink	17	1:50	Epitomics

Calsequestrin	Polyclonal	Rabbit	WB	55	1:2000	Affinity Bioreagents
CamKII	Monoclonal IgG1 G-1	Mouse	WB	50	1:1000	Cell signaling
Connexin43	Monoclonal IgG1 4E6.2	Mouse	WB	43-47	1:1000	Millipore
FKBP12.6	Polyclonal	Rabbit	Duolink	12	1:50	Novus biologicals
GFP	Polyclonal	Mouse	WB	27	1:30000	Clontech
Glyceraldehyde-3-Phopsphate-Dehydrogenase (GAPDH)	Monoclonal IgG1 6C5	Mouse	WB	38	1:30000	Millipore
Phospho-Connexin 43 (Ser368)	Polyclonal	Rabbit	WB	43-47	1:1000	Millipore
Phospholamban	Monoclonal IgG2a sD12	Mouse	WB	5-25	1:5000	Thermo Scientific
Phospho-Phospholamban (Ser16)	Polyclonal	Rabbit	WB	5	1:5000	Upstate
Phospho-Phospholamban (Thr17)	Polyclonal	Rabbit	WB	5	1:5000	Badrilla
Phospho-RyR2 (Ser2808)	Polyclonal	Rabbit	WB	350	1:1000	Badrilla
Phospho-RyR2 (Ser2814)	Polyclonal	Rabbit	WB	350	1:1000	Badrilla
Ryanodine Receptor	Monoclonal IgG1 C3-33	Mouse	Duolink	350	1:50	Abcam
Ryanodine Receptor	Monoclonal IgG1 C3-33	Mouse	WB/ IP	350	1:1000	Thermo Scientific
S100A1	Polyclonal	Rabbit	WB/ Duolink/ IF	10	1:1000/ 1:50/1:200	Acris
Serca2	Polyclonal N-19	Goat	WB	100	1:2000	Santa Cruz
s-Nitroso-Cysteine (SNO-Cys)	Polyclonal	Rabbit	Duolink	---	1:50	Sigma-Aldrich
Sorcin	Polyclonal	Rabbit	Duolink	12	1:50	Acris
α-Actinin (sarcomeric)	Monoclonal IgG1 EA-53	Mouse	IF	100	1:800	Sigma Aldrich

Secondary Antibody	**Host**	**Emission**	**Application**	**Dilution**	**Obtained from**
Anti-goat	donkey	680	WB	1:10000	LI-COR Biosciences
Anti-mouse	goat	680/800	WB	1:10000	LI-COR Biosciences
Anti-rabbit	goat	680/800	WB	1:10000	LI-COR Biosciences
Anti-mouse	goat	488/568	IF	1:200	Invitrogen
Anti-rabbit	goat	488/568	IF	1:200	Invitrogen

3.1.6 Prepared buffers, solutions and media

Buffers and stock solutions were prepared in deionized water unless noted otherwise. Buffers were titrated with sodium hydrochloride.

Buffer/Solution	Preparation Protocol
1.3 g/ml CsCl	402.4 mg/ml in H_2O
1.4 g/ml CsCl	548.3 mg/ml in H_2O
ACM medium	5.4 mM KCl, 3.5 mM $MgSO_4$, 0.05 mM NaPyruvate, 20 mM $NaHCO_3$, 10 mM glucose, 20 mM HEPES, 23.5 mM NaGlutamate, 4.87 mM NaAcetate, 0.05 mM phenol red, 15 mM butaedionemonoxime, 20 mM creatinine, 15 mM creatinphosphate, 15 mM taurine, 27 IU/ml Insulin, adjusted to pH 7.2, sterile filtrated
ACM-EDTA medium	5.4 mM KCl, 3.5 mM $MgSO_4$, 0.05 mM NaPyruvate, 20 mM $NaHCO_3$, 10 mM glucose, 20 mM HEPES, 23.5 mM NaGlutamate, 4.87 mM NaAcetate, 100 µM EDTA, 0.05 mM phenol red, 15 mM butaedionemonoxime, 20 mM creatinine, 15 mM creatinphosphate, 15 mM taurine, 27 IU/ml Insulin, adjusted to pH 7.2, sterile filtrated
Anode buffer	1 M Tris adjusted to pH 8.6
BlueJuice 3x loading dye	150 mM Tris, 6% SDS, 0.3% bromphenolblue, 10% glycerol, 5% β-mercaptoethanol, adjusted to pH 6.8
Ca^{2+} buffer	10% glycerol, 135 mM Nacl, 1 mM $CaCl_2$, 20 mM Tris-HCl, adjust to pH 7.4
Ca^{2+}-NP40 buffer	1% NP-40, 10% glycerol, 135 mM NaCl, 1 mM $CaCl_2$, 20 mM Tris-HCl, adjust to pH 7.4
Digestion-solution	1.5 ml sterile-filtrated Trypsin (10 ml Stock; 1g Trypsin (1:250) for 10 ml HBSS), 300 U/ml DNAse I, 2% P/S, 40 mM HEPES, 3.2 µM NaOH
EHT-Medium	DMEM low glucose, 10% horse serum, 2% chicken embryo extract, 1% P/S
I-Block blocking solution	0.2% (w/v) Tropix I Block, 1% Tween 20 in TBS
Kathode buffer	0.1 M taurine, 0.1 M Tris, 0.1% SDS
modified - M199	Medium 199 supplemented with 5 mM taurine, 5 mM carnitine, 5 mM creatine, 5 mM N-mercaptoproprionyl glycine, 27 IU/ml insulin, 1% P/S, adjusted to pH 7.25, sterile filtrated
NCF-Medium	DMEM high glucose, 10% FCS, 1% P/S
NCM-Medium	Medium 199, 10/0.5% FCS, 1% l-glutamine, 1 mM $CaCl_2$, 1% P/S
PFA	4% PFA in H_2O, adjusted to pH 7.2
SDS-lysis buffer	PBS, 1 mM EDTA, 1 mM EGTA, 1% SDS, 1% phosphatase inhibitor 2 and 3, 1 tablet protease inhibitor in 10ml
Stop-solution	4% FCS, 300 U/ml DNAse I, 2% P/S, 60 mM HEPES
TBS -Tween	0.1% (v/v) Tween in 1x TBS
Transfer buffer	20% methanol, 15 mM Tris-HCl, 15 mM taurine
Tris buffer (TBS)	25 mM Tris, 150 mM NaCl, 1 mM $CaCl_2$, adjusted to pH 7
Tyrode solution	119.8 mM NaCl, 5.4 mM KCl, 1.05 mM $MgCl_2$, 0.2 mM $CaCl_2$, 0.42 NaH_2PO_4, 22.6 mM $NaHCO_3$, 5.05 mM glucose, 0.05 mM Na_2EDTA, 0.28 mM ascorbic acid (total Na^+ 142.9 mM, total Cl^- 130.9 mM, O_2/CO_2(%) 95/5), pH adjusted by gassing

Virus buffer	10 mM Tris pH 8.1, 10% glycerol, 150 mM NaCl, 1 mM MgCl

3.1.7 Non-standard software

Software version	Author/ company
Lab Chart v7.1.2	ADI Instruments
ImageJ Version 1.43u	National Institute of Health
MyIQ Optical System Software Version 1.0	BioRad
Odyssey Infrared Imaging Software Version 2.0	LI-COR Biosciences
Prism Version 5.01	GraphPad software Inc.
Xcellence rt1.2	Olympus soft Imaging Solutions GmbH
Endnote X6	Thomson Reuters

3.2 Methods

3.2.1 Cell culture techniques

All cells were incubated in a humidified 37°C incubator gassed with 5% CO_2.

3.2.1.1 Virus production

3.2.1.1.1 General cell culture

Human embryonic kidney carcinoma 293A cells (Hek293A) were used for the production of recombinant adenoviruses. This cell line was established by transforming normal embryonic kidney cells with the adenovirus 5.[153] Thus, Hek293A cells contain genes that are needed for adenovirus replication. In that way, replication-deficient viruses can be produced from preexisting virus stocks.
Hek293A were grown in 10% FCS DMEM-Medium and were used between passages 20-40. For subculturing, culture medium was removed and cells washed with PBS once. Trypsin was added and incubated for 3 minutes (min) at 37°C. The reaction was stopped by adding the double amount of culture medium and the cells were carefully resuspended. Subculturing was performed when cells had reached 80% confluence by splitting in ratio 1:5.

3.2.1.1.2 Amplification of replication-deficient adenoviruses

Adenoviruses are used for the transduction of cardiomyocytes, which are difficult to transfect with standard reagents.[154] Current adenoviral vectors are depleted for viral genes that control replication (Early 1 and 3 genes, E1/E3), however they are still infectious and can integrate into the host genome. Cloning techniques allow the insertion of target gene cDNA, so that adenoviruses can be used for overexpression studies.

For this study, an adenovirus system described by He et. al. (1998) was used to drive expression for the human S100A1 cDNA.[155] The virus was constructed with two promoters, driving S100A1 and GFP expression under two separate basal CMV promoters (AdS100A1). As control vector, a virus containing only GFP was used (AdGFP).[133] Thus, GFP expression could directly be monitored after transduction of primary cells to monitor transduction efficiency.

The production of adenoviruses was performed in Hek293A cells, which contain the E1/E3 genes that are missing in the recombinant adenovirus. Virus amplification was performed according to Akther et al.[156]

Hek293A cells were grown on 20 25 cm dishes until they reached 80% confluence and were transduced with 80 µl of working aliquots of AdGFP or AdS100A1 (titer approx. $2 \cdot 10^{11}$ VP/ml). From the next day on, cells were monitored three times a day for GFP expression and morphological changes. When all cells displayed GFP expression and first cells started to detach (after 1-3 days), cells were carefully harvested with a cell scraper or by carefully washing the cells of the plate with the cell culture medium. The cell suspension was centrifuged for 15 min at 1200 g and 4°C. The supernatant was discarded and the cell pellet, which had a greenish color, was stored at -80°C until further processed. For one virus batch, the virus production was repeated twice. For cell lysis, 1 ml of PBS per cell pellet was added and 3 freeze-thaw cycles in liquid nitrogen and a 37°C water bath performed. To eliminate Hek293A cell DNA and inhibit clotting of broken viruses particles, DNAse digestion was performed (2 U/ml) for 30 min at 37°C. Afterwards, residual cell debris was removed by a centrifugation steps at max. speed (ca. 4800 g) for 10 min at 4°C. The supernatant containing the adenovirus was kept and the centrifugation step repeated 3 times. The virus solution was directly subjected to virus enrichment by cesium chloride density gradient centrifugation.

3.2.1.1.3 Virus enrichment by cesium chloride density gradient centrifugation

Virus enrichment was performed by a modified protocol from Tollefsen et al. using a cesium chloride (CsCl) density gradient.[157]

CsCl density gradients were prepared in ultracentrifugation tubes by carefully sublayering 3 ml of the heavy CsCl-solution (1.4 g/ml) under 3 ml of light CsCl-solution (1.3 g/ml). 4 ml of virus solution was layered on top filling the tubes to the edge. The first centrifugation step was performed for 2-4 hours (h) at 220000 g and 4°C in an ultracentrifuge (rotor SW41 Ti). As the virus has a density of about 1.33 g/ml, it appeared as a whitish-bluish band slightly above the border between the two CsCl-solutions (Fig. 7). Another lighter band was visible slightly above the proper virus, which most likely contained empty virus capsid. The correct virus band was punctured with a 16 G needle and 2 ml syringe and layered on top of another CsCl density gradient for further enrichment. The second gradient was run over night (ON). The final amount of concentrated virus (about 1-2 ml) was complemented with 25 µl 40% sucrose-solution in PBS and dialyzed in 10000 dalton molecular weight cut off dialyzation cassettes against PBS for two times for 4 h and one time ON. Finally, 10% glycerol were added to the dialyzed virus solution

and aliquoted à 100-200 µl for subsequent experiments or à 20 µl for titer determination and stored at -80°C.

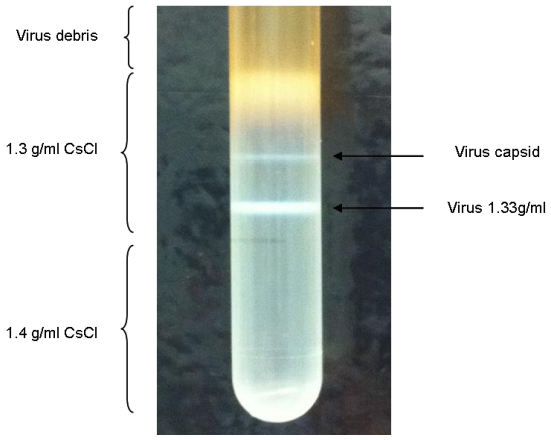

Figure 7: CsCl density gradient after first centrifugation step
After the first centrifugation for 2-4 h, the virus is concentrated between the heavy and light CsCl solution and manifests as whitish/ bluish band. Above the proper virus is another band, which consists only of virus capsid and has a lower density. For preparation of the second gradient, the virus was removed by punctuation with a 16 G needle.

3.2.1.1.4 Titer determination

Titer determination was performed with the end point dilution assay in Hek293A cells. Hek293A cells were seeded at a density of 20000 cells/well in 96 well plates and grown ON. The next day, sequential virus dilutions were performed, from $1 \cdot 10^{-2}$ to $1 \cdot 10^{-12}$ in 8 replicates for each concentration. After 24 h, GFP expression was inspected by eye and wells were scored positive if one cell/well was green. The viral titer was calculated by the following deviation according to the Spearman-Kärber formula:

Titer (pfu/ml)= $10^{(1+Z(X-0.5)}$
Z= log 10 of starting dilution (for 1:100 Z=2)
X= the sum of the fraction of positive wells (number of positive wells/number of total wells for each dilution)

Typical virus yields were between $1 \cdot 10^{11}$-$2 \cdot 10^{12}$ pfu/ml. Virus enrichment after ultracentrifugation was about 100-fold compared to before.
Exact virus titration was performed in neonatal rat cardiomyocytes. For this purpose, virus stocks were thawed on ice, diluted according to the virus concentration with virus buffer and shock frozen in liquid nitrogen in 20 µl working aliquots. Different multiplicities of infections (MOIs) (1-50) of new virus were added to neonatal rat cardiomyocyte cultures, incubated ON and subjected to western blot analysis for S100A1 overexpression. MOIs yielding desired S100A1 overexpression was 4-8-fold compared to control and were chosen for subsequent experiments. GFP expression was always adapted so that both viruses had matching GFP expression.

3.2.1.2 Isolation and cultivation of neonatal rat cardiomyocytes

Neonatal rat cardiomyocytes (NCM) were isolated by gradual trypsin digestion.

One to three day old neonatal Wistar rat pubs (normally 28-36) were decapitated and the chest opened with a medial incision. The heart was removed and transferred to a 25 cm culture dish with ice-cold HBSS containing 2% P/S. Next, the adjacent tissue, remaining atria and vessels were removed and the heart pieces transferred to a small 6 cm culture dish. Hearts were minced using a tissue chopper (medium blade force and speed, pieces size 8.00 mm, one time longitudinal, one time transverse chopping). 5 ml digestion solution was added, heart pieces transferred to a 50 ml reaction tube and washed twice with digestion solution. To remove the supernatant, heart pieces were allowed to sediment by gravity for some seconds and the supernatant removed. Next, 10 ml digestion solution was added and incubated under constant shaking for 10 min at room temperature (RT). 10 ml stop solution was added and tissue mechanically homogenized using a 25 ml serological pipette for 30 times. The tissue was allowed to sediment and the supernatant, containing heart cells, transferred to 2.5 ml pre-cooled FCS and stored on ice. These digestion steps were repeated 9 times. At the end, almost all tissue pieces were digested. Cells were centrifuged for 15 min at 60 g at 4°C and pellets carefully resuspended in 50 ml 10% FCS M199. 2 ml DNAse solution was added to inhibit cell clotting and the cell solution was filtered through a cell strainer (100 µm pore size) to remove residual tissue pieces. For the generation of EHT, cells were counted and the desired cell number doffed of. For the cultivation of neonatal cardiomyocytes, the cell suspension was transferred to a 25 cm dish and pre-plated to deplete for cardiac fibroblasts for 90 min at 37°C. As fibroblast attach faster to tissue culture surfaces, the cardiomyocyte fraction was enriched by this procedure from approx. 45% to 70%.[126] Afterwards, the culture dish was carefully hit on the bench to detach slightly adherent cardiomyocytes, the supernatant transferred to a 50 ml tube and carefully homogenized with a 25 ml serological pipette. Cells were counted using a Neubauer counting chamber and plated with a density of $2 \cdot 10^6$ cells/well in 6 well plates. The next day, cells were washed once with PBS and new medium was added. On the second day, medium was changed to 0.5% FCS M199. Experiments were normally started on day 3 or 4.

3.2.1.3 Cultivation of neonatal rat cardiac fibroblasts

Neonatal rat cardiac fibroblasts (NCF) attach faster to plastic surfaces than cardiomyocytes. After pre-plating of NCM, the culture dish was filled with 10% FCS DMEM medium and cells were allowed to attach ON. The next day, cells were washed twice with PBS and medium changed. When cells had reached 90% confluence (after 3 days) they were subcultured in the ratio 1:3 as described above. As this passage still contained cardiomyocytes, cell were passaged one or two more times for pure NCF cultures. For experiments, cells in passage 2 or 3 were used in 6 well plates by splitting one T175 culture dish in four 6 well plates.

3.2.1.4 Generation and cultivation of Engineered Heart Tissue (EHT)

3.2.1.4.1 Generation of EHT

EHT is a 3-dimensional cell culture model, that outmatches conventional 2-dimensional cell culture, as neonatal rat cells (whole heart isolates) are cultivated in a collagen matrix under cyclic stretch (referred to as loaded conditions), which, after almost two weeks of maturation, resembles adult myocardium and forms a functional syncytium.[151, 152] EHT were produced in ring-shaped form, which eases its handling.

EHT was constructed as described previously.[151] After isolation of neonatal rat cells, before the pre-plating step to enrich cardiomyocyte fraction, cells were counted using a Neubauer counting chamber and the desired number of cells ($2.75 \cdot 10^6$ cells/EHT) centrifuged at 60 g for 15 min. The pellet was resuspended in the according volume of cold EHT Medium. For each ring, 0.9 mg rat tail type I collagen were mixed with the same amount of 2x concentrated DMEM medium and neutralized with 0.1 M NaOH until neutral color change (reddish to pinkish). 10% Matrigel and $2.75 \cdot 10^6$ isolated heart cells were added for 1 EHT (final volume 1 ml). 1 ml of this mixture was pipetted into ring-shaped casting molds and allowed to solidify for 1 h in a CO_2 incubator (Fig. 8.1). Afterwards, the medium was carefully added and changed every 2nd day thereafter. After 7 days, hardened EHT (Fig. 8.2) were transferred onto custom-made stretching device to facilitate phasic stretch (from 100 to 110% of length at 2 Hz) (Fig. 8.3). EHT were stimulated with ET-1 (day 8) or transduced with AdGFP or AdS100A1 (day 10) at the indicated time points. EHT were completely matured on day 12 (Fig. 8.4)

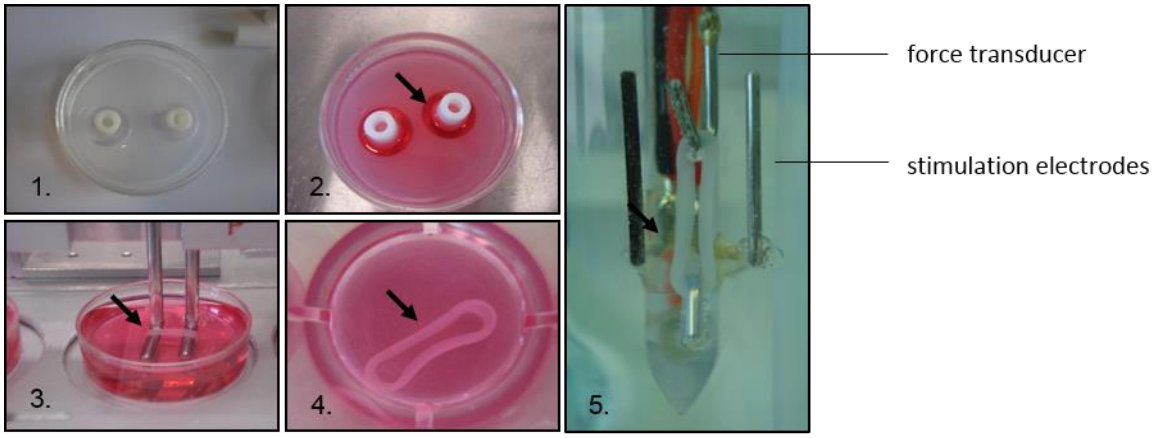

Figure 8: Setup for EHT preparation, culture and analysis of contractile function:
1. Casting mold assembly, 2. EHT condensation around the central cylinder until culture day 7, 3. EHT after transfer onto a stretching apparatus (10% unidirectional and cyclic stretch at 2 Hz), 4. Mature EHT at day 12, 5. EHT in a thermostated organ bath for isometric force measurement under pulsefield stimulation (37°C, 2Hz, 5ms, 100 mA). Arrow point towards ring shaped EHT.

3.2.1.4.2 Functional analyses of EHT

On day 12, isometric contraction experiments were performed: EHT were subjected to fluorescent microscopy to monitor GFP expression, if transduced with adenovirus, before being transferred to an

organ bath equipment. EHT were hung between hook and force transducer (Fig. 8.5) and were allowed to equilibrate for 30 min without pacing in tyrode solution (0.2 mM Ca^{2+}). Then, EHT were electrically stimulated with rectangular pulses (2 Hz, 5 ms, 100-120 mA) for another 30 min at 1 mM Ca^{2+}. Length of EHT was adjusted to maximal force generation, which most likely resembles optimal sarcomere length. Tyrode solution was changes twice and contractility was recorded with LabChart software for cumulative Ca^{2+} concentrations (0.2 mM-1.6 mM) with a recording period of approx. 150 sec/step (Fig. 9).

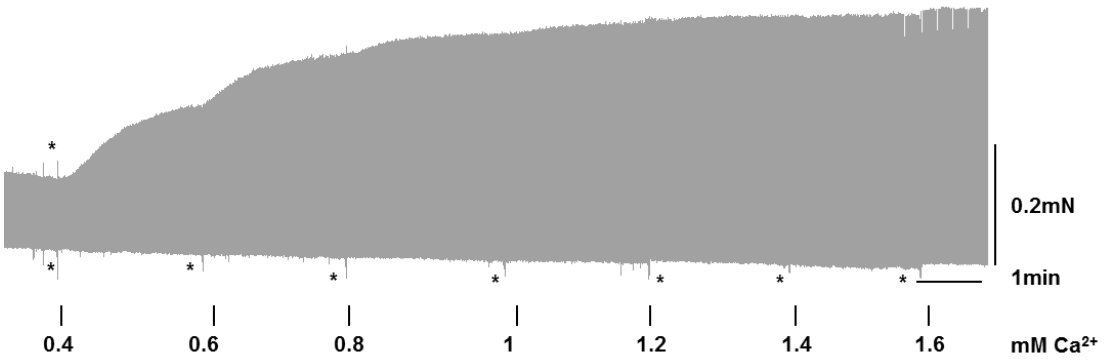

Figure 9: Original force recording of Ca^{2+} stimulated EHT
Ca^{2+} in the tyrode solution was increased stepwise and contractility recorded with LabChart. Addition of Ca^{2+} increased twitch tension to its maximum at 1.6 mM Ca^{2+}. Asterisks indicate artifacts from the force transducer when Ca^{2+} was added manually.

Contractile performance was analyzed in offline mode with a semiautomatic custom designed plugin. Figure 10 displays a representative twitch: Twitch tension (TT) was calculated as amplitude between TT_{max}-TT_{min}. Time to peak (TTP) was calculated as start of twitch until TT_{max}. Tau, the relaxation constant was integrated from the relaxation velocity.

After functional recordings, EHTs were shock-frozen in liquid nitrogen and stored at -20°C until further processing.

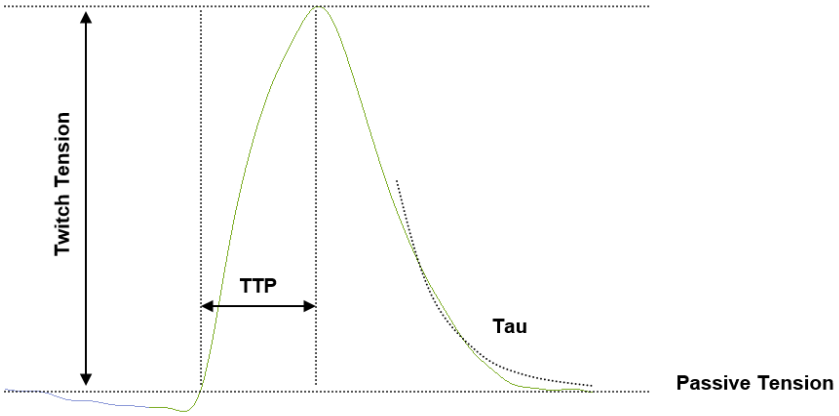

Figure 10: Schema of twitch measurement and functional parameters deduced from it
Twitch tension (TT), Time to peak (TTP) and tau were analyzed using Labchart software and a semiautomatic plugin.

3.2.1.4.3 Arrhythmia-Assay

For the arrhythmia assay, EHT was equilibrated as described above. Ca^{2+} in the tyrode solution was adjusted to 0.2 mM and stepwise increased up to 4 mM with a recording period of approx. 150 sec/step. For quantifications of after-contractions, the number of after-contractions was counted manually for each Ca^{2+} concentration and the recorded time. The incidence of after-contractions was calculated as ratio number of after-contractions to total number contractions. For quality control, at 0.2 and 0.4mM Ca^{2+}, EHT should not display any after-contractions and at 4 mM Ca^{2+}, all EHT should display 100% after-contractions. By applying this method, 10% of EHT were discarded from the analysis. For combined Ca^{2+}/ β-AR stimulation, after adjustment in 0.2 mM Ca^{2+}, 1 µM Iso was added before incrementally increasing Ca^{2+} to 2 mM. Again, EHT that displayed after-contractions at 0.2 mM Ca^{2+} or 1 µM Iso were excluded from the analysis.

For the experiments with ryanodine or Flecainide, EHT was adjusted to 1.6 mM Ca^{2+} (EC50 for control EHT) for 10 min. 50 nM ryanodine/ 3 µM Flecainide were added to the tyrode solutions and after-contractions analyzed for further 10 min as described before.

3.2.1.5 Isolation of adult rat cardiomyocytes

Isolation of adult rat cardiomyocytes (ACM) was performed according to a protocol from Piper.[158] Male wistar rats were anesthetized with 1 ml thiopental until expiration of adverse-effect reflexes. The thorax was opened with a median incision and 10 U heparin injected into the vena cava inferior to prevent blood clotting. Afterwards, the heart was dissected and placed into pre-cooled 0.9% NaCl solution. The aorta was probed on a 1.5 mm wash point penetrometer and placed into a Langendorf equipment. Ca^{2+} free ACM-EDTA medium was infused retrograde in an open circle with a flow rate of 12 ml/min to wash out residual free Ca^{2+}. After 5 min, circular flow was established and 2 mg/ml collagenase added in ACM medium. After approx. 30 min the digestion was stopped, the heart transferred to a 6 cm dish and minced using a tissue chopper (medium blade force and speed, size 7.17 mm, twice along both axes). The heart pieces were resuspended in ACM-EDTA medium and passed through a cell strainer (pore size 200 µm). The obtained cell suspension was subjected to several Ca^{2+} toleration steps, where Ca^{2+} in the ACM medium was increased stepwise (0 mM, 0.05 mM, 0.1 mM, 0.2 mM, 1 mM, 2.5 mM final). Cells were allowed to sediment for 10 min at each step, the supernatant removed and new medium with higher Ca^{2+} concentration was added. After the last step, cells were resuspended in modified-M199. Laminin was added in a final concentration of 1:100 and cells were plated in 6 well plates for immunoprecipitation (IP) and western blot analysis or in 8 well chamber slides for immunofluorescence/ PLA assay. After 1 h incubation, medium was changed and viral transduction was performed as indicated.

3.2.2 Biochemical methods

3.2.2.1 Western blot

3.2.2.1.1 Isolation of proteins

For preparation of cell homogenates, frozen EHT were transferred to a reaction tube containing 150 µl SDS-lysis buffer or 200 µl Ca^{2+}-NP40 buffer and 4 ceramic balls. They were homogenized using a tissue lyser (1 min, 5500 rpm) and the debris was removed by centrifugation for 10 min at 13000 g. The supernatant was transferred to a new reaction tube and stored at 4°C until used for SDS-page or stored at -20°C until used for IP.

ACM and NCM were harvested by pooling two 6 wells in 80-100 µl of the same SDS-lysis buffer/ Ca^{2+}-NP40 buffer using a cell scraper and homogenized by passing through a 32 G needle with a syringe 5-10 times. Homogenates were centrifuged at 13000 g for 10 min, the supernatant transferred to a new reaction tube and stored at 4°C or -20°C until used for SDS-page or IP. As previous experiments indicated that protein concentrations did not vary between different stimulations and experiments, there was no routine measurement of protein concentration but samples were rather loaded by volume.

3.2.2.1.2 Sodium dodecyl sulfate polyacrylamide gel electrophoresis (SDS page)

Separation of proteins was performed by SDS page according to the system described by Laemmli with some modifications.[159]

Approx. 130 µg from EHT and 80 µg from ACM/ NCM protein lysates (always 25 µl) were mixed with 5 µl loading dye and boiled for 3 min at 95°C before loading on pre-casted gradient tris-glycine gels (4-20%). Gels were run with anode and cathode buffer for approx. 2 h at 100 V until the tracking dye reached the end of the gel.

3.2.2.1.3 Immunological detection

Prior to immunological detection, proteins from tris-glycine gels were transferred onto PVDF membranes using a custom made tank blot western blot apparatus.[160]

PVDF membranes were activated for 10 sec in 100% methanol and placed into transfer buffer for 2 min. The gel was also pre-soaked in transfer buffer for 2 min. The gel and membrane were mounted between presoaked filter paper and proteins transferred for 2 h at 50 V onto the membrane. Transfer efficiency was controlled by complete marker transfer. Afterwards, the membrane was washed 3 times with TBS to remove residual methanol. Unspecific binding sites were blocked for 1 h at RT with I-block solution on a shaker. For immunological detection, membranes were probed with the appropriate set of primary antibodies in I-block solution according to table 3.2.5 ON at 4°C under constant shaking. After 3 short washing steps with TBS-Tween, the fluorescent-labelled secondary antibody were incubated for 1 h at RT in the dark on a shaker. After 3 further washing step with TBS-Tween, the membrane was washed 3 additional time in TBS to remove the tween before scanning. Proteins were visualized with a LI-COR

infrared imager directly afterward and quantitative densiometric analysis was performed. Signals were normalized to GAPDH densiometric levels or others as indicated.

3.2.2.2 Immunoprecipitation (IP)

IPs were performed to enrich RyR2 proteins from ACM and EHT, as this protein shows too low abundance for straight western blotting.

All steps were carried out on ice. EHT and ACM protein lysates were prepared as described above. As protein material from one EHT was too little, two EHT were pooled for one IP. Protein suspension was filled up to 500 µl to guarantee optimal stirring during rotation. After incubation of protein homogenates for 30 min on ice and centrifugation for 15 min at 13000 g, 25 µl protein A/G-Agarose was added and rotated for 2-4 h. Lysates were centrifuged again at 2000 g for 5 min to remove protein non-specifically bound to agarose beads. The supernatants were then mixed with 4 µl precipitating RyR2 antibodies and rotated ON at 4°C. Again, 25 µl protein A/G-Agarose was added, samples rotated for additional 6 h and centrifuged at 3000 g for 5 min. Pellets were washed three times with Ca^{2+} buffer and 20 µl loading dye without bromophenolblue was added. Samples were boiled at 95°C for 3 min, centrifuged at 2000 g for 5 min at RT and the supernatant was subjected to SDS page as described above.

3.2.3 Cell biological methods

3.2.3.1 Immunofluorescence Staining

Immunfluorescence stainings (IF) were performed to visualize protein localization in NCM, ACM and EHT. Control EHT was embedded in mounting medium, frozen in liquid nitrogen and stored at -80°C until further analysis. 10 µm thick sections along the longitudinal axis were cut on a cryotom and transferred to Superfrost slides. Slides were shortly rinsed with ice-cold PBS and fixed with PFA for 15 min.

NCM and ACM were grown on cover slips or 6 well chamber slides. Before PFA fixation for 15 min, they were washed with ice cooled PBS.

After washing 3 times with PBS for 5 min, all cells were permeabilized with 0.5% Triton in PBS for 5 min. After another washing step, unspecific binding was blocked with I-block for 1 h. Primary antibodies were diluted in I-block according to table 3.2.5 and incubated ON at 4°C. The next day, cells were washed with PBS 3 times for 5 min before adding secondary antibody (in I-block) for 1-2 h at RT. After a final washing step, cells were mounted with Vectashield and allow to dry ON at RT before long time storage at 4°C in the dark. Negative controls were produced in the same manner without using primary antibodies.

3.2.3.2 Proximity Ligation Assay (PLA)

The proximity ligation assay detects protein interaction *in situ*, when the distance between two proteins is 40 nm or less. Primary antibodies raised in different species are used to recognize the target antigen. Species-specific PLA probes, which have a unique short DNA strand attached to it, bind to primary antibodies. If PLA probes are in close proximity (<40 nm), ligation of the oligonucleotides is possible. Rolling circle amplification enables a several-hundredfold replication of the DNA circle, which encodes a fluorescent signal. This becomes visible as a distinct bright dot under a fluorescence microscope.[161] ACM were grown on 6 well chamber slides and transduced with AdGFP or AdS100A1. Stimulation with isoproterenol (Iso, $1 \cdot 10^{-7}$ M) was performed for 10 min and cells were treated as described under 3.3.3.1 until blocking. Primary antibodies (see table 3.2.5) were diluted in antibody diluent and incubated ON at 4°C. Cells were washed with wash buffer A three times and then incubated for 1 h at 37°C with the corresponding PLA probes (PLUS and MINUS probes depending on primary antibody) diluted in blocking buffer 1:5. For detection, cells were again washed three times with wash buffer A and ligase mixture (1:40 in Ligation stock) was added and incubated on each sample for 30 min at 37°C. After another washing step, polymerase solution (1:80 in amplification buffer) was added following an incubation period of 100 min at 37°C. Final washing was performed with wash buffer B before mounting using Vectashield. Negatives controls were obtained by omitting primary antibodies. Slides were allowed to dry at RT ON before long time storage at 4°C in the dark.

3.2.3.3 TUNEL staining

For apoptosis staining, the TdT-mediated dUTP-biotin nick end labeling (TUNEL) assay was performed according to the user manual. For the staining procedure, EHT slides were fixed with PFA for 20 min at RT. After a washing step with PBS, slides were permeabilized with 0.2% Triton-X in PBS for 2 min before another washing step with PBS was performed. 50 µl of enzyme solution were mixed with 450 µl of label solution and incubated for 60 min at 37°C in a humidified chamber. For negative controls, label solution without enzyme solution was used. After another washing step with PBS, slides were mounted using Vectashield and allowed to dry ON at RT. For long time storage, slides were stored at 4°C. For quantification of TUNEL positive cells, at least four pictures from two slides were taken for each replicate with 3 replicates for each condition.

3.2.3.4 Microscopy

Images were taken with a 10 x, 40 x objective or 60 x oil immersion objective with an Olympus IX81 microscope. For quantification, images were subjected to deconvolution using Xcellence rt 1.2 software with the following settings: numerical apparatus 1.35, spherical apparatus 1.5, no neighbor deconvolution, haze removal factor 70%, sub-volume overlap 10, spherical aberration detection off. Images were further processed using Image J.

3.2.4 Molecular biology methods

3.2.4.1 RNA Isolation

Isolation of entire RNA from EHT was performed using phenol-chloroform extraction with trizol reagent. All steps were performed on ice. After functional recordings, EHT was transferred to 1 ml trizol and vortexed for 5 min to dissolve EHTs. 200 µl chloroform was added and briefly mixed. Phase separation was performed by centrifugation for 15 min at 14000 g and 4°C. The aqueous phase (approx. 400 µl), which contained the RNA, was transferred to a new reaction tube. To increase RNA yield, 1.5 µl of polyacryl carrier was added. RNA was precipitated by adding 400 µl ice-cold isopropanol and incubated at -20°C ON before centrifugation for 15 min at 14000 g and 4°C. The pellet was washed twice with ice-cold 70% ethanol and allowed to dry for 15 min at RT. After dissolving in 20 µl DEPC-treated H_2O, RNA concentration was measured using a Nano Drop and stored at -20°C or directly subjected to reverse transcription.

3.2.4.2 Reverse Transcription

cDNA synthesis was performed using iScript cDNA synthesis kit according to the manufactures instructions: 1 µg RNA was mixed with 4 µl RT buffer, 1 µl reverse transcriptase in a total of 20 µl. Reverse transcription was performed at 25°C for 5 min, extended at 42°C for 30 min and inactivated at 85°C for 5 min and stored on ice. The obtained cDNA was diluted 1:100 in DEPC-treated H_2O and stored at -20°C if not used for real-time PCR.

3.2.4.3 Real-time PCR

The real-time PCR reaction was set up mixing 7.5 µl iQ SYBR Green Supermix, 0.5µl 3 µM forward and reversed primer (see table 3.2.4) and 6.5 µl diluted cDNA. 40 cycles were applied in the MyIQ PCR cycler:

First, incubation at 95°C for 3 min, denaturation at 95°C for 10 sec, annealing at 57°C or 63.5°C for 45 sec, elongation at 72°C for 30 sec, final denaturation at 95°C for 1 min and final elongation at 55°C for 1 min. Fluorescence intensity was measured after each elongation step. Melting curves were performed routinely after each run by increasing the temperature stepwise by 0.5°C from 55-90°C. Fluorescence intensity was recorded at the end of each temperature step to ensure that only one product was amplified.

3.2.5 Statistics

All values shown are mean ± SEM unless indicated otherwise. An unpaired two-tailed Student's t-test was performed for statistical comparison of two groups. One-way ANOVA or two-way repeated ANOVA with Bonferroni-post test were performed to compare more than two groups and with two variables, respectively. For all tests, a p value of $p<0.05$ was considered significant.

4. Results

4.1 Engineered Heart Tissue resembles functional syncytium

Engineered Heart Tissue (EHT) has been widely appreciated as a model of functional syncytium, similar to isolated papillary muscle. Over the culture period, cardiomyocytes (CMs) in EHT form a dense network of muscle bundles. Despite made of neonatal CMs, CMs in EHT adopt an adult-like phenotype over time, which manifests itself in high sarcomeric organization, increased numbers of mitochondria and a striated pattern of CMs. Immunofluorescence staining of EHT sections confirmed a longitudinal orientation of CM along the stretching axis in the EHT matrix (Fig. 11A), displaying a striated pattern. S100A1 showed a similar striated pattern. Comparative staining in adult and neonatal rat CMs (ACM and NCM respectively) showed that ACM had a similar degree of structural organization, as S100A1 also displayed a striated pattern (Fig. 11B). In contrary, NCM had less structural organization, as S100A1 did not show the striated pattern (Fig. 11C). Thus, CMs in EHT showed a similar adult-like structural organization than isolated adult CMs.

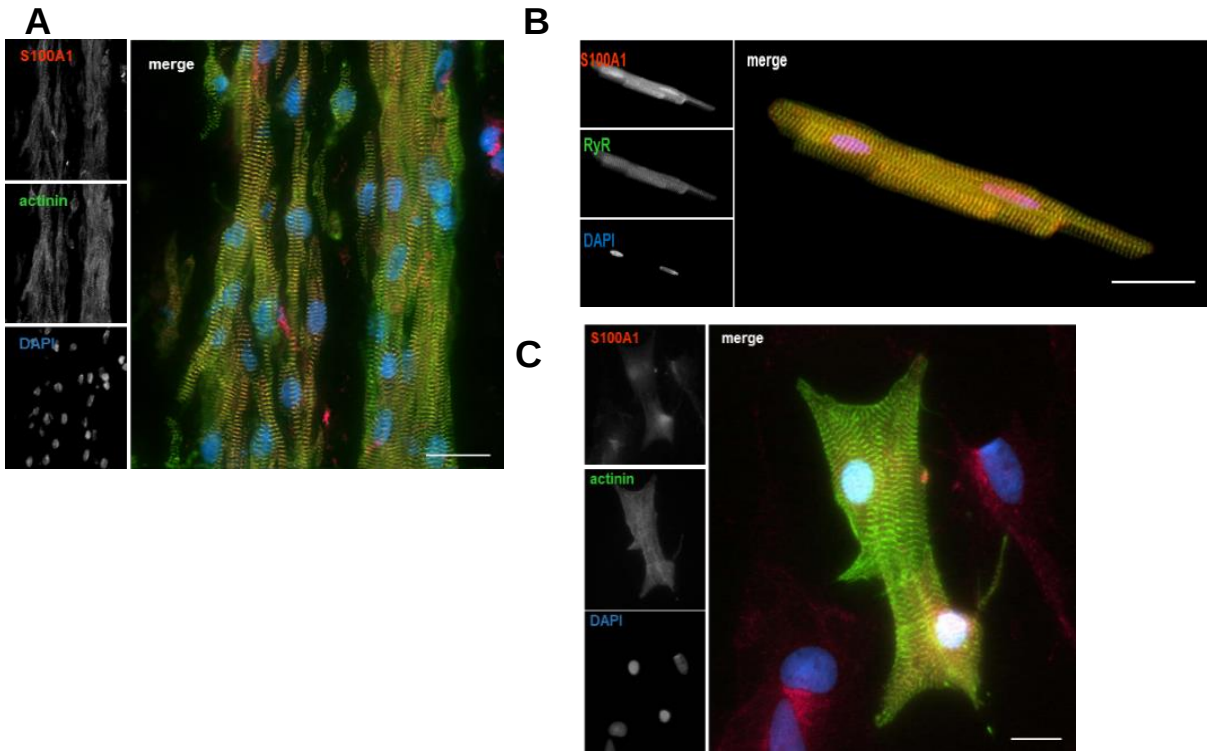

Figure 11: EHT shows an adult-like structural organization
A) Representative immunofluorescent image of cardiomyocytes in EHT. EHT were cryopreserved, cut into 10 µm thick sections and stained for S100A1 (red, upper left). CMs were labeled with α-actinin (green, middle left). CMs formed muscle bundles along the stretching axis and displayed a striated pattern. S100A1 co-localized with α-actinin, indicating an adult-like phenotype. **B)** Representative staining of S100A1 (red, upper left) in ACMs. CMS were labeled with RyR2 (green, middle left). In ACM, S100A1 also displays a striated pattern. **B)** Representative staining of S100A1 (red) in NCM. Cardiomyocytes were counterstained with and α-actinin (green). S100A1 did not show a striated pattern. Scale bare represent 20 µm.

EHT has been used to monitor cardiac contractile function *in vitro*, again showing similar features as isolated papillary muscle. However, EHT is more easily to produce and culture than isolated muscle. Previous studies reported that EHT develop increased force in response to external stimuli as Ca^{2+} and β-AR agonists. Indeed, increasing Ca^{2+} concentrations ([Ca^{2+}]) in the recording solution increased force generation in a concentration dependent manner (Fig. 12A). Here, maximum contractility (0.3 mN) was achieved at 1.6 mM Ca^{2+}, which was also reported by Zimmermann et. al. [151] Similarly, stimulation with β-AR agonist isoproterenol (Iso) also increased twitch tension (TT) (Fig. 12B), while maximum contractility (0.3 mN) was achieved at 1 µM Iso/0.4 mM Ca^{2+}. The half-maximum of the force–calcium curve, expressed as EC50, can be interpreted as the "calcium sensitivity" of muscle cells. When Ca^{2+} sensitivity is decreased, more Ca^{2+} is required to get force to the midpoint and when Ca^{2+} sensitivity is increased, less Ca^{2+} is required to get the force to the midpoint.[162]

After Iso stimulation EC50 was reduced from 0.43 mM Ca^{2+} to 0.24 mM Ca^{2+} in comparison to exclusive Ca^{2+} stimulation (Fig. 12C). Thus, β-AR agonist stimulation sensitized EHT to lower Ca^{2+} levels, despite equal maximum force generation.

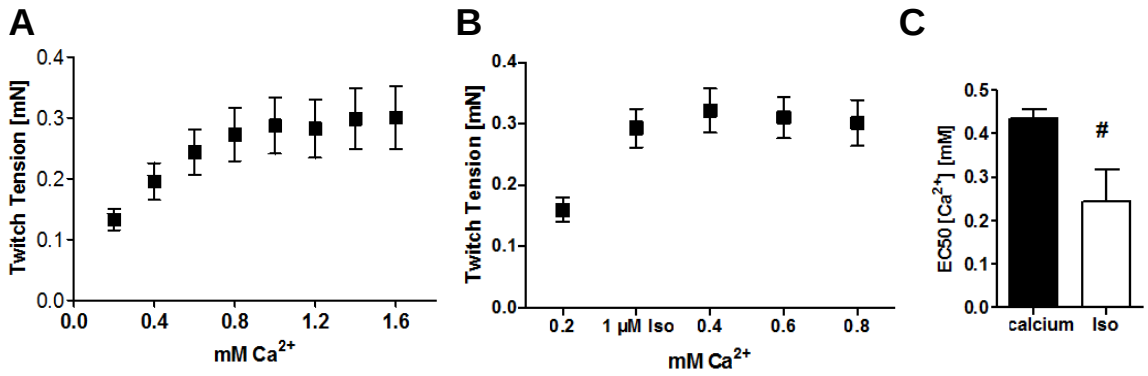

Figure 12: Dose-respond curves of Ca^{2+} and Iso stimulated EHT
A) Ca^{2+} in the tyrode solution was increased stepwise and contractility recorded with LabChart. Addition of Ca^{2+} increased TT to its maximum of 0.3 mN at 1.6 mM Ca^{2+}. n=22 **B)** Similarly, stimulation with Iso also increased TT to its maximum of 0.3 mN at 1 µM Iso/0.4 mM Ca^{2+}. n=3 **C)** Calculated EC50 from A and B. Stimulation with Iso increased Ca^{2+} sensitivity of EHT and reduced EC50. # $p<0.05$ vs. calcium; student's t-test.

Summarizing, EHT could be generated in a reproducible manner and showed similar features as in previous studies. Thus, they can be used a model system in the subsequent work.

4.2 Development of an EHT model with contractile impairment

Until recently, it was not possible to generate EHT from failing CM and test therapeutic interventions in these EHT. However most recently, a similar model of fibrin-based EHT was reported to show contractile impairment and hypertrophic remodeling in respond to afterload enhancement and stimulation with hypertrophic factors as endothelin-1 (ET-1) or phenylephrine (PE).[163] Still, this model was constructed in a different way than in this study. Thus, the first part of this work aimed to

establish a model of hypertrophic or HF-like EHT, which shows most features of failing hearts *in vivo* using pharmacological stimuli.

For this reason, EHT were chronically stimulated with ET-1 to induce hypertrophic remodeling. These first experiments focused on the comprehensive characterization of ET-1 stimulated EHT and its effect on contractile performance and cellular remodeling.

4.2.1 Chronic ET-1 treatment diminishes contractile performance of EHT

EHT were stimulated with $4 \cdot 10^{-8}$ M ET-1 for 96 h. After 48 h, they were transduced with the control virus (AdGFP) for 48 h with continuing ET-1 stimulation. Dose-respond-curves were recorded from 0.2 mM-1.6 mM Ca^{2+} and contractile performance was analyzed.

An increase in Ca^{2+}_{extra} (Ca^{2+} in the tyrode solution) from 0.4 to 1.6 mM resulted in an increase in twitch tension from 0.14 mN to 0.3 mN in control (AdGFP transduced) EHT (Fig. 13A, B). Chronically ET-1 stimulation severely impaired contractility: Basal twitch tension (0.4 mM Ca^{2+}) was strongly diminished to 0.04 mN and Ca^{2+} stimulation (1.6 mM Ca^{2+}) only increased twitch tension to the level of control basal (0.16 mN). This reduced twitch tension manifested in a reduced sensitivity to Ca^{2+}, as EC50 was increased from 0.43 mN to 0.68 mN in ET-1 stimulated EHT.

Time to peak (TTP) was only slightly increased after ET-1 treatment at 0.4 mM Ca^{2+} (from 63.7 ms to 71 ms). However, at 1.6 mM Ca^{2+}, TTP significantly increased from 69.8 ms to 88.6 ms, indicating stronger effects at higher [Ca^{2+}]. Similarly, Tau was only slightly increased after ET-1 treatment (from 0.03 s to 0.032 s). Yet, calcium stimulation did not affect Tau further.

Thus, chronic ET-1 stimulation resulted in a severe systolic contractile impairment, measured as a reduction in TT. Nevertheless, responsiveness to Ca^{2+} stimulation was maintained. Effects on TTP were not very pronounced and only manifested at higher [Ca^{2+}]. Tau, which indicates diastolic function, displayed a tendency towards reduced relaxation.

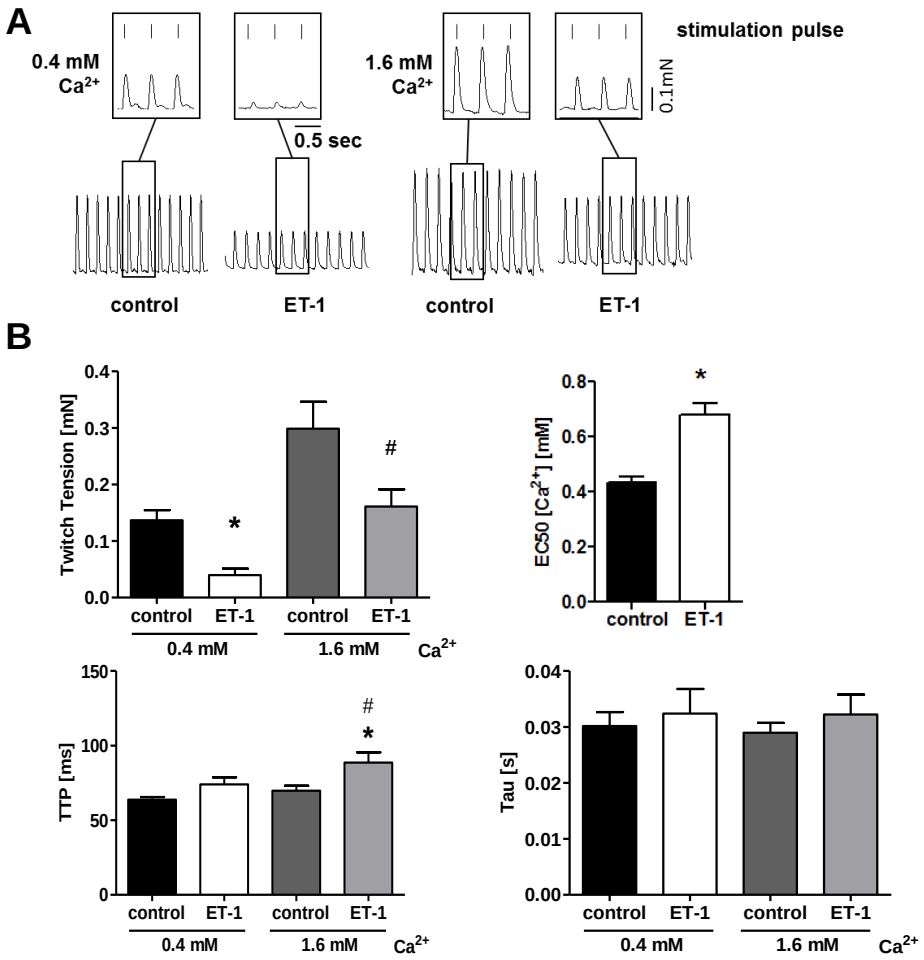

Figure 13: Chronic ET-1 treatment impairs contractility of EHT
A) Representative isometric force twitches from control and ET-1 treated EHT at 0.4 mM Ca^{2+} and 1.6 mM Ca^{2+}. EHT were stimulated with low dose ET-1 ($4 \cdot 10^{-8}$ M) for 96 h and subjected to contractile force analysis afterwards. Cells were stimulated with a biphasic pulse of 5 ms length and 110 mA at 2 Hz. $[Ca^{2+}]_{extra}$ was stepwise increased after a recording time of 150 sec and contractile parameter analyzed. **B)** Corresponding quantification of twitch tension, EC50, Tau and time to peak (TTP) at 0.4 mM and 1.6 mM Ca^{2+}. ET-1 stimulation resulted in an overall impaired contractile performance. n=17 control, n=13 ET-1, from at least 6 isolations; * $p<0.05$ vs. 0.4 mM Ca^{2+}, # $p<0.05$ vs. 1.6 mM Ca^{2+}; 2-way ANOVA/ student's t-test.

4.2.2 Chronic ET-1 treatment induces cellular remodeling

Next, the cellular effects of chronic ET-1 treatment were investigated to confirm HF-like remodeling. Common marker proteins and genes that indicate failing remodeling of CMs were analyzed by western blotting or real-timer PCR. As a common marker of hypertrophy and the activation of fetal gene program, ANP mRNA levels were analyzed by real-time PCR. They increased approx. 2-fold after chronic ET-1 treatment (Fig. 14B). Similarly, S100A1, Serca2 and PLB protein levels as well as RyR2 mRNA levels were also downregulated to approx. 50% of control levels (Fig. 14A, B). These effects are in line with the current understanding of hypertrophic remodeling during the progression towards HF. In conflict to this, NCX mRNA levels were also reduced, which are reported to be increased in chronic HF *in vivo*.[52, 68, 164]

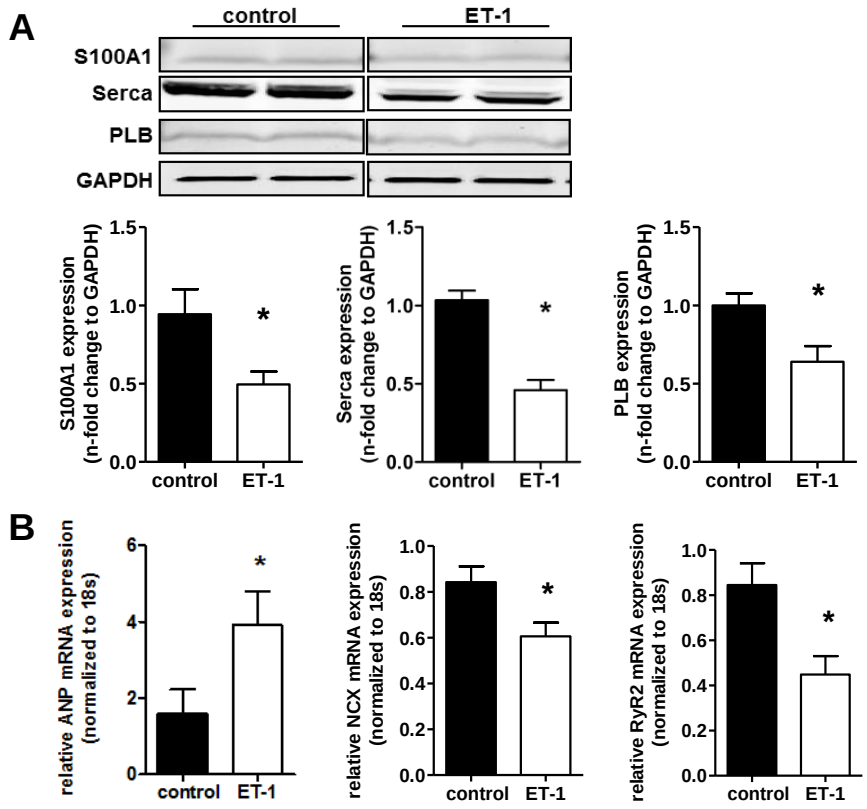

Figure 14: **ET-1 treatment induces marker gene expression reminiscent of HF-like remodeling**
A) Representative immunoblots and statistical analysis for S100A1, Serca2 and PLB protein expression from control and ET-1 treated EHT. After functional recordings, proteins were isolated and subjected to western blot analysis for S100A1, Serca2 and PLB expression, which were all reduced to about 50%. Two duplicates for each condition were depicted and densiometric values were normalized to GAPDH. n=4, from 4 isolations; * $p<0.05$ vs. control; student's t-test. **B)** mRNA analysis for ANP, RyR2 and NCX. mRNA levels were analyzed with real-time PCR and normalized to 18s. ANP levels were increased approx. 2-fold, whereas RyR2 and NCX expression levels were reduced. n=4, from 4 isolations; * $p<0.05$ vs. control; student's t-test.

Furthermore, the effects of chronic ET-1 treatment on typical fibrosis and inflammation markers were analyzed. Both CMs as well as cardiac fibroblast can be activated by ET-1, resulting in a pro-inflammatory and pro-fibrotic remodeling.[165]

In EHT, ET-1 stimulation increased mRNA expression of connective tissue growth factor (CTGF), a general marker of fibroblast activation (Fig. 15). Furthermore, pro-fibrotic markers as smooth muscle actin (SMA) and collagen-1 were increased as well as inflammatory markers as interleukin 6 (IL-6) and intercellular adhesion molecule 1 (ICAM-1). Yet, the increase in collagen-1 and IL-6 expression levels was not significant. Besides, there were no effects on transforming growth factor β (TGF-β) and tumor necrosis factor α (TNF-α) mRNA levels after ET-1 treatment (data not shown). In conclusion, ET-1 treatment induced pro-inflammatory and pro-fibrotic gene activation.

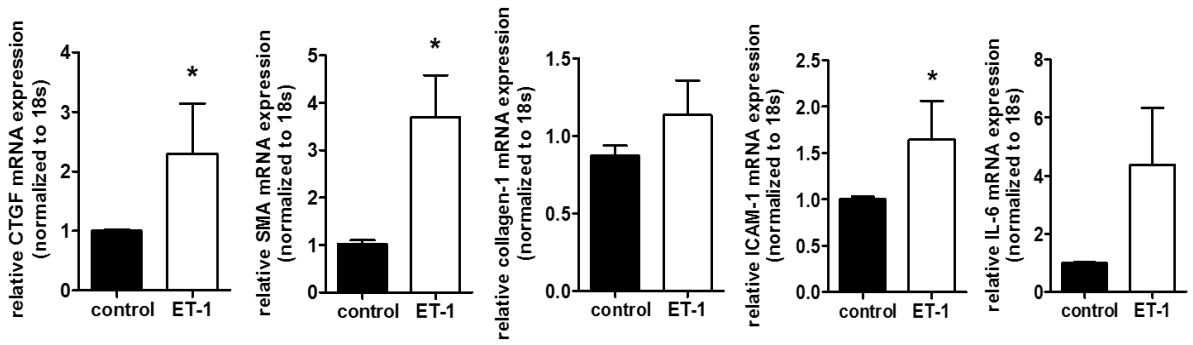

Figure 15: ET-1 treatment induces pro-inflammatory and fibrotic gene activation
EHT were stimulated with ET-1 ($4 \cdot 10^{-8}$ M) for 96 h before subjected to mRNA analysis by real-time PCR for CTGF, SMA, collagen-1, ICAM-1 and Il-6. CTGF, SMA and ICAM-1 expression levels were significantly increased after ET-1 treatment. mRNA expression was normalized to 18s. n=4; * $p<0.05$ vs. control; student's t-test.

4.2.3 Chronic ET-1 treatment might induce necrosis

One explanation for the massive loss of contractility could be substantial cell death by apoptosis, necrosis or other forms of cell deaths. For this reason, comprehensive cell death analyses were performed.

After 96 h of ET-1 treatment, cell culture supernatants were collected and subjected to analyses for high sensitive Troponin T (hsTNT) and lactate dehydrogenase (LDH) by enzyme linked immunosorbent assay (ELISA) in the analysis center of the University Hospital Heidelberg. These are two markers that are used to monitor tissue damage and can indicate necrosis. hsTNT is a standard marker for the diagnosis of myocardial infarction (MI), as it is released from damaged tissue can be measures with high sensitivity at low levels.[166] Similarly, increased LDH levels have been measured in culture supernatants from necrotic CMs.[167] As there was a strong increase in hsTNT levels in cell culture supernatants after ET-1 treatment (544 pg/ml vs.1667 pg/ml) and a slight increase in LDH levels (57 U/l vs. 80 U/l) (Fig. 16), this indicated that ET-1 stimulation induced necrosis in EHT.

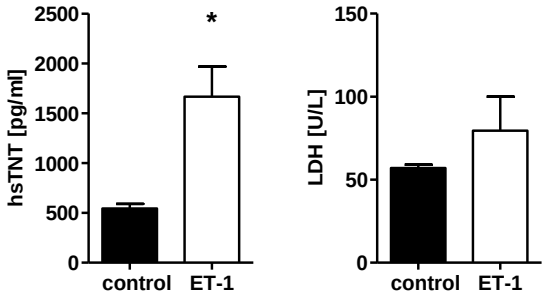

Figure 16: Chronic ET-1 treatment increases hsTNT and LDH levels in culture medium
After stimulation with ET-1 for 96 h, supernatant of cell cultures was collected and analyzed for hsTNT and LDH levels in the analysis center of the University Hospital Heidelberg. hsTNT increased significantly after ET-1 treatment, but LDH levels only slightly. n=2; * $p<0.05$ vs. control; student's t-test.

Next, apoptotic cell death in EHT was determined. Terminal deoxynucleotidyl transferase dUTP nick end labeling (TUNEL) allows to specifically label apoptotic cells in tissue sections or isolated cells.

EHT was cryopreserved after 96 h of ET-1 treatment and cut into sections on the cryotom. After the specific TUNEL staining, cells were counterstained with DAPI to calculate percentage of TUNEL positive cells (Fig. 17A). The overall apoptosis rate of cells in EHT was about 4%, which is in line with previous reports about small numbers of apoptotic cell death in EHT (Fig. 17B).[151, 152] However, there was no increase in TUNEL positive cells after ET-1 stimulation, indicating that ET-1 stimulation did not induce apoptosis.

The same slides allowed calculations about absolute cell numbers per slide to quantify cell numbers in EHT after ET-1 stimulation. Although counting nuclei is only a rough approximation of the overall cell number, this still gives a good estimation if nuclei numbers change essentially during different stimulations. Control slide contained 260 nuclei, whereas after ET-1 treatment there was a slight increase in nuclei (386) (Fig. 17B).

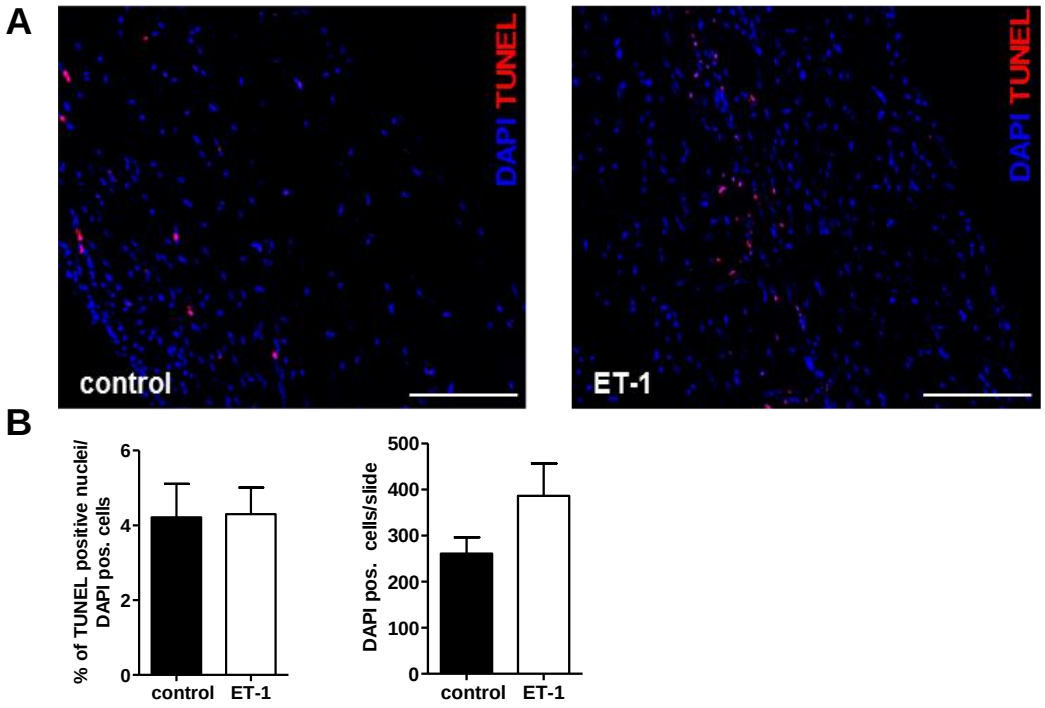

Figure 17: Chronic ET-1 treatment does not induce apoptosis
A) Cryopreserved EHT was cut into 10 µm thick sections and TUNEL staining performed (red signal). Nuclei were counterstained with DAPI (blue). **B)** Quantification of A. About 4% of cells were TUNEL positive in control and ET-1 treated EHT. Nuclei numbers per slide slightly increased after ET-1 treatment. For quantification of TUNEL positive nuclei and nuclei/ slide, at least 3 images were taken from each section. Two sections from different layers were analyzed for each EHT. n=4 different isolations; student's t-test. Scale bar represents 200 µm.

The slight increase in nuclei number can have two major reasons: Either specifically fibroblasts proliferate and CMs die after ET-1 stimulation, or the total cell number does not change and CMs become polynucleated, which has been described after hypertrophy of isolated CMs before.[152, 168] For this reason, protein expression of calsequestrin (CSQ) was analyzed to estimate changes in CM content after ET-1 treatment. CSQ is only expressed in CMs and loss of CMs should lead to a decreased

CSQ expression. However, western blotting confirmed no changes in CSQ protein expression after ET-1 treatment (Fig. 18).

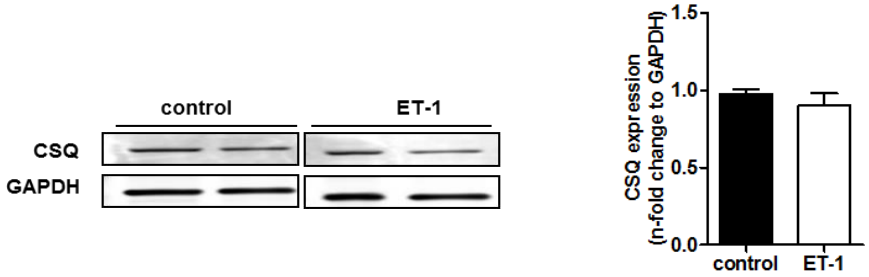

Figure 18: Chronic ET-1 treatment does not reduce CSQ protein expression
Representative immunoblots (left) and statistical analysis (right) for CSQ from control and ET-1 treated EHT. After functional recordings, proteins were isolated and subjected to western blot analysis for CSQ expression. Two duplicates for each condition were depicted and densiometric values were normalized to GAPDH. n=4, from 4 isolations; student's t-test.

In conclusion, these data indicate that necrosis might have occurred after ET-1 stimulation in EHT, similar to the *in vivo* situation after MI. Still, there was no increase in apoptosis and no specific loss of CMs after ET-1 treatment, which could be responsible for the massive loss of contractility.

Since ET-1 treated EHT showed most characteristics of hypertrophic remodeling in addition to a strong contractile impairment, they will be referred to as failing or HF-like EHT form here on.

4.3 Induction of store-overload induced Ca^{2+} release (SOICR) in EHT

The previous paragraph confirmed that EHT can be stimulated with pharmacological substances as ET-1 to induce a HF-like phenotype, which resulted in strong diminished contractile force and hypertrophic remodeling. The next part aimed to establish a protocol where possible arrhythmogenic events can be analyzed in this model under isometric stretch.

4.3.1 Ca^{2+}-Stress and β-AR stimulation induce after-contractions

Cellular Ca^{2+} overload is known to inhibit proper RyR2 closure during diastole, rendering RyR2 "leaky". This SOICR in turn can result in extra-contractions, which might lead to cellular arrhythmias.[26, 37, 58] If this mechanism also acts in part in EHT was tested by stimulating EHT with incremental doses of Ca^{2+}. These exceeded physiological levels (up to 4 mM Ca^{2+}_{extra}) and might potentially induce SOICR, finally leading to pro-arrhythmogenic extra-contractions.

As shown before, an increase in Ca^{2+}_{extra} resulted in an improved contractility as depicted in Fig.1. With increasing Ca^{2+} concentrations, non-stimulated after-contractions occurred first sporadically but then with increasing frequency (Fig. 19). At the same time, force from stimulated twitches started to decline.

By further raising Ca^{2+}_{extra}, all normal contractions were followed by these after-contractions, so that overall twitch tension was strongly diminished. Tracking of individual recordings elucidated that after-contractions originated after stimulated, normal contractions. Therefore, they were called after-contractions.

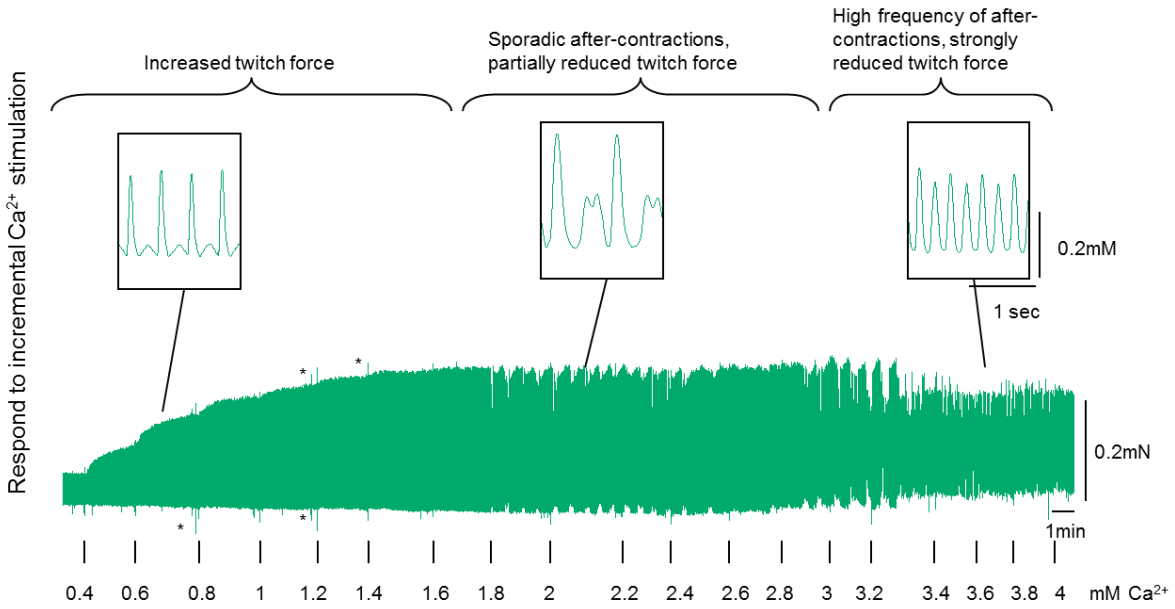

Figure 19: Ca^{2+}-Stress induces after-contractions in a concentration-dependent manner
Representative isometric force twitches of Ca^{2+} stressed EHT. Ca^{2+}_{extra} was stepwise increased from 0.2 mM to 4 mM during functional recordings. An increase in Ca^{2+} first increased twitch tension to its maximum. At higher [Ca^{2+}], non-stimulated extra-contractions occurred first sporadically which reduced amplitude of stimulated twitches. By further increasing Ca^{2+}_{extra}, their frequency increased, until all stimulated contractions were followed by extra-contractions and the overall twitch tension was strongly diminished. Asterisks indicate artifacts from the force transducer when Ca^{2+} was added manually.

To test if these after-contractions originate from RyR2 malfunction, ryanodine was added in low concentrations when after-contractions occurred. Ryanodine specifically binds to the RyR2 and inhibits channel opening without further affecting systolic Ca^{2+} handling.[169] Application of low dose ryanodine (50 nM) was able to profoundly inhibit after-contractions at 1.6 mM Ca^{2+} from 43% to 16%, while overall twitch amplitude was maintained (Fig. 20A, B). Similarly, Flecainide (class Ic anti-arrhythmic agent that blocks diastolic RyR2 opening as well as the Nav1.5 sodium channel) was also able to inhibit after-contractions, however, this effect was not that strong (Fig. 20C).

Thus, Ca^{2+} stimulation was able to induce pro-arrhythmogenic after-contractions that might originate from diastolic RyR2 malfunction.

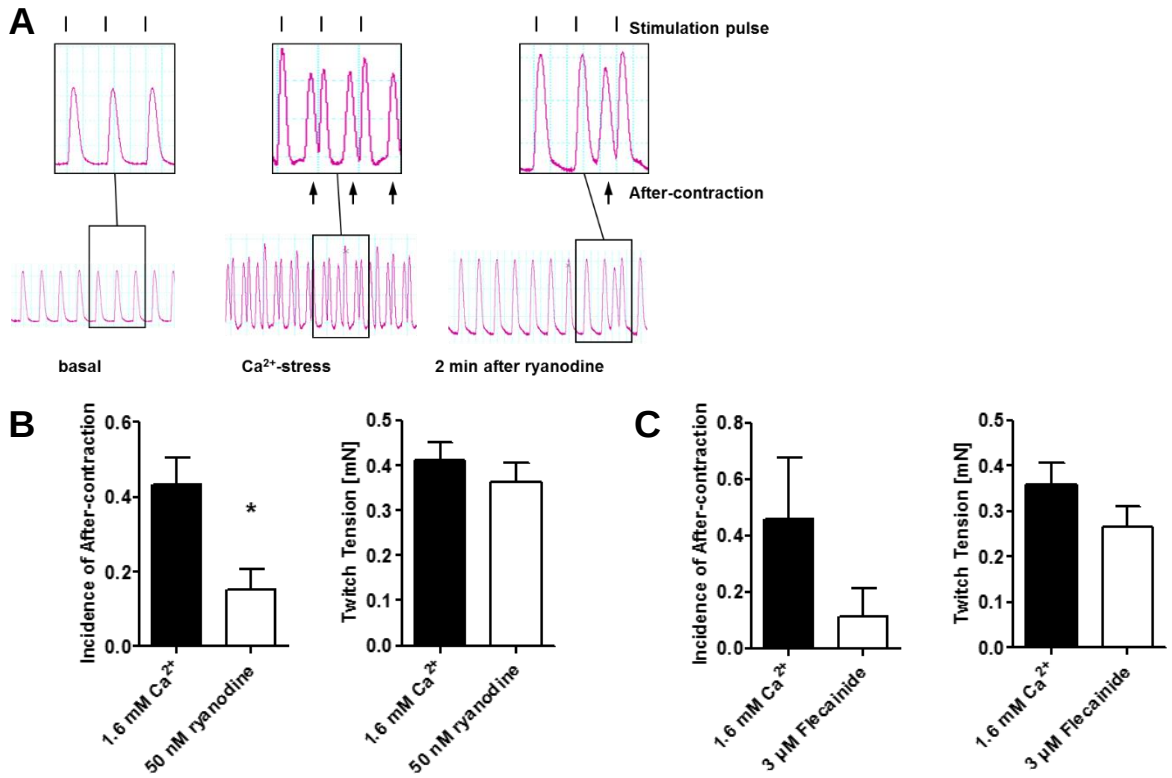

Figure 20: Ca^{2+}-Stress induces after-contractions that can be inhibited by low-dose ryanodine
A) Representative isometric force twitches of Ca^{2+} stressed EHT. Lines above indicate stimulation pulses (110 mA, 5 ms width, 2 Hz), which induce a regular twitch; arrows below indicate non-stimulated after-contraction. Ca^{2+}-stress increased the development of extra-contractions that originate after stimulated contractions (→after-contractions). Administration of low dose ryanodine (50 nM) profoundly inhibited the appearance of after-contractions. **B)** Quantification of after-contractions. Stimulation of 1.6 mM Ca^{2+} increased the incidence of after-contractions to 43%, whereas application of 50 nM ryanodine reduced it to 16%. Overall twitch tension was maintained after the addition of ryanodine. n=15; * $p<0.05$ vs. control; student's t-test. **C)** Quantification of after-contractions after addition of Flecainide. Flecainide was also able to reduce the incidence of after-contractions, whereas twitch tension was maintained. n=5; student's t-test.

Inducing SOICR and after-contraction could also be obtained by combining Ca^{2+} and β-AR-stimulation: EHT were stimulated with 1 µM Isoproterenol (Iso) before incrementally increasing Ca^{2+}_{extra} to 2 mM. This combined stimulated also resulted in a dose-dependent increase of after-contractions (Fig. 21); however they started at much lower Ca^{2+} concentrations, as β-AR-stimulation normally increases SR Ca^{2+} load, thereby lowering the threshold for diastolic Ca^{2+} leakage.[86] Thus, β-AR-stimulation increased the sensitivity for Ca^{2+}-overload-induced after-contractions in EHT.

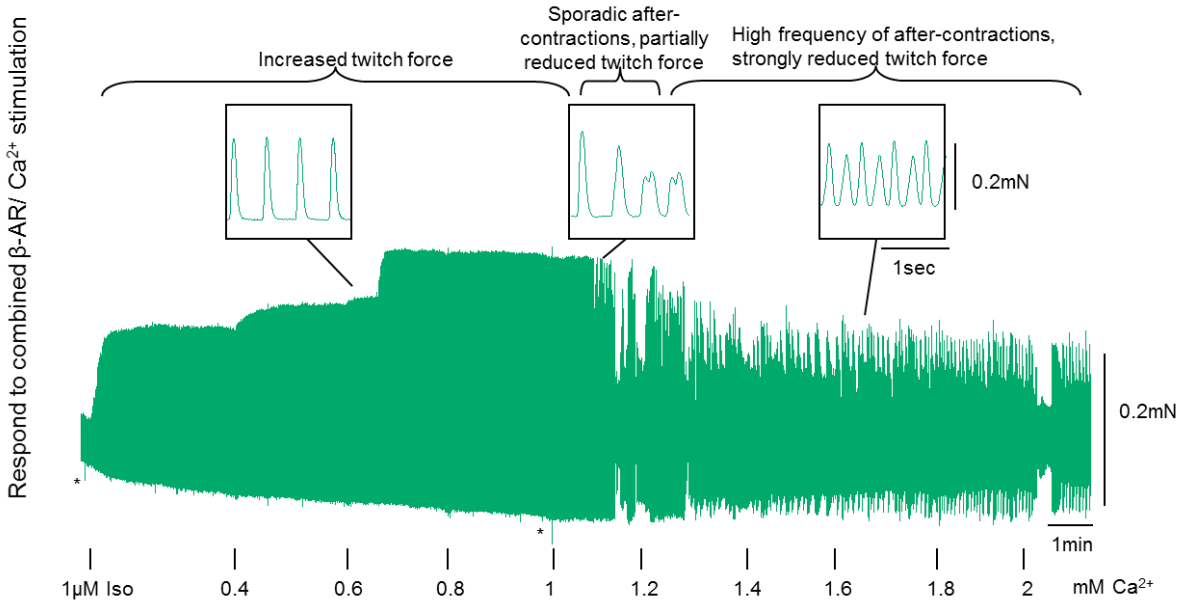

Figure 21: Combined β-AR/ Ca^{2+} stimulation induces after-contractions
Representative isometric force twitches of β-AR/ Ca^{2+} stressed EHT. After addition of 1 µM Iso, Ca^{2+}_{extra} was stepwise increased from 0.2 mM Ca^{2+} to 2 mM during functional recordings. An increase in Ca^{2+}_{extra} first increased twitch tension to its maximum. At higher [Ca^{2+}], non-stimulated extra-contractions occurred, which reduced amplitude of stimulated twitches. With further increasing Ca^{2+}_{extra}, their frequency increased, until all stimulated contractions were followed by extra-contractions and the overall twitch tension was strongly diminished. Asterisks indicate artifacts from the force transducer when Iso/ Ca^{2+} was added manually.

Summing up, EHT can be used to monitor effects of SOICR after Ca^{2+} and β-AR stimulation. After-contractions represent the correlate of diastolic Ca^{2+} leakage that is normally analyzed in isolated cardiomyocytes.

4.4 S100A1-mediated gene transfer in normal and failing EHT

Having established that chronic ET-1 stimulation induced a HF-like phenotype in EHT and that Ca^{2+} and β-AR stimulation induced pro-arrhythmogenic after-contractions, I next aimed to investigate the impact of S100A1 overexpression on contractile performance in normal and HF-like EHT and its impact of Ca^{2+} and β-AR triggered after-contractions.

4.4.1 Adenoviral-mediated S100A1 overexpression increases S100A1 protein levels in EHT

For all experiments, an adenovirus with CMV-promoter driving either expression of GFP (AdGFP, control virus) or a two-promoter virus co-expressing GFP and S100A1 (AdS100A1, S100A1) was used

(see 3.3.1.1.2). GFP expression was monitored directly after viral transduction in living cells to estimate transduction efficiency.

To test in which cell type the adenovirus constructs are preferentially expressed, comparable adenoviral transductions were performed in monolayer cell cultures with AdGFP for 24 h. Although CMV promoter is supposed to drive general protein expression in all cell types, GFP expression was mainly detectable in cardiomyocytes: Applying same multiplicity of infection of (MOI) of 10, pure neonatal rat cardiac fibroblasts (NCF) showed only weak and rare GFP expression (Fig. 22), whereas NCM cultures (mixed population of cardiomyocytes and fibroblasts) showed a more homogeneous GFP expression and a stronger intensity. Thus, cardiomyocytes seem to be the major target of adenoviral expression and it can be assumed that similar expression pattern will be seen in EHT cultures, which consist of equal amounts of cardiomyocytes and cardiac fibroblasts.

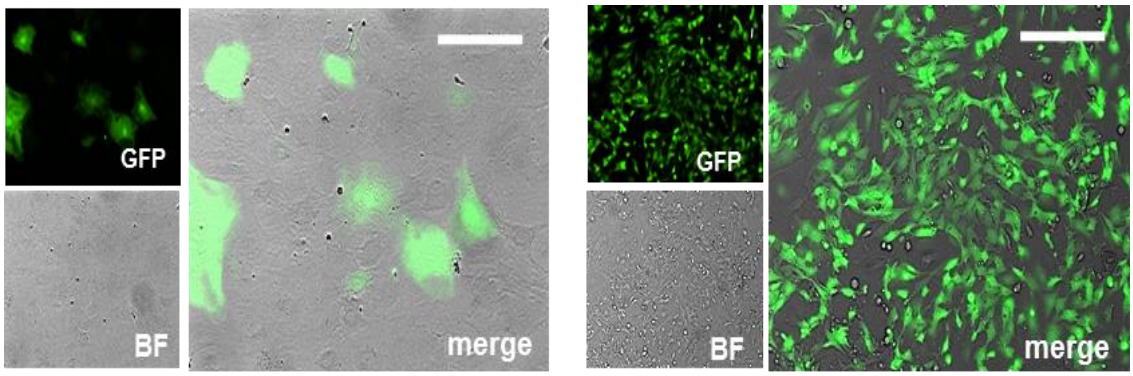

Figure 22: AdGFP is predominantly expressed in cardiomyocytes
Representative fluorescent (upper left) and transmission (lower left) images of NCF (P3, **left**) and NCM (**right**) 24h after adenoviral transduction with AdGFP with MOI 10. Only few NCF showed GFP expression (left, merge), whereas NCM showed almost homogeneous GFP expression (right, merge). Scale bar represents 200 µm.

In EHT cultures, higher MOI needed to be applied in order to establish adequate transduction rates. 48 h after adenoviral transduction with MOI 50, EHT showed a robust and nearly homogeneous GFP expression using both vectors (Fig. 23). Although GFP expression was slightly enhanced at the border regions and a little weaker at the inner center of the rings, all layers were transduced. Transduction with an MOI 50 resulted in an approximately 70-80% transduction efficiency (estimated values from light and fluorescent microscopy). 100% transduction efficiency was not achieved, as GFP expression at the border regions would increase dramatically and harm cells in the outer layers before homogenously transfecting all cells in the inner layer.

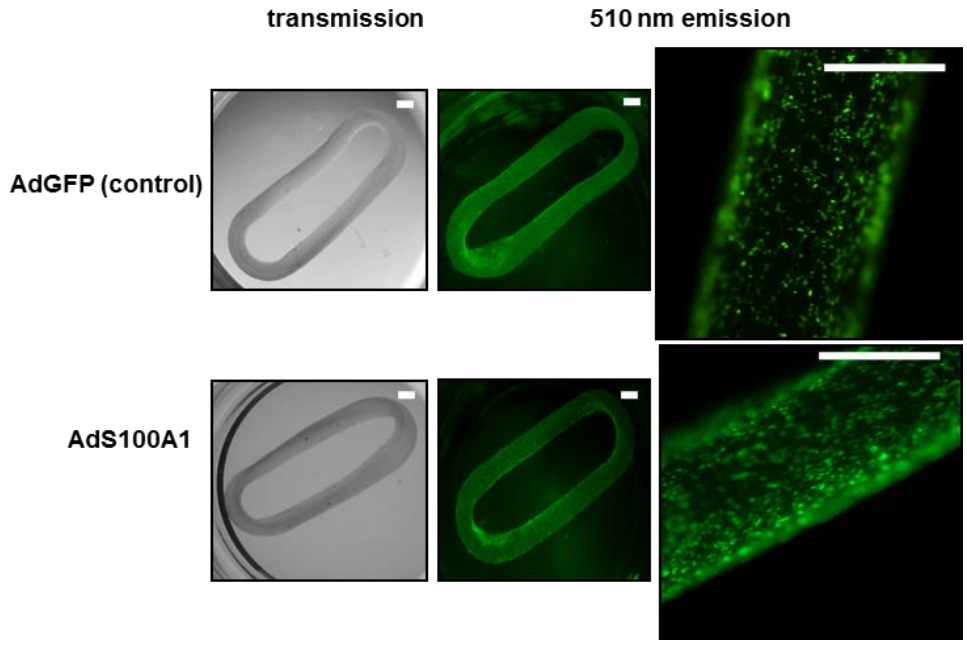

Figure 23: Adenoviral-mediated gene transfer in EHT
Representative transmission (left) and epifluorescent images (middle, right) of control (AdGFP) and S100A1 (AdS100A1) transduced EHT. Images were taken 48 h after adenoviral transduction with a multiplicity of infection of 50 (MOI 50) from living cells. Adenoviral transduction with AdGFP (upper panels) and AdS100A1 (lower panel) showed homogeneous GFP expression through all cell layers and was comparable between both vectors. Scale bar represents 1mm.

In protein lysates, western blotting analysis confirmed an 8-fold increase in S100A1 protein levels in AdS100A1 transduced EHT in comparison to AdGFP transduced control EHT. GFP expression was similar between both groups. In failing EHT, S100A1 overexpression increased 3-fold compared to control (Fig. 24A, B). Again, GFP expression levels did not differ between failing EHT and failing/S100A1 overexpressing EHT while still matching control levels. Real-time PCR based analysis of human S100A1 mRNA levels, which is only expressed after S100A1 overexpression, confirmed equal expression in S100A1 overexpressing and failing/S100A1 overexpressing EHT (Fig. 24C). Thus, viral expression seemed to be equal between control and failing EHT.

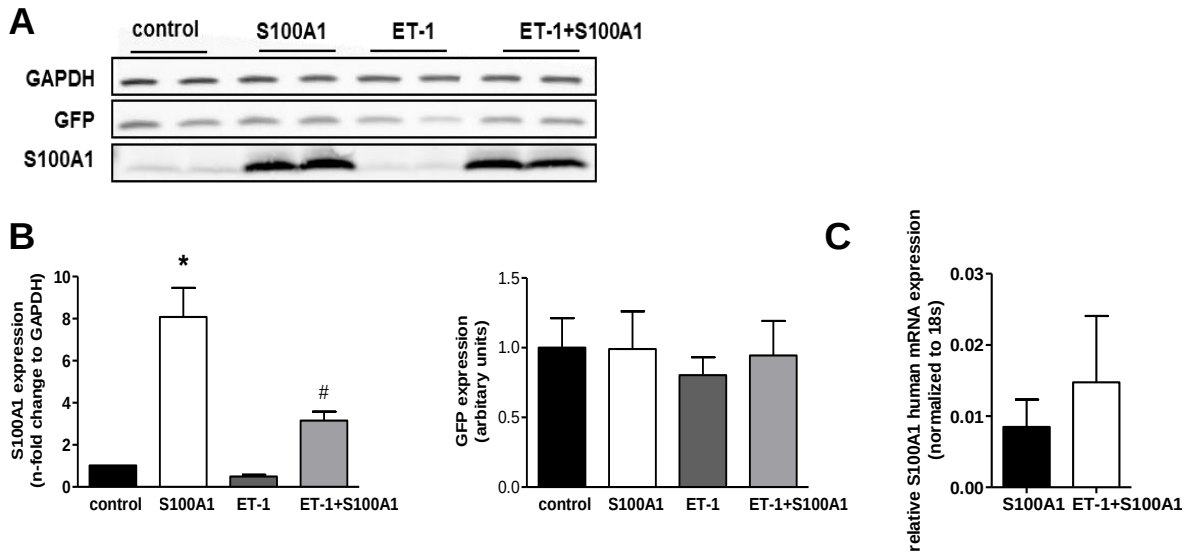

Figure 24: S100A1 overexpression increases S100A1 protein levels in normal and normalizes S100A1 protein expression in HF-like EHT
A) Representative immunoblots for S100A1 and GFP expression from control and ET-1 stimulated EHT after adenoviral transduction. EHT were stimulated with $4 \cdot 10^{-8}$ M ET-1 for 96 h, transduced for 48 h with an MOI 50 with either AdGFP or AdS100A1, protein isolated and subjected to western blot analysis for GFP and S100A1. Two duplicates for each condition were depicted and densiometric values were normalized to GAPDH. **B)** Statistical analysis from A. S100A1 protein expression increased 8-fold after S100A1 overexpression in normal EHT and 3-fold in failing EHT, while GFP expression was matching between all groups. n=10 control, n=5 ET-1, from at least 5 isolations; # $p<0.05$ vs. ET-1, * $p<0.05$ vs. control; 1-way ANOVA. **C)** mRNA analysis for human S100A1. Human S100A1 expression did not differ between S100A1 and ET-1+S100A1. mRNA expression was normalized to 18s. n=4; student's t-test.

4.4.2 S100A1 overexpression increases isometric force generation in EHT

As western blot and real-time PCR analysis confirmed increased S100A1 protein and mRNA levels, the next step was to analyze the functional outcome of these increased S100A1 levels in normal and failing EHT.

Again, EHT were transduced with a MOI 50 with either AdFGP (control) or AdS100A1 (S100A1). For rescue experiments, EHT were stimulated with $4 \cdot 10^{-8}$ M ET-1 for 48 h before adenoviral transduction was performed. EHT were cultured for further 48 h with continuing ET-1 treatment before dose-respond-curves were recorded in the presence of 0.2 mM-1.6 mM Ca^{2+}.
Maximum contractility was again achieved at 1.6 mM Ca^{2+}. S100A1 overexpression resulted in superior contractility at both Ca^{2+} concentrations, increasing twitch tension from 0.27 mN to 0.48 mN (Fig. 25). In the same manner, S100A1 overexpression reduced TTP to 56.6 ms at 0.4 mM Ca^{2+}, however there was only a marginal increase to 58.1 ms at 1.6 mM Ca^{2+}. Additionally, S100A1 overexpression slightly reduced Tau from 0.025 to 0.021 s. However, the effects of S100A1 overexpression on TTP and Tau were only significant at high [Ca^{2+}].
Where TT was strongly impaired in failing EHT, S100A1 overexpression normalized it to 0.11 mN at 0.4 mM Ca^{2+}, which is comparable to the level of control EHT. At 1.6 mM Ca^{2+}, S100A1 overexpression

again normalized TT to 0.35 mN (level of control Ca^{2+} stimulated). Similarly, S100A1 overexpression slightly reduced TTP at 0.4 mM Ca^{2+} to 74 ms and to 78 ms at 1.6 mM Ca^{2+} in failing EHT, however, TTP was still higher than in control EHT. In failing EHT, S100A1 overexpression had no effects on Tau. Ca^{2+} sensitivity, measured as EC50, was slightly increased after S100A1 overexpression (from 0.43 to 0.38 mM Ca^{2+}). Stronger effects were seen in failing EHT, where S100A1 overexpression almost normalized EC50 (0.68 in failing EHT vs. 0.53 mM Ca^{2+} in S100A1/ failing EHT) (Fig. 25C).

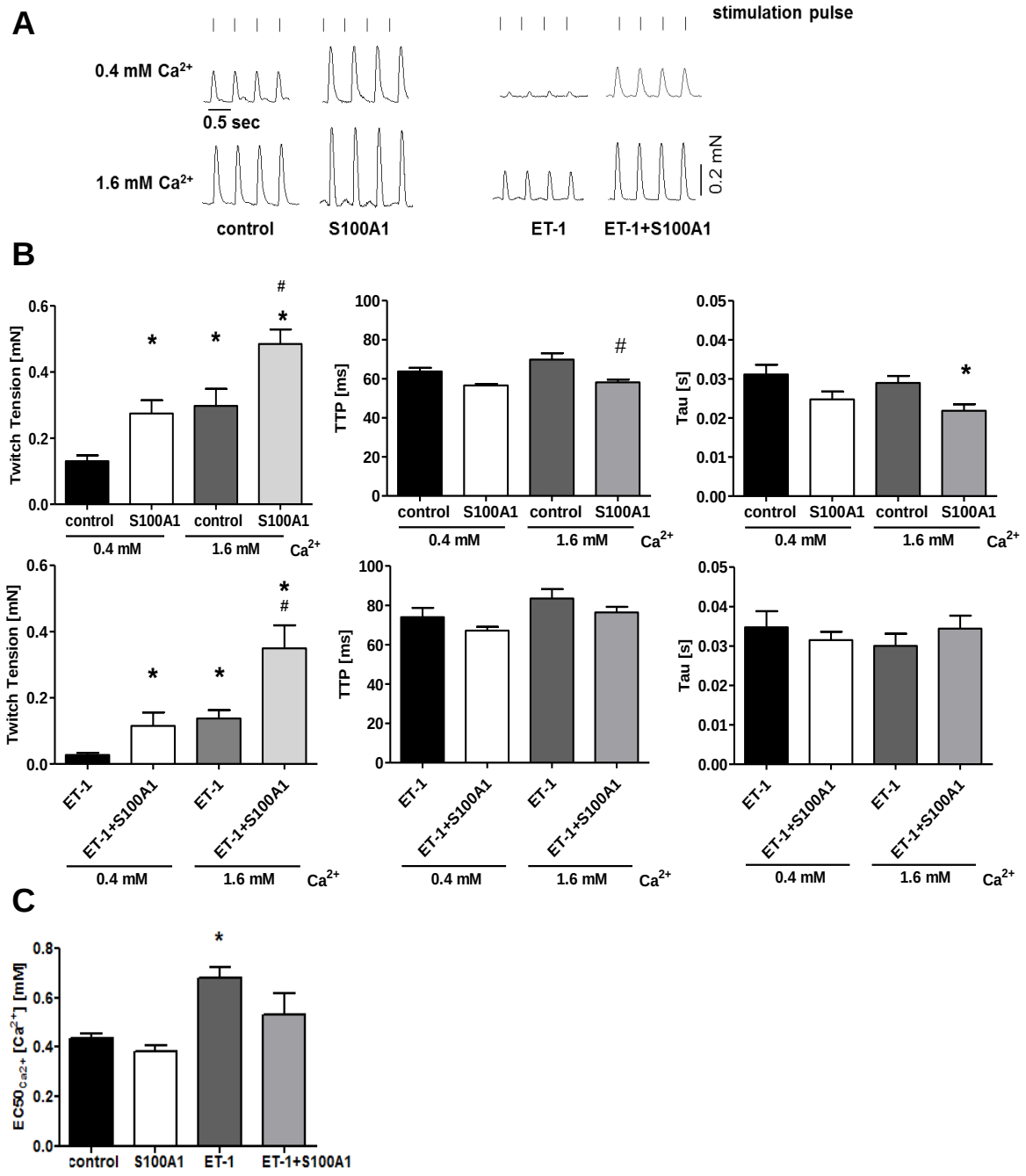

Figure 25: S100A1 overexpression increases isometric force generation in normal and failing EHT
A) Representative isometric force twitches from control and ET-1 treated EHT ($4 \cdot 10^{-8}$ M for 96 h) with S100A1 overexpression at 0.4 mM Ca^{2+} and 1.6 mM Ca^{2+}. EHT were stimulated with a pulse of 5 ms length and 110 mA at 2 Hz. $[Ca^{2+}]_{extra}$ was stepwise increased after a recording time of 150 sec and contractile parameter analyzed. **B)** Corresponding quantification of TT, TTP and Tau from control and failing EHT and with S100A1 overexpression at 0.4 mM Ca^{2+} and 1.6 mM Ca^{2+}. S100A1 overexpression resulted in superior contractile performance. n=17

control, n=13 ET-1 from at least 6 isolations; * p<0.05 vs. 0.4 mM Ca^{2+}, # p<0.05 vs. 1.6 mM Ca^{2+}; 2-way ANOVA. **C)** Corresponding quantification of EC50. n=20 control, n=6 ET-1; * p<0.05 vs. control; 1-way ANOVA.

Summarizing, these data provided evidence that S100A1 overexpression increased systolic contractile performance in normal EHT, independent of its Ca^{2+} load. In failing EHT, S100A1 overexpression was able to normalize TT to the levels of control EHT. Still, S100A1 overexpression had not such a strong impact on other contractile parameters as TTP and Tau.

As the effects of S100A1 overexpression were independent of the Ca^{2+}-load in EHT, functional recordings were repeated with Iso stimulation to test if S100A1's effect are also independent of β-AR activity (Fig. 26). Again, S100A1 overexpression increased TT after Iso stimulation from 0.2 mN to 0.44 mN (vs. 0.16 mN to 0.31 mN in control). Iso stimulation slightly reduced TTP from 60 ms to 58 ms, whereas S100A1 overexpression had no further impact. Similarly, Tau was slightly reduced after S100A1 overexpression (0.25 s vs. 0.28 s in control), however, Iso stimulation had no impact on Tau. Thus, S100A1 effects on contractile performance were also independent of β-AR stimulation.

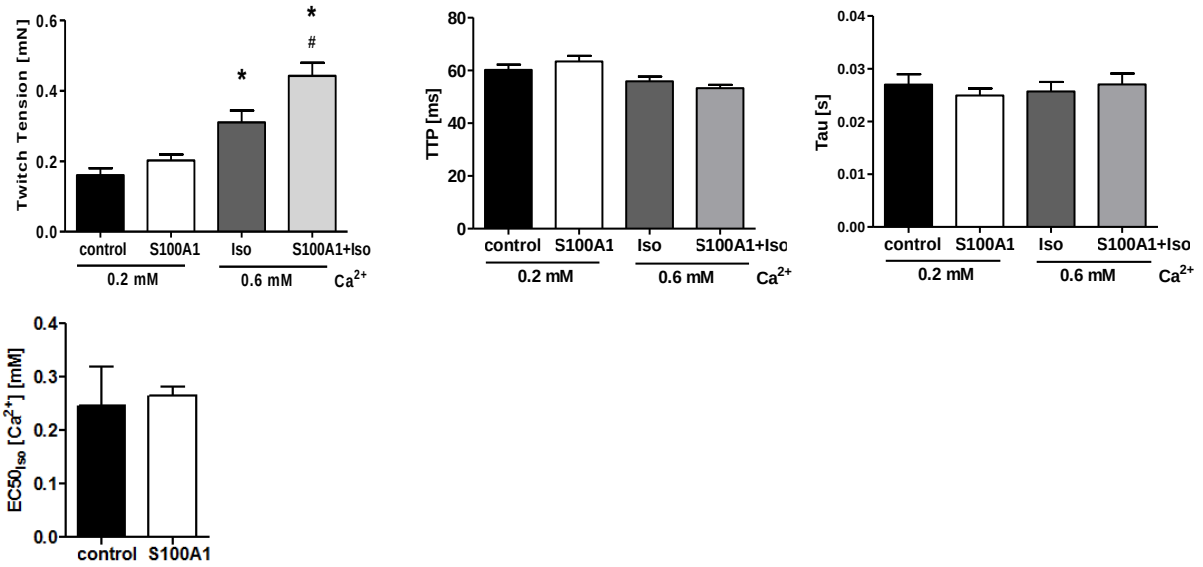

Figure 26: S100A1 overexpression increases isometric force generation after β-AR stimulation
Quantification of TT, TTP and Tau from control and S100A1 overexpressing EHT at 0.2 mM Ca^{2+} and 1 µM Iso/0.6 mM Ca^{2+}. S100A1 overexpression resulted in superior contractile performance. n=20, from at least 6 isolations; * p<0.05 vs. 0.2 mM Ca^{2+}, # p<0.05 vs. 1µM Iso/0.6 mM Ca^{2+}; 2-way ANOVA.

4.4.3 S100A1 overexpression prevents Ca^{2+}-induced after-contractions

As shown in the previous section, S100A1 overexpression increased contractile force in normal and failing EHT. Given that positive inotropic interventions harbor the risk of triggering pro-arrhythmogenic events by increasing SR Ca^{2+} load, the next part focused on the potential arrhythmogenic potential of S100A1 in EHT. Previous work could already show that S100A1 overexpression reduces Ca^{2+} spark frequency and amplitude and protects against β-AR-triggered Ca^{2+} waves in normal and failing isolated adult cardiomyocytes (unpublished data). Still, unloaded cardiomyocytes *in vitro* do not properly

recapitulate the complex situation in intact tissue, where cardiomyocyte-cardiomyocyte and cardiomyocyte-fibroblast interaction can contribute to arrhythmogenesis. Similarly, Ca^{2+} waves must not necessarily translate into real arrhythmogenic contraction. For these reasons, the EHT model was chosen to analyze potential anti-arrhythmic effects in a minimalistic model, where cells are physically coupled and isometric force generation is analyzed.

Normal and failing EHT were transduced with either AdGFP (control) or AdS100A1 (S100A1) and exposed to incremental Ca^{2+} stress (0.2 mM to 4 mM). The occurrence of after-contractions was counted manually and the incidence of after-contractions calculated from the number of total stimulated contractions.

In control EHT, incremental increase in Ca^{2+} resulted in a dose-dependent increase in after-contractions (Fig. 27A). At 1.6 mM Ca^{2+}, 50% of all normal contractions were followed by after-contractions and at 3.2 mM Ca^{2+}, all (100%) contractions were followed by after-contractions (Fig. 27B). In contrast to that, S100A1 overexpression desensitized EHT to Ca^{2+} overload, as only 10% of after-contractions originated at 1.6 mM Ca^{2+}. However, this effect was not present at all Ca^{2+} concentrations, as at 3.2 mM Ca^{2+}, the incidence of after-contractions also reached 100%. Hence, S100A1 overexpression shifted EC50 from 1.6 mM to 2.1 mM Ca^{2+} and reduced the sensitivity to after-contractions.

Similar experiments were performed in failing EHT. In general, failing EHT were much less sensitive to Ca^{2+} stress, which might be a consequence of diminished Serca2, PLB and NXC expression. EC50 in failing EHT was 1.8 mM Ca^{2+}; however, S100A1 overexpression was still able to rescue the phenotype and increased EC50 further to 2.8 mM Ca^{2+} (Fig. 27B).

These experiments in normal EHT were repeated with combined β-AR- and Ca^{2+} stimulation. In general, sensitivity to after-contractions was enhanced after Iso stimulation. However, S100A1 overexpression was still able to protect EHT against triggered after-contractions and shifted EC50 from 0.68 to 0.82 mM Ca^{2+} (Fig. 27C).

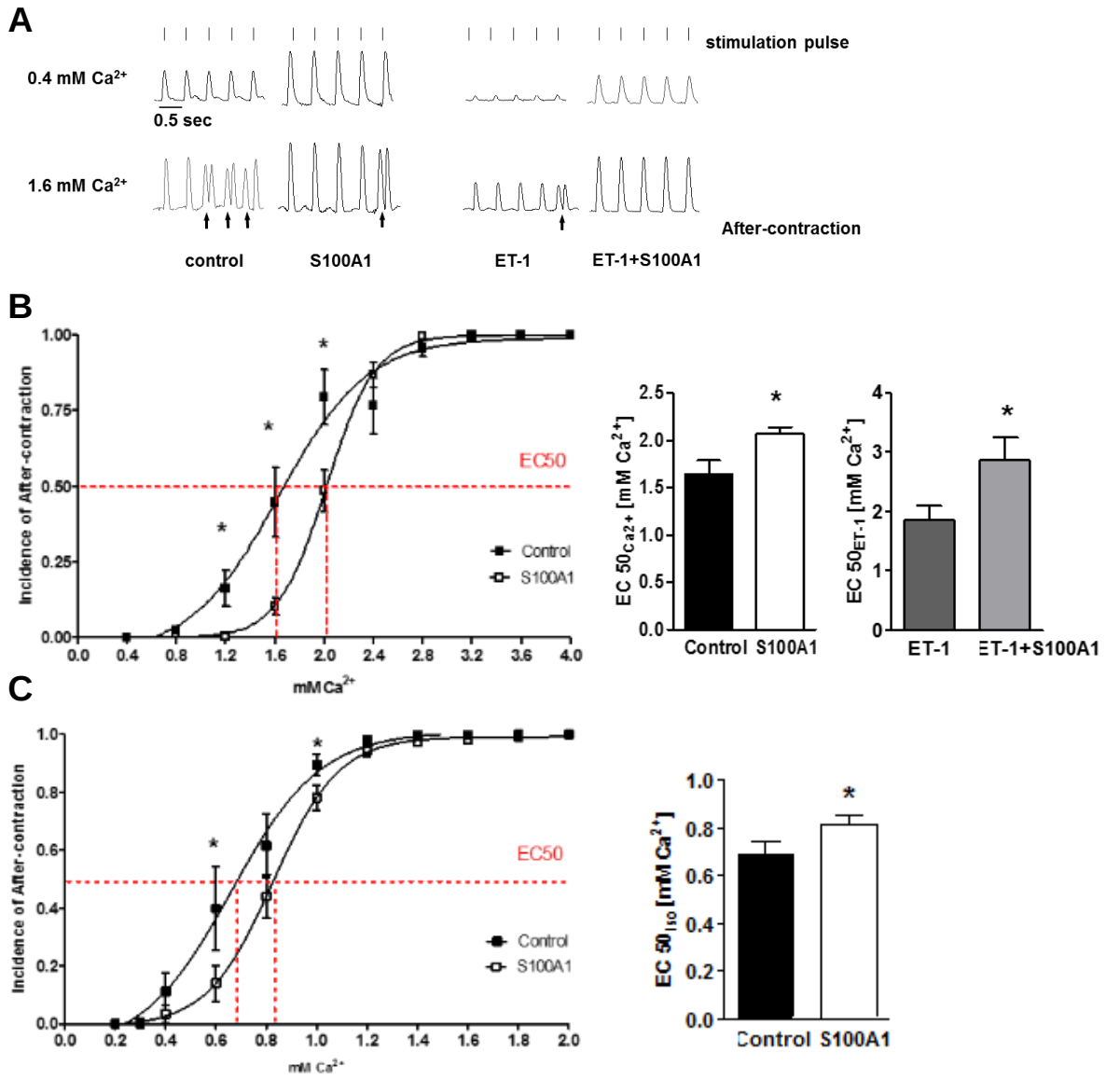

Figure 27: S100A1 overexpression reduces the incidence of calcium-triggered after-contractions in normal and failing EHT
A) Representative isometric force twitches of control and S100A1 overexpressing normal and failing EHT. EHT were stimulated with $4 \cdot 10^{-8}$ M ET-1 for 96 h and transduced with an MOI 50 of AdGFP (control) or AdS100A1 (S100A1) for 48 h before subjected to functional force recordings. $[Ca^{2+}]_{extra}$ was stepwise increased after a recording time of 150 sec and after-contractions counted manually. Lines above indicate stimulation pulses (110 mA, 5 ms width, 2 Hz), arrows below indicate non-stimulated after-contraction. **B)** Quantification of the incidence of after-contractions. $Ca^{2+}{}_{extra}$ was plotted against the calculated incidence of after-contractions. Incremental Ca^{2+} stress resulted in a dose-dependent increase in after-contractions that formed a sigmoidal curve and allowed for calculation of EC50 in normal and failing EHT. n=17 control, n=9 ET-1; * $p<0.05$ vs. control; student's t-test. **C)** Quantification of the incidence of after-contractions after Ca^{2+}/ β-AR stimulation. n=11; * $p<0.05$ vs. control/ET-1; student's t-test.

In summary, S100A1 overexpression protected normal EHT from Ca^{2+}-induced after-contractions, inhibiting pro-arrhythmogenic events. Despite overall reduced sensitivity for Ca^{2+}, failing EHT were also protected from after-contractions after S100A1 overexpression. β-AR stimulation sensitized normal EHT to after-contractions, while S100A1 acted protective.

Thus, despite increasing cellular inotropy, S100A overexpression also prevented Ca^{2+}- and β-AR-triggered after-contractions.

4.5 Elucidating S100A1's molecular effects

The previous paragraph confirmed that S100A1 is a profound inotropic agent, yet with similar anti-arrhythmic potency, protecting against Ca^{2+} and β-AR-stimulated after-contractions. Key mechanisms that could explain these effects can originate from changes in protein expression, phosphorylation pathways as well as in RyR2 activity. Thus, the next experiments aimed to identify the underlying mechanism of this anti-arrhythmic potency.

4.5.1 S100A1 overexpression does not change expression of major Ca^{2+}-handling proteins

Changes in contractile performance can originate from different expression levels of major Ca^{2+} handling proteins which are involved in cardiomyocyte EC coupling.

However, Serca2 and PLB protein levels in normal and failing EHT did not change after S100A1 overexpression, despite reduced expression after ET-1 stimulation (Fig. 28A). Similarly, mRNA levels of RyR2 and NCX also did not differ after S100A1 overexpression (Fig. 28B). Thus, changes in protein or mRNA expression are most likely not responsible for increased contractile performance and anti-arrhythmic potency. This is in line with previous results in isolated adult cardiomyocytes and *in vivo* experiments, which demonstrated that enhanced activity of S100A1's target proteins most likely to account for the enhanced contractile performance.[134, 137] Complementary analyses also confirmed unchanged hsTNT and LDH levels as well as TUNEL positive cells after S100A1 overexpression in normal and failing EHT (data not shown).

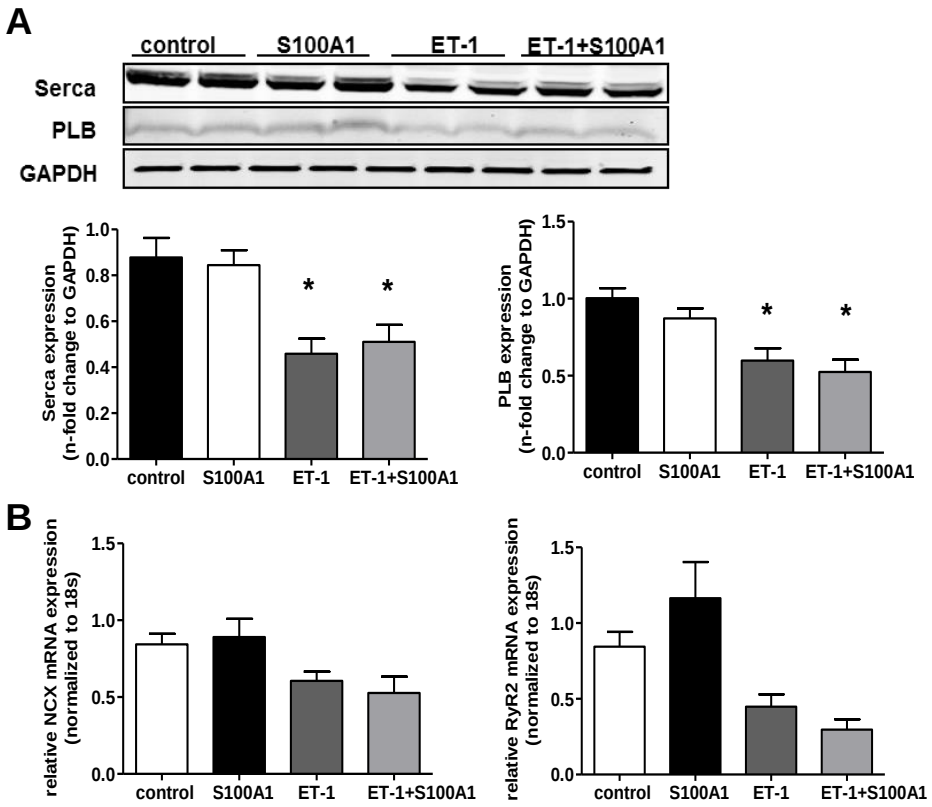

Figure 28: S100A1 overexpression does not changes expression of Serca2, PLB, RyR2 and NCX
A) Representative immunoblots and statistical analysis for Serca2 and PLB protein expression from control and S100A1 transduced EHT. After functional recordings, proteins were isolated and subjected to western blot analysis for Serca2 and PLB expression, which did not alter between control and S100A1. Two duplicates for each condition were depicted and densiometric values were normalized to GAPDH. n=5 from 5 different isolations; *p<0.05; 1-way ANOVA. **B)** mRNA analysis for RyR2 and NCX, which did not differ between control and S100A1. mRNA expression was normalized to 18s. n=4 from 4 different isolation; 1-way ANOVA.

4.5.2 S100A1 overexpression might reduce pro-inflammatory activation

Next, the pro-inflammatory and pro-fibrotic remodeling of normal and failing EHT after S100A1 overexpression was analyzed (Fig. 29).

Il-6 mRNA levels were increased 4-fold in failing EHT, while S100A1 overexpression reduced Il-6 expression after S100A1 overexpression in failing EHT to control levels. Similarly, ICAM-1 expression levels were increased 2-fold in failing EHT and S100A1 overexpression normalized ICAM-1 expression levels to control levels. However, these effects were not statistically significant. In contrast, S100A1 overexpression had no effect on ANP, SMA and collagen-1 mRNA expression levels in failing EHT. However, due to unstable PCR values, these effects were also not statistically significant.

Still, S100A1 overexpression seems to have no effect on pro-fibrotic markers but rather reduced the increase in pro-inflammatory markers.

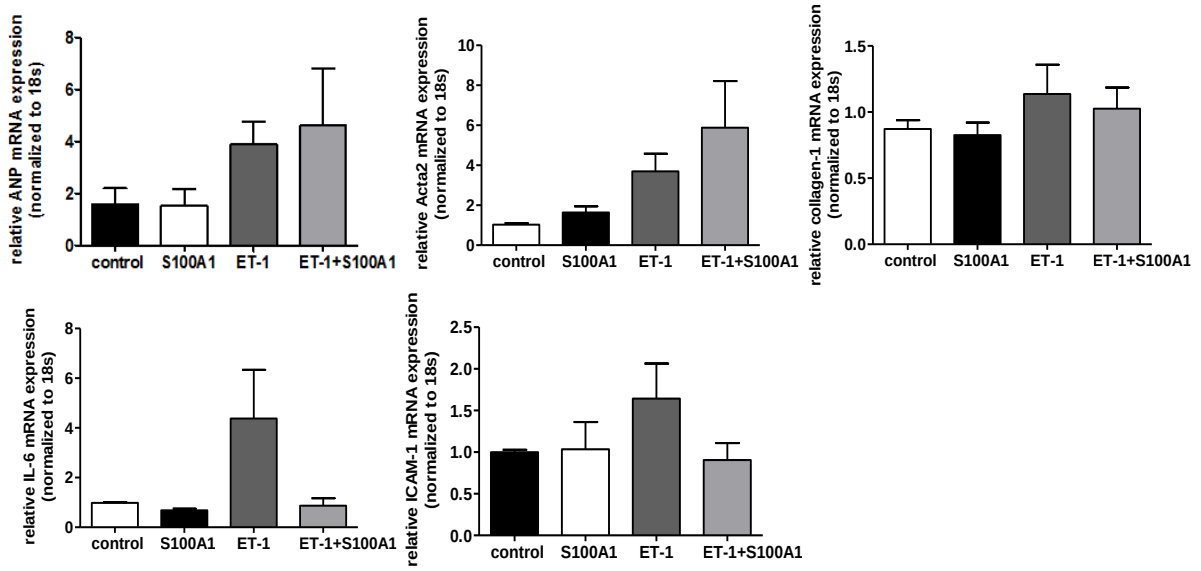

Figure 29: S100A1 overexpression after ET-1 treatment reduces pro-inflammatory activation
mRNA analysis for ANP, SMA, collagen-1 and ICAM-1 in control, failing EHT and after S100A1 overexpression. While pro-fibrotic markers as collagen-1 and SMA did not change after S100A1 overexpression in normal and failing EHT, pro-inflammatory markers IL-6 and ICAM-1 increased in failing EHT, yet were comparable to control levels in failing EHT with S100A1 overexpression. However, this effect was not statistical significant. mRNA expression was normalized to 18s. n=4; 1-way ANOVA.

4.5.3 S100A1 overexpression does not change Cx43 expression in EHT

EHT is a 3-dimensional tissue model where CMs interact with neighboring cells, forming complex structures and resembling intact heart tissue. Thus, changes in electrical coupling and electrical conductance might also be responsible for the anti-arrhythmic effect.

Among others, Connexin43 (Cx43) is the major gap junction proteins coupling cardiomyocytes and changes in its expression, phosphorylation and localization have been linked to arrhythmogenesis. Additionally, cardiomyocyte-fibroblast interactions by Cx43 have been reported as well.[170-172] Thus, changes in electrical conductance might originate from changed Cx43 expression or phosphorylation levels.

However, S100A1 overexpression had no effect on Cx43 expression and its phosphorylation status (Fig. 30). Failing EHT showed a slight increase in Cx34 expression and a reduction in Cx43 phosphorylation, but this tendency was not significant. Still, there was no effect of S100A1 overexpression in normal and failing EHT neither on Cx43 expression nor on its phosphorylation. Hence, changes in Cx43 expression or its phosphorylation are probably not accountable for S100A1's effects.

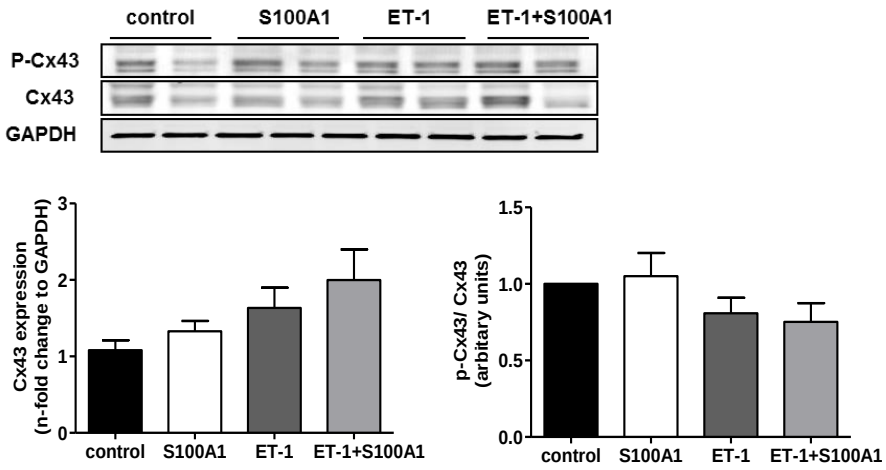

Figure 30: S100A1 overexpression does not change Cx43 expression and phosphorylation
Representative immunoblots and statistical analysis from control, failing and S100A1 overexpressing EHT. After functional recordings, proteins were isolated and subjected to western blot analysis for Cx43 and p-Cx43 expression. Two duplicates for each condition were depicted and densiometric values were normalized to GAPDH or total Cx43. In failing EHT, Cx43 expression was slightly increased and Cx43 phosphorylation was slightly reduced; however there were no further change after S100A1 overexpression. n=4 from 4 isolations; 1-way ANOVA.

4.5.4 S100A1 overexpression does not change global PKA or CamKII downstream signaling

Increased PKA- and CamKII-activity have been linked to triggered arrhythmias *in vitro* and *in vivo*. Most important, RyR2 phosphorylation at serine 2808 (Ser-2808, PKA-mediated) and at serine 2814 (Ser-2814, CamKII-mediated) have been shown to promote cellular arrhythmias.[46, 74, 75, 81] Global changes in PKA- and CamKII activity can be analyzed by PLB phosphorylation. PKA phosphorylates PLB at serine 16 (Ser-16) and CamKII at threonine 17 (Thr-17); however, local kinase activity at the RyR2 is often more important.

First, PLB phosphorylation was analyzed in normal and failing EHT to estimate changes in global PKA and CamKII activity. Before and after functional recordings, EHT were subjected to western blot analysis for PLB phosphorylation (Fig. 31).
Ca^{2+} stimulation (4 mM) resulted in an exclusive increase in PLB Thr-17 phosphorylation. PLB Ser-16 phosphorylation was not affected by Ca^{2+} stimulation, indicating that Ca^{2+}-stress activates selectively CamKII. After S100A1 overexpression, PLB phosphorylation pattern did not change.
In failing EHT, basal (0.2 mM Ca^{2+}) PLB Thr-17 phosphorylation levels were comparable to normal EHT. Ca^{2+} stimulation (4 mM) however dramatically increased PLB Thr-17 phosphorylation. Again, Ca^{2+} stimulation had no effect von PLB Ser-16 phosphorylation in failing EHT, but phosphorylation levels were slightly enhanced compared to normal EHT. Again, increasing S100A1 protein levels did not interfere with PLB phosphorylation pattern.

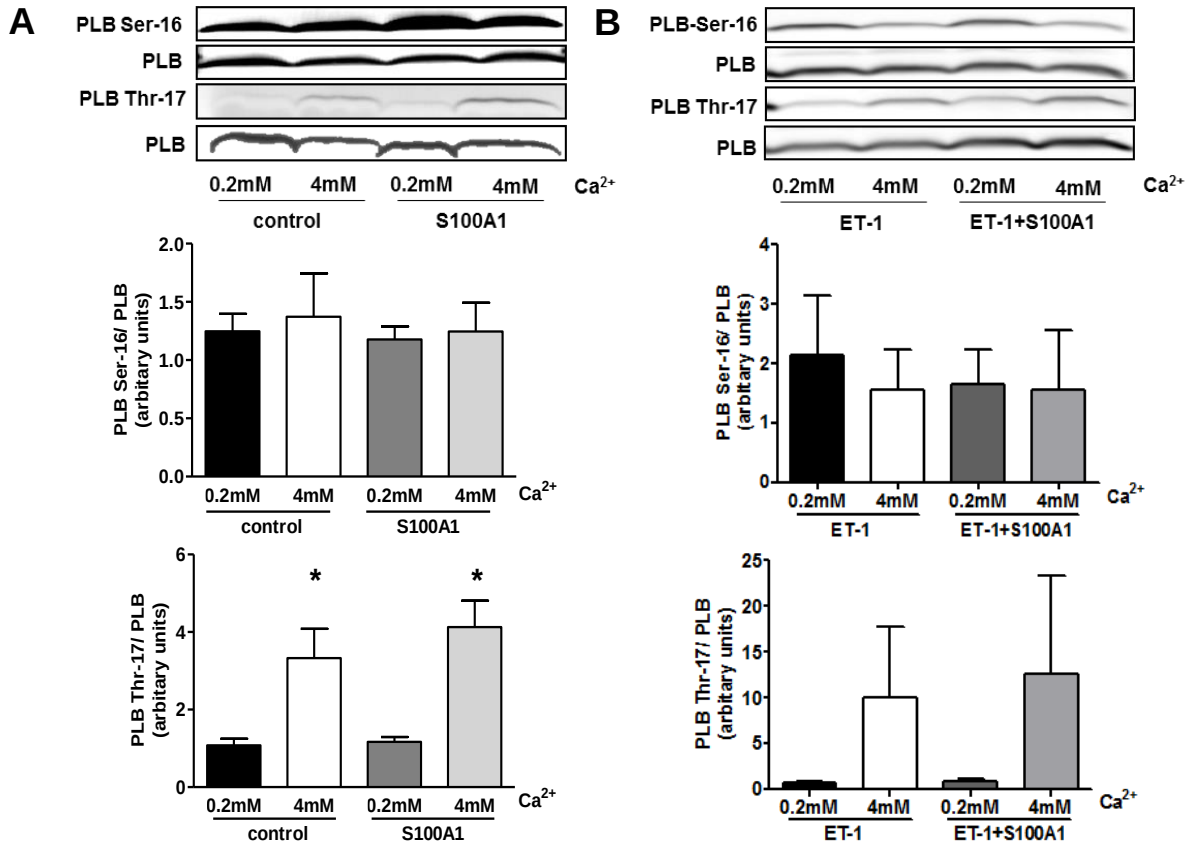

Figure 31: S100A1 overexpression does not change PLB phosphorylation after Ca^{2+} stimulation
Representative immunoblots and statistical analysis from control and S100A1 overexpressing normal **(A)** and failing EHT **(B)** before (0.2 mM Ca^{2+}) and after Ca^{2+} stimulation (4 mM Ca^{2+}). Before or after functional recordings, proteins were isolated and subjected to western blot analysis for PLB, P-PLB serine 16 and P-PLB threonine 17 expressions. Densiometric values were normalized to PLB. Ca^{2+} stimulation increased P-PLB Thr-17 in normal and failing EHT, however there was no change in phosphorylation pattern after S100A1 overexpression. control n=5, ET-1 n=4 from 4 isolations; * $p<0.05$ vs. 0.2mM Ca^{2+}; 1-way ANOVA.

As sole Ca^{2+} stimulation did not activate PKA, β-AR stimulation dependent PLB phosphorylation was also analyzed in normal EHT (Fig. 32). Iso stimulation increased both PLB Ser-16 and Thr-17 phosphorylation, as increased cAMP levels are known to increase cytosolic Ca^{2+}, activating CamKII indirectly.[21] As shown before, S100A1 overexpression did not interfere with PLB phosphorylation pattern after β-AR stimulation.

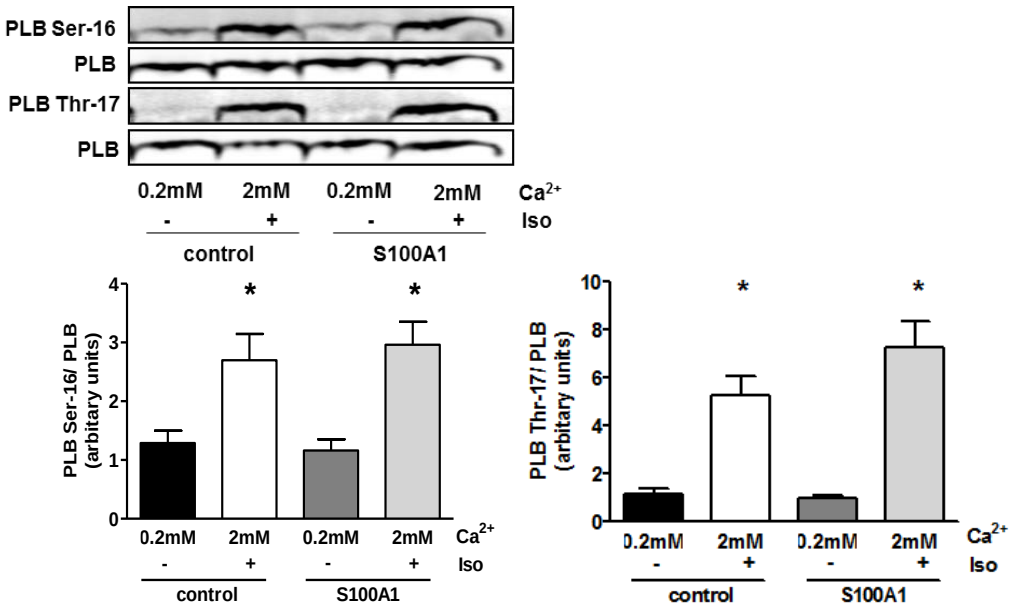

Figure 32: S100A1 overexpression does not change PLB phosphorylation after β-AR stimulation
Representative immunoblots and statistical analysis from control and S100A1 overexpressing EHT after Iso stimulation. Iso (1 µM/ 2 mM Ca^{2+}) stimulation increased P-PLB Ser-16 and Thr-17 in normal EHT, however there was no change in PLB phosphorylation pattern after S100A1 overexpression. control n=5, from 4 isolations; * $p<0.05$ vs. 0.2 mM Ca^{2+}; 1-way ANOVA.

Thus, S100A1 overexpression did not change PLB phosphorylation in normal and failing EHT, indicating that S100A1 does not interfere with global PKA- and CamKII-activity.

4.5.5 S100A1 overexpression does not change RyR2 phosphorylation

Next, RyR2 immunoprecipitations (IPs) were performed to analyze local PKA- and CamKII-activity at the RyR2. Again, RyR2 phosphorylation was analyzed before and after functional recordings. Ca^{2+} stimulation (4 mM) resulted in a profound increase in RyR2 Ser-2814 phosphorylation, but RyR2 Ser-2808 phosphorylation was also slightly increased, which indicated increased PKA- and CamKII-mediated RyR2 phosphorylation (Fig. 33). S100A1 overexpression did not change RyR2 phosphorylation pattern but resulted in an increase in co-precipitating S100A1 protein, which demonstrated enhanced binding to the RyR2 after S100A1 overexpression. Similarly, Iso stimulation increased RyR Ser-2808 phosphorylation, but Ser-2814 phosphorylation was difficult to analyze due to overall low quality of western blot bands.

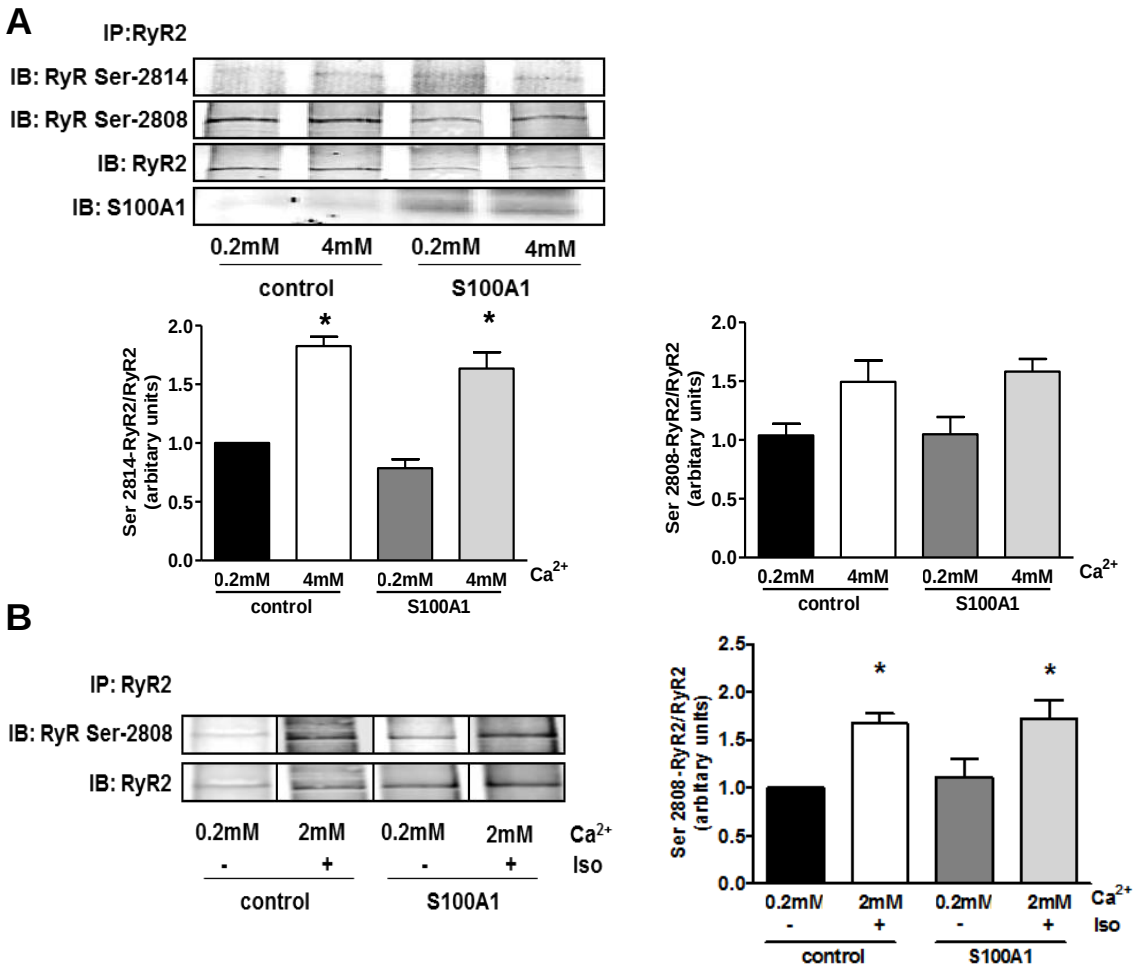

Figure 33: S100A1 overexpression does not change RyR2 phosphorylation
A) Representative immunoblots and statistical analysis from control and S100A1 overexpressing EHT after Ca^{2+} stimulation. Before (0.2 mM Ca^{2+}) and after (4 mM Ca^{2+}) functional recordings, two EHT were pooled and RyR2 was immunoprecipitated. Precipitates were subjected to western blot analysis for RyR2, P-RyR2 Ser-2808 and P-RyR2 Ser-2814 expression. Densiometric values were normalized to total RyR2. Ca^{2+} stimulation increased P-RyR Ser-2814 in EHT, but there was no change in phosphorylation pattern after S100A1 overexpression. However, S100A1 overexpression increased co-precipitating S100A1. n=5, from 5 isolations; * $p<0.05$ vs. 0.2mM Ca^{2+}; 1-way ANOVA. **B)** Representative immunoblots and statistical analysis from control and S100A1 overexpressing EHT after Iso stimulation. Before (0.2 mM Ca^{2+}) and after (1 µM Iso/2 mM Ca^{2+}) functional recordings, two EHT were pooled and RyR2 was immunoprecipitated. Precipitates were subjected to western blot analysis for RyR2, P-RyR2 Ser-2808 and P-RyR2 Ser-2814 expressions. Densiometric values were normalized to total RyR2. Iso stimulation increased P-RyR2 Ser-2814 in EHT, but there was no change in phosphorylation pattern after S100A1 overexpression. n=5, from 5 isolations; * $p<0.05$ vs. 0.2 mM Ca^{2+}; 1-way ANOVA

These experiments were only performed in normal and not in failing EHT, as it was difficult to generate enough material. As PLB phosphorylation pattern did not change after S100A1 overexpression in failing EHT, it is reasonable to assume that RyR2 phosphorylation pattern might also not change after S100A1 overexpression in failing EHT.

Thus, S100A1 did not change PKA- and CamKII downstream signaling and this mechanism can be excluded from possible explanations for S100A1 anti-arrhythmic effects.

4.6 Impact of S100A1 on the RyR2 macrocomplex

The previous paragraph demonstrated that S100A1 overexpression had no effect on PKA- and CamKII-mediated RyR2 phosphorylation. Next, the impact of S100A1 on the binding of accessory proteins was analyzed, as several studies reported that differential binding of CaM, FKBP12.6 or sorcin can change systolic and diastolic RyR2 function.

As these experiment were difficult to perform in EHT, especially with regard to immunohistochemistry, isolated adult rat cardiomyocytes (ACM) were used. A most recent study (see introduction) demonstrated that S100A1 overexpression increased Ca^{2+} transient amplitudes and reduced Ca^{2+} spark frequency and waves in normal and failing ACM, which renders these cells suitable to investigate S100A1's positive inotropic and anti-arrhythmic effects. First, biochemical analyses were repeated under the same conditions to confirm unchanged PKA- and CamKII activity before investigating RyR2 complex formation.

4.6.1 S100A1 overexpression increases S100A1 protein levels in ACM

S100A1 overexpression in ACM was analyzed 24 h after adenoviral transduction. Transduction of ACM with MOI 5 of AdGFP (control) or AdS100A1 (S100A1) resulted in a homogeneous GFP expression in all cells. Western blot analysis confirmed a 6-fold increase in S100A1 protein levels and comparable GFP expression levels in control and S100A1 transduced ACM (Fig. 34).

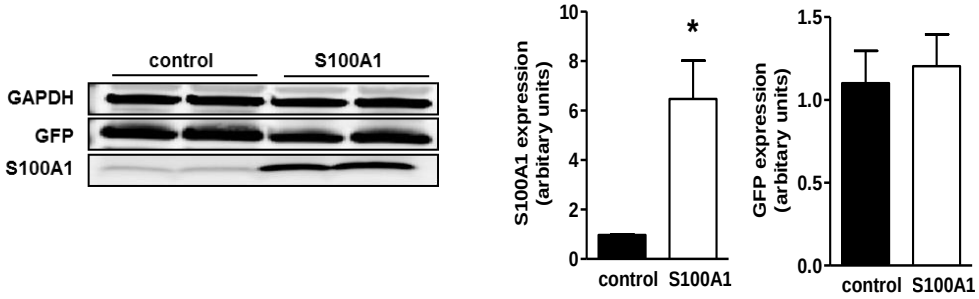

Figure 34: S100A1 overexpression increases S100A1 protein levels in adult rat cardiomyocytes
Representative immunoblots and statistical analysis from control and S100A1 overexpressing ACM. 24 h after adenoviral transduction, proteins were isolated and subjected to western blot analysis for S100A1 and GFP expression. S100A1 overexpression increased 6-fold after adenoviral transduction with AdS100A1. GFP levels were matching between both viruses. Two duplicates were depicted and densiometric values were normalized to GAPDH. n=4, from 4 isolations; * $p<0.05$ vs. control; student's t-test.

4.6.2 S100A1 overexpression does not change PKA or CamKII downstream signaling

As the analysis in EHT indicated that S100A1 overexpression has no effect on PKA- and CamKII-mediated PLB and RyR2 phosphorylation, these results first had to be confirmed in ACM to approve similar response to external stressors in both models. Here, β-AR stimulation with Iso was chosen, at the analysis in EHT indicated that Iso activates both PKA and CamKII.

β-AR stimulation with Iso (10^{-7} M, 10 min) strongly increased PLB Ser-16 phosphorylation (30-fold) and slightly increased PLB Thr-17 phosphorylation (2-fold). However, there were no changes in phosphorylation pattern after S100A1 overexpression (Fig. 35A).

Similar results were obtained after RyR2 IP for RyR Ser-2808 and Ser-2814 phosphorylation: Iso stimulation increased Ser-2808 phosphorylation 2-fold and Ser-2814 phosphorylation 1.5 fold, but S100A1 overexpression did not change phosphorylation levels further (Fig. 35B). As already seen in EHT immunoprecipitates, S100A1 overexpression increased co-precipitating S100A1 protein.

Thus, ACM showed similar effects of PKA and CamKII activation in response to Iso stimulation and can be used to further investigate RyR2 complex formation.

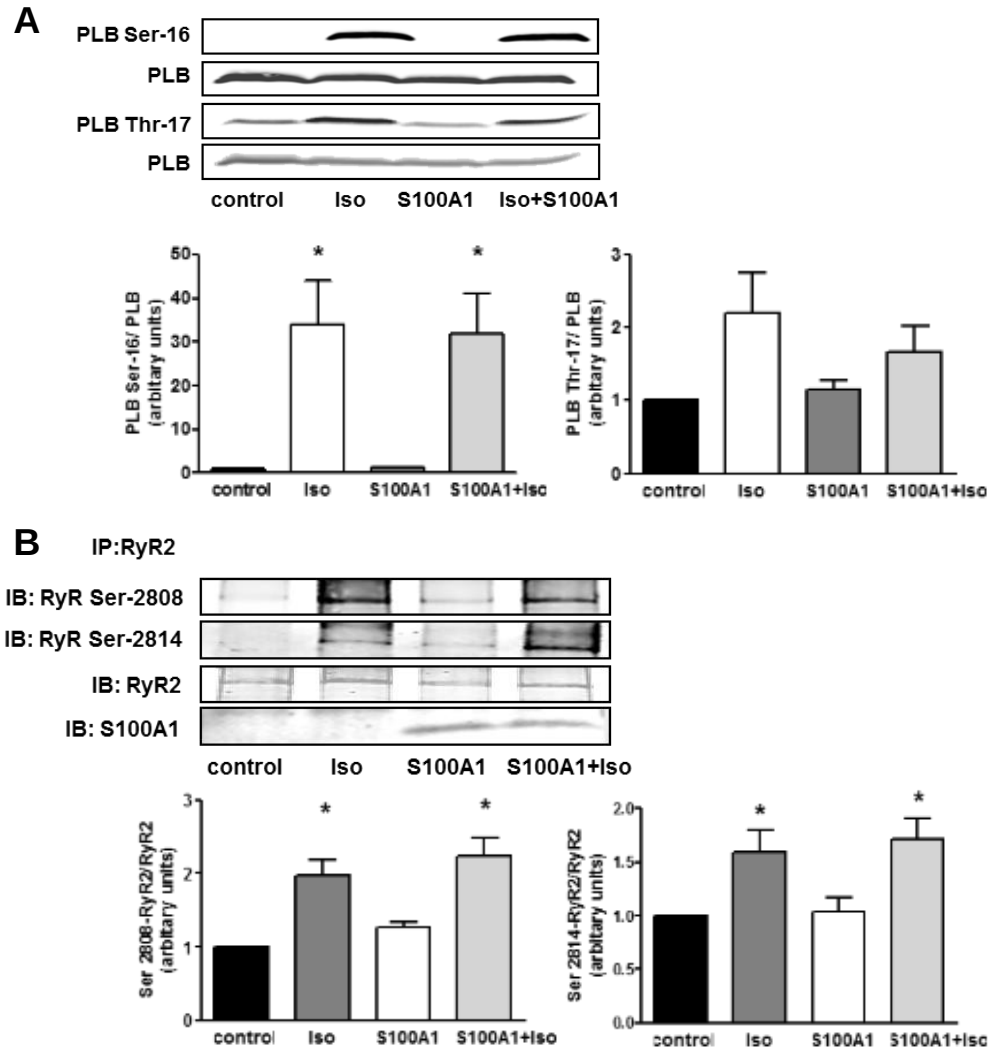

Figure 35: S100A1 overexpression does not change PLB and RyR2 phosphorylation pattern
Representative immunoblots and statistical analysis from control and S100A1 overexpressing ACM. 24 h after adenoviral transduction, proteins were isolated or RyR2 IPs performed and subjected to western blot analysis for PLB, P-PLB Ser-16, P-PLB Thr-17, **(A)** RyR2, P-RyR Ser-2808 and P-RyR2 Ser-2814 expression **(B)**. Iso stimulation increased P-PLB and P-RyR2 by PKA and CamKII but phosphorylation pattern did not change after S100A1 overexpression. Densiometric values were normalized to GAPDH. n=4, from 4 isolations; * $p<0.05$ vs. control; 1-way ANOVA.

4.6.3 S100A1 overexpression does not change complex formation of RyR2

Accessory proteins of the RyR2 have been shown to modulate systolic as well as diastolic RyR2 function *in vivo* and *in vitro*. In general, CaM, FKBP12.6 and sorcin have all been reported to inhibit RyR2 function.[71]

Thus, the proximity ligation assay (PLA) was performed to analyze the binding properties of CaM, FKBP12.6 and sorcin to RyR2 after S100A1 overexpression. This assay allows *in situ* analysis of protein interactions in the intact cell, when the distance between two proteins/ primary antibodies is less than 40 nm. This protein interaction can be visualized as immunofluorescent dot in the microscope (Fig. 36A). As each dot represents one protein/protein interaction, this can be quantified.

Again, ACM were transduced with either AdGFP or AdS100A1, stimulated with Iso and PLA was performed (Fig. 36B). Iso stimulation slightly reduced CaM/RyR2 interaction. Interestingly, S100A1 overexpression did not change this under basal conditions as well as after Iso stimulation. In contrast, Sorcin/RyR2 interaction was increased after Iso stimulation but again S100A1 overexpression had no effect on this interaction. Finally, FKBP12.6/RyR2 interaction did not change at all after Iso stimulation. However, all changes were not statistically significant, indicating only tendencies towards changed interactions after Iso stimulation.

Thus, S100A1 overexpression had no effect on the binding properties of accessory proteins to the RyR2, indicating that S100A1 had no impact on complex assembly of the RyR2.

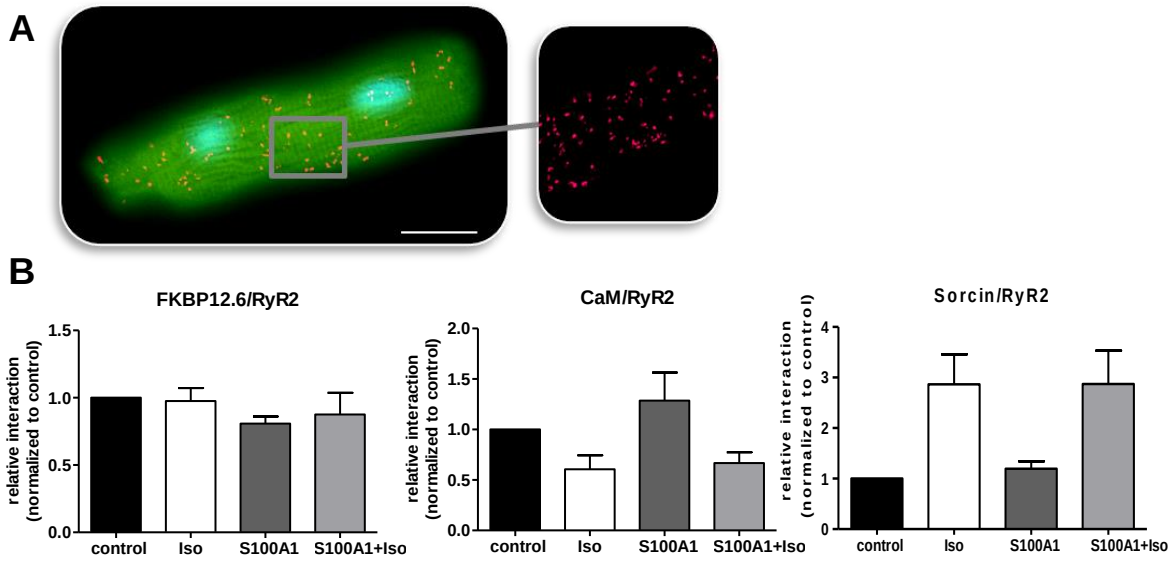

Figure 36: S100A1 overexpression does not change CaM/RyR2, FKBP12.6/RyR2 and Sorcin/RyR2 interaction

A) Representative immunofluorescence image of PLA in ACM. Each red dot represents one protein/protein interaction that can be quantified using ImageJ. Scale bar represent 20 µm. **B)** Statistical analysis from control and S100A1 overexpressing ACM and with Iso stimulation. 24 h after adenoviral transduction, cells were stimulated with Iso (10^{-7} M, 10 min) and PLA were performed to analyze CaM/RyR2, FKBP12.6/RyR2 and sorcin/RyR2 interaction. Iso stimulation reduced CaM/RyR2 interaction, increased sorcin/RyR2 interaction and had no impact on FKBP12.6/RyR2 interaction. However, S100A1 overexpression did not change stoichiometry further. n=4, from 4 isolations; 1-way ANOVA.

4.6.4 S100A1 overexpression enhances S100A1/RyR2 interaction

Although already shown by Co-IP, PLA was additionally performed to quantify increased S100A1 binding to the RyR2 and monitor possible changes during β-AR stimulation. Previous studies demonstrated that a 3-4 fold S100A1 overexpression increased S100A1/RyR2 ratio 2-fold as analyzed by Co-IP (unpublished data).

PLA confirmed that Iso stimulation had no effect on S100A1/RyR2 interaction but S100A1 overexpression increased S100A1/RyR2 ratio 2-fold as analyzed by PLA (Fig. 37).

Thus, direct interaction of S100A1 with RyR2 could be confirmed with the PLA technology and also indicated unchanged binding after β-AR stimulation. This might preferentially account for the anti-arrhythmic effects of S100A1 overexpression on the RyR2, however, if this is due to allosteric regulation of the channel or of different origin remains unclear.

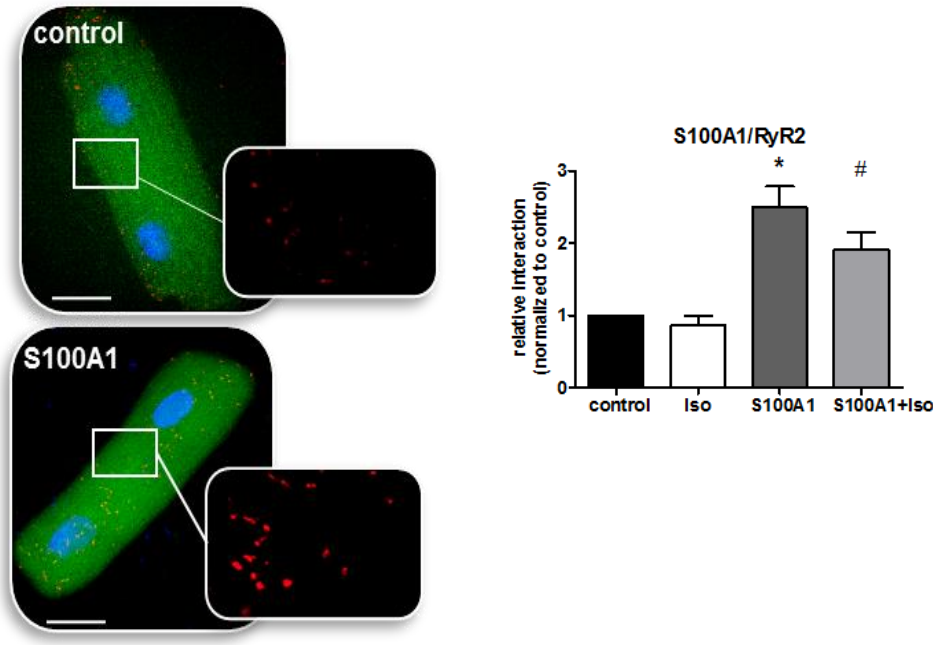

Figure 37: S100A1 overexpression enhances S100A1/RyR2 stoichiometry
Representative immunofluorescence images (left) and statistical analysis (right) from control and S100A1 overexpressing ACM. 24 h after adenoviral transduction, cells were stimulated with Iso (10^{-7} M, 10 min) and PLA was performed to analyze S100A1/RyR2 interaction. Iso stimulation had no effect on S100A1/RyR2 interaction but S100A1 overexpression enhanced S100A1/RyR2 ratio. n=3, from 3 isolations; * $p<0.05$ vs. control; 1-way ANOVA. Scale bar represents 20 µm.

4.6.5 S100A1 overexpression blunts RyR2 s-nitrosylation after β-AR stimulation

Changes in cellular redox-state and especially changes in RyR S-nitrosylation (SNO) have recently been made responsible for short-term regulation of RyR2 function and its open probability (P_o).[87, 101, 102, 108, 109]

As standard assays for the detection of nitrosylated proteins were difficult to perform (due to low abundance of RyR2 in isolated cells), PLA was performed to specifically link s-nitrosylation to

RyR2.[173] By combining a general SNO-antibody with a specific RyR2 antibody, RyR2-SNO could specifically be detected (Fig. 38).

Iso stimulated resulted in increased in RyR2-SNO (2-fold). S100A1 overexpression had no effect on RyR2-SNO under basal conditions. Interestingly, the increase in RyR2-SNO after Iso stimulation was blunted after S100A1 overexpression and even below control levels.

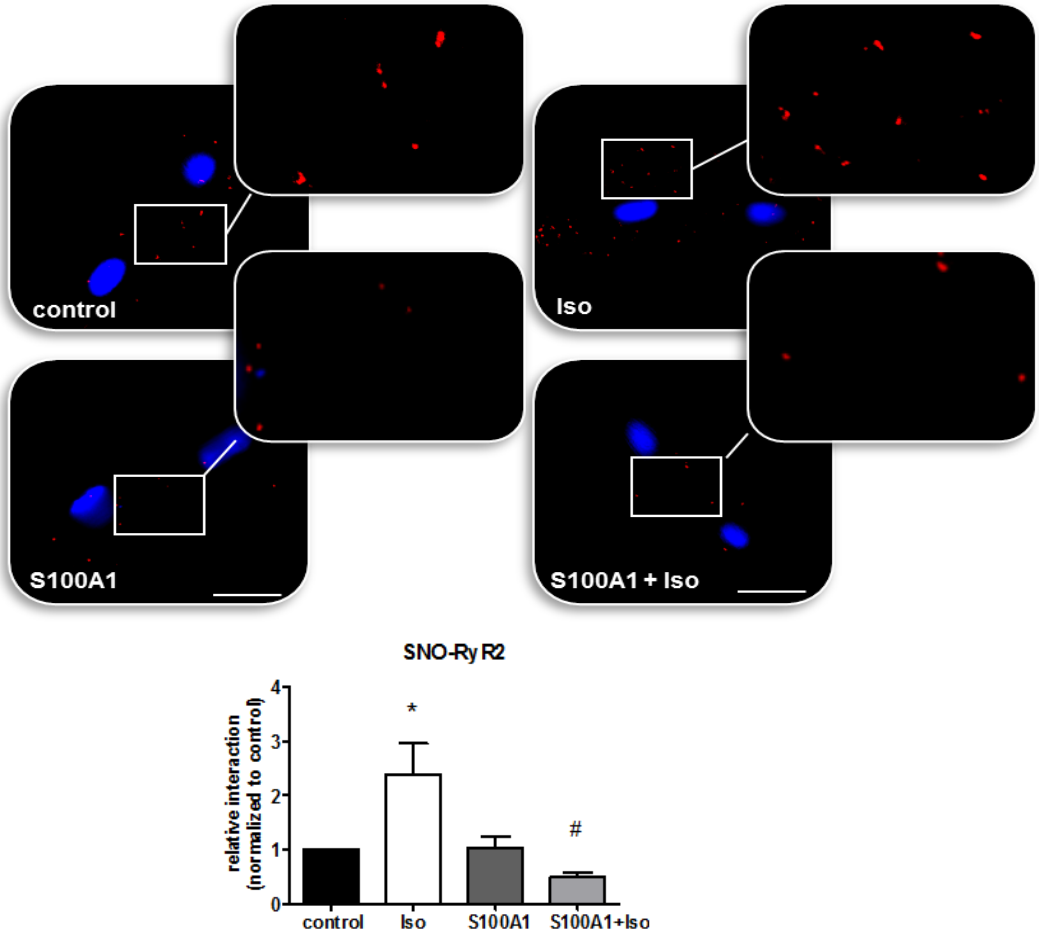

Figure 38: S100A1 overexpression normalized RyR s-nitrosylation
Representative immunofluorescence images (left) and statistical analysis (right) from control and S100A1 overexpressing ACM. 24 h after adenoviral transduction, PLA was performed to analyze RyR2-SNO. Iso stimulation increased RyR-SNO, whereas S100A1 overexpression blunted the increase after Iso stimulation.
n=3, from 3 isolations; * $p<0.05$ vs. control, # $p<0.05$ vs. Iso; 1-way ANOVA. Scale bar represent 20 µm.

For the first time, altered RyR2-SNO after S100A1 overexpression might explain S100A1's differential effects on RyR2 function. However, if different redox-modifications (oxidation, glutathionylation) are also changed after S100A1 overexpression and if these changes in the redox-status have a functional implication need to be investigated in greater detail.

5 Discussion

The small Ca^{2+} binding protein S100A1 controls major Ca^{2+} driven networks within the CM. The positive inotropic actions of S100A1 are mainly dependent on enhanced Ca^{2+} transients and are preserved under β-adrenergic receptor (β-AR) stimulation without affecting cAMP-dependent kinase activities.[133-135, 137, 138, 141, 145, 146, 174] In contrast to the current understanding of the action of positive inotropes, S100A1 overexpression is in accordance with a reduced diastolic Ca^{2+} leak in isolated cells *in vitro* (unpublished data). However, until now it remained unclear if the inhibition of the diastolic Ca^{2+} leak also impedes mature arrhythmogenic contractions.

Within this work, I analyzed the impact of S100A1 on diastolic contraction abnormalities in a multicellular tissue model under isometric conditions and unveiled some important mechanistic properties.

5.1 Pharmacological stimulation of EHT with ET-1 – an *in vitro* model of failing cardiac tissue

5.1.1 Classification of EHT into current models for cardiac hypertrophy or heart failure

Understanding the basic mechanisms of diseases requires experimental *in vitro* and *in vivo* models, which allow to reconstruct the disease state.

Rodent models are widely appreciated to understand the etiology of various cardiovascular diseases and to study the effects of therapeutic interventions *in vivo*.[175-177] Still, it is difficult to discriminate between direct alterations from systemic and humoral effects seen in these *in vivo* models. For this reason, *in vitro* models of neonatal and adult rat and mice cardiomyocytes have been utilized to circumvent this limitation. For example neonatal and adult rat cardiomyocytes have been stimulated with α-AR agonists, endothelin-1, or cultured on silicon membranes and subjected to phasic stretch to induce hypertrophy.[154, 178-180] Still, they do not adequately recapitulate changes occurring *in vivo* and have major limitations: First, cardiomyocytes (CMs) in cell culture are distributed diffusely. This may limit their informative values as CMs in the heart tissue are highly organized in a 3-dimensional network. Second, standard 2-dimensional monolayer cell cultures do not allow measurement of contractile function, an important parameter to distinguish hypertrophied from failing CMs. Third and even more important, neonatal CMs do not exhibit the same characteristic and mechanistic features as adult myocardium as they are not completely differentiated and have an immature phenotype.[181] This might bias outcomes of certain studies and lead to false assumptions of regulatory mechanisms in the intact heart.[182] Culturing adult CMs can only be performed in good quality for a maximum of 48 h, which renders the time period for pharmacological and therapeutic interventions extremely short (own observations).[154]

To overcome some of these limitations, the model of Engineered Heart Tissue (EHT) was developed. Despite build of neonatal rat cells, CMs develop an adult-like phenotype over the culture period (12 days), which also allows enough time for pharmacological manipulations.[151, 152] Although initially developed as tissue repair model to support failing myocardium, current research focuses on the utilization of EHT as model system for cardiac hypertrophy, ischemic damage and therapeutic testing.[163, 182-188]

In this work, according to the state-of-the art methods in neonatal cultures, EHT were stimulated with low-dose of ET-1 ($4 \cdot 10^{-8}$ M for 96 h) to induce heart failure (HF)-like remodeling.[189] This resulted in a strong impairment of systolic contractility, as measured by reduced twitch tension (TT). The duration of the contraction, measured as time to peak (TTP), was longer in failing EHT at high [Ca^{2+}], which indicates stronger effects at higher Ca^{2+} levels. However, diastolic function, measured by tau, was not affected, which points towards an exclusive impairment of systolic function. Furthermore, Ca^{2+} sensitivity was reduced in failing EHT, where similar effects have been shown in isolated muscle fibers of failing heart.[190]

Functional impairment was accompanied by a complex cellular remodeling: In line with the current concepts of heart failure, PLB, Serca2 and RyR2 expression were all downregulated and ANP expression was upregulated. In contrast, NCX expression was also downregulated in this model, where increased expression levels had been reported in failing hearts.[47, 52, 164] Still, it has to be considered that this model system might regulate not all proteins in the same way than in the intact heart.

S100A1 expression has been reported to be reduced in failing hearts, whereas compensated hypertrophy showed no reduction is S100A1 levels *in vivo*.[191] Similarly, stimulation of neonatal rat cardiomyocytes with hypertrophic factors resulted in a time and concentration dependent reduction in S100A1 expression levels, which might be part of the fetal gene program.[138] Here, S100A1 expression was also strongly diminished, which underlines a HF-like remodeling.[192]

Increased fibroblast activation in HF has been attributed to increased smooth muscle actin (SMA), collagen-1 and connective tissue growth factor (CTGF) expression.[165, 193] Despite an increase in SMA and CTGF levels, there was no change in collagen-1 expression in failing EHT, which might originate from the vast amount of collagen in the matrix. Inflammatory markers as interleukin 6 (IL-6) and intercellular adhesion molecule 1 (ICAM-1) were also increased, which indicates inflammatory remodeling.[194] Thus, failing EHT express markers for pathological cardiomyocyte dysfunction and fibroblast activation.

Furthermore, cell death analysis pointed towards increased necrosis in failing EHT, but no increase of apoptotic cell death. Most recently, necrosis has been appreciated to occur in failing hearts *in vivo*, whereas apoptosis occurred only at lower levels in the chronic state.[195, 196] Hence, cell death analysis in EHT emphasize on similar effects than the *in vivo* situation.

In contrast to this, nuclei numbers in failing EHT were slightly increased, which suggests no substantial increase in cell death. However, in early stages of necrosis, DNA is still intact, thus cell numbers might not decrease despite ongoing necrosis.[196] Increased nuclei number might also originate from polynucleation of cardiomyocytes or proliferation of fibroblast, which both have been reported to occur in failing hearts.[168] Similarly, polynucleation of cardiomyocytes in EHT has been reported after ET-1 stimulation.[152]

Altogether, failing EHT showed most features of failing hearts *in vitro*. Still, heart failure is a clinical syndrome and not easily transferable to the culture dish. Although, *in vivo* experiments will remain the gold standard for analysis of functional recovery following myocardial injury and pharmacological interventions, EHT might be an attractive model to replace the adult heart to study the effects of different stressors and treatments on contractile performance and molecular expression changes.

5.1.2 After-contractions – a model for Ca^{2+}-triggered arrhythmias

Triggered ventricular arrhythmias are characterized by an abnormal heartbeat, which can become life-threatening when the heart is unable to fill or empty completely and support the body with oxygenated blood. Mechanisms for the origin of ventricular arrhythmias are multifaceted as well as the models which have been utilized for their analysis *in vivo*.[170]

Investigating this effect *in vitro* exposed Ca^{2+} mishandling as major cause of arrhythmias in ventricular CMs: Ca^{2+} overload results in diastolic Ca^{2+} leakage, which in turn can induce delayed after-depolarizations (DADs) that lead to mature action potentials and extra contractions.[9, 48-50] State-of-the-art techniques for the analysis of abnormal diastolic Ca^{2+} handling include confocal Ca^{2+} imaging of Ca^{2+} sparks and Ca^{2+} waves and action potential recordings to monitor DADs.[197] However, these effects are mainly explored in isolated ACMs, which are not cultivated under loaded conditions. Additionally, cell-cell interactions, which might contribute to arrhythmogenesis, are not considered.[171, 172] Thus, EHT may represent a more refined model to analyze arrhythmogenesis as cells are cultivated under loaded conditions and contraction abnormalities can be recorded under isometric conditions.

Although described before, optical imaging techniques as FURA-2-based Ca^{2+} imaging and di-4-ANEPPS-based electrical recording remained difficult in EHT, as penetration of the dye into the EHT matrix was incomplete and a special setup for the optical recording additionally to the force recordings would have been needed.[185] Moreover, the conduction of electric currents during force recordings was unmanageable, as artefacts from the stimulation electrodes were too strong to detect electrical currents. Thus, it was not possible to resolve Ca^{2+} cycling or electrical currents in combination with functional recordings.

On a cellular level, Ca^{2+} overload is known to induce store-overload-induced Ca^{2+}-release (SOICR) in single cells, which can manifest itself in extra contractions.[50, 57] Thus, this mechanisms might also

take place in EHT. Indeed, increasing [Ca^{2+}] in the tyrode solution (above physiological levels) did not only increase contractile force of EHT, but after accomplishment of max. TT, Ca^{2+} overload induced concentration-dependent contraction abnormalities, referred to as after-contractions. Thus, it is quite plausible that cellular Ca^{2+} overload also occurs in EHT and triggers diastolic Ca^{2+} leakage, resulting in mature contractions. Additionally, these after-contractions were profoundly inhibited by ryanodine and known anti-arrhythmic drugs as Flecainide without loss of overall TT, supporting that known cellular mechanisms are the origin of after-contractions.

Similarly, Schaaf et al. reported the nascent of contraction abnormalities in respond to pro-arrhythmogenic drugs in a similar model of reconstituted heart tissue from human embryonic stem cells.[187] Automatically detection of irregular beating pattern was used to describe the arrhythmogenic potential, which is similar to the manual tracking of after-contractions applied for this study.

Here, the contraction abnormalities, or after-contractions, were counted manually over a wide range of [Ca^{2+}] (0.2 mM-4 mM Ca^{2+}). First, after-contractions originated sporadically with no loss of overall TT. During this phase, the SR might still be able to compensate diastolic Ca^{2+} loss and maintain SR Ca^{2+} load. With increasing [Ca^{2+}], after-contractions were more pronounced, which was accompanied by a strong decrease in TT. This might originate from improper diastolic SR filling due to massive diastolic Ca^{2+} loss.[47] Unfortunately, standard methods for the estimation of SR Ca^{2+} load (e.g. by the rapid application of high doses caffeine or rapid cooling to 4°C) were unsuccessful, as the diffusion into the tissue might take to long for homogeneous effects. Additionally, β-AR stimulation with isoproterenol (Iso) sensitized EHT to much lower Ca^{2+} concentrations ($EC50_{Ca}$=1.8 mM Ca^{2+}, $EC50_{Iso}$=0.7 mM Ca^{2+}). β-AR stimulation is known to further increase SR Ca^{2+} load, promoting SOICR and supporting the diastolic Ca^{2+} leak.[86] Knowing this underlying mechanism in single cells and the combined treatment with anti-arrhythmic drugs argue for SOICR as basis for the origin of after-contractions.

All in all, this model showed a simple and robust induction of after-contractions that will be useful in evaluating potential therapeutic anti-arrhythmic approaches.

5.2 Validation of S100A1's therapeutic potential in normal and failing EHT

Therapeutic effects of S100A1 have been demonstrated in different studies *in vivo* and *in vitro*.[133-135, 137-139, 141, 145, 146] So why use another model to investigate S100A1 effects if different *in vivo* and *in vitro* models are available and therapeutic effects have already been shown? Animal models are great to demonstrate efficacy of therapeutic interventions and to investigate if side effect or compensatory mechanisms take place. Yet, when it comes down to the identification of the underlying mechanism, the whole body might be too complex to elucidate key mechanisms. Just the other way

around, i*n vitro* models are great to investigate cellular effects and decipher the exact mechanism, however if these mechanisms also take place in intact heart tissue remains elusive.
Thus, EHT represents an intermediate model, where the effects of S100A1 can be analyzed in a minimalistic system. Here, cells are cultivated under cyclic stretch and functional recordings are performed under isometric conditions. This allows analysis of functional effects as well as the breakdown of key mechanisms. Furthermore, novel therapeutic actions might be unveiled that cannot be seen in isolated cells and have not been uncovered *in vivo* yet.

5.2.1 S100A1 acts positive inotropic *and* anti-arrhythmic in EHT

Positive inotropic effects of S100A1 have been shown in various experimental HF models *in vivo* and *in vitro.*[133-135, 137-139, 141, 145, 146] Therefore, positive inotropic effects of S100A1 in EHT were first validated to show efficacy of adenoviral-mediated S100A1 gene transfer in this model.
As expected, S100A1 overexpression in normal EHT showed superior systolic contractility, which was preserved under Ca^{2+} and β-AR stimulation. Improved contraction duration (TTP) and relaxation (tau) were only seen at high [Ca^{2+}]. This might indicate that S100A1's effects are even more pronounced at high [Ca^{2+}]. S100A1 overexpression in failing EHT demonstrated normalized systolic contractility comparable to control EHT. Here, not effects on other contractility parameters were seen, but S100A1 normalized Ca^{2+} sensitivity of failing EHT.
Summarizing, S100A1 inotropy could be confirmed in this model, which demonstrates feasibility and efficacy of S100A1 gene transfer in EHT. Applying different inotropic stimulation (Ca^{2+} alone or combined β-AR/ Ca^{2+} stimulation) revealed that S100A1 acts on top of Ca^{2+}/ cAMP-dependent pathways.

The potential **anti-arrhythmic effect of S100A1** has only been shown in isolated adult CMs so far. A most recent study by Völkers et al. (unpublished data) demonstrated that adenoviral-mediated overexpression of S100A1 in normal and failing adult rat CMs was able to inhibit SOICR. This reduced the diastolic Ca^{2+} leak, which manifested in a diminished frequency of triggered Ca^{2+} sparks and Ca^{2+} waves.
Thus, the inhibition of after-contractions by S100A1 in normal and failing EHT was able to confirm and even extend these data: Manual counting of after-contractions after Ca^{2+} and β-AR stimulation was used to quantify susceptibly to triggered arrhythmias and subsequent calculation of EC50 allowed estimation of the therapeutic potential. Thus, S100A1 overexpression increased EC50 both after Ca^{2+} as well as after β-AR stimulation, suggesting enhanced resistance against Ca^{2+} triggered after-contractions.
Although failing EHT were much less sensitive to Ca^{2+}, S100A1 overexpression also prevented Ca^{2+} triggered after-contractions in these EHT. The reduced sensitivity of failing EHT to Ca^{2+} could originate from the great reduced contractile performance and the reduced expression of Ca^{2+} handling proteins.

This would lead to general reduced cytosolic Ca^{2+} uptake, reduced SR Ca^{2+} load and subsequently reduced $[Ca^{2+}]_i$, that would be too little to trigger after-contractions.

Previous experiments in isolated CM only used β-AR stimulation a stressor, focusing on the impact of S100A1 on diastolic Ca^{2+} handling after β-AR stimulation. In this study, experiments were conducted with exclusive Ca^{2+} stimulation as well as combined β-AR stimulation. This indicates that S100A1 does not rely on cAMP-dependent signal pathways but directly targets the Ca^{2+} mishandling.

For therapeutic purpose, it would be interesting to perform further pharmacological studies and test current anti-arrhythmic drugs that target different steps in the development of Ca^{2+} triggered arrhythmias against S100A1 and see if S100A1's effects are on top of other anti-arrhythmic drugs. However, these experiments were beyond the scope of this study.

5.2.2 S100A1 effects are independent of changes in contractile protein expression pattern

In previous studies, expression analyses yielded that S100A1-mediated effects on Ca^{2+} cycling and contractile performance did not result from an altered abundance of SR proteins, but changes in S100A1's target protein activity might account for these effects.[134, 137] Here, S100A1 overexpression also had no effect on the expression on major Ca^{2+} handling proteins in normal and failing EHT. More precisely, despite persistent changes in protein and mRNA expression pattern, S100A1 acted positive inotropic and anti-arrhythmic.

Anti-hypertrophic and anti-fibrotic effects of S100A1 have only been demonstrated *in vivo* so far and analysis in isolated cells could not confirm any anti-hypertrophic or -fibrotic effects of S100A1.[135, 138, 141] Therefore it can be assumed that feedback mechanisms, potentially by normalized catecholamine levels, most probably account for these effects *in vivo* which do not take place in isolated cells. In this study, S100A1 overexpression also had no effect on hypertrophic or fibrotic remodeling in EHT, as neurohumoral regulation does not take place in this model.

Although negligible in isolated cells, electrical coupling in intact tissue can have a major impact on electrical coupling, action potential propagation and the development of arrhythmias.[170] As depicted before, the recording of the electrical current was impossible in the organ bath setup and analysis with fluorescent dyes also failed. Thus, a more easy readout to measure electrical conductance in EHT was chosen: Cardiomyocytes are electrically coupled via gap junctions, which consist of Connexin43 (Cx43), Connexin40 and 50. Cx43 is the most abundant gap junction protein and altered expression, phosphorylation and localization have been linked to arrhythmogenesis.[170-172] Thus, analysis of Cx43 expression and phosphorylation pattern might shed light on the conduction properties in EHT. However, there were no changes neither in expression nor on the phosphorylation of Cx43 between normal and failing EHT and after S100A1 overexpression. Thus, changes in electrical coupling do mostly likely not account for the anti-arrhythmic effects of S100A1 in EHT.

5.3 Challenging current concepts for the development of Ca^{2+} triggered arrhythmias

5.3.1 S100A1 acts independent of PKA/CamKII signaling

Changes in local PKA- and CamKII signaling at the RyR2 have been made responsible for the development of cellular arrhythmias.[39, 74, 75, 198] Current research focusses on RyR2 phosphorylation by PKA (Ser-2808) and CamKII (Ser-2814) as important regulators of RyR2 function. In heart failure, hyperphosphorylation by both kinases is supposed to mediate the diastolic Ca^{2+} leak. However, not all groups have been able to reproduce these results and there is an ongoing debate which kinase is more important.[74, 75, 198, 199] Still, most researchers agree on the fact that RyR2 phosphorylation is important for its function.

Illuminating the impact of S100A1 on RyR2 phosphorylation showed no changes is phosphorylation patterns: In EHT, Ca^{2+} stimulation activated exclusively CamKII as analyzed by phosphorylation of PLB Thr-17 and RyR2 Ser-2814 in normal EHT. Failing EHT showed not increase in PLB Thr-17 under basal conditions, however PLB Thr-17 phosphorylation was exaggerated after Ca^{2+} stimulation, indicating enhanced CamKII activity in failing EHT. Still, S100A overexpression had no effect on PLB phosphorylation pattern. As analysis of RyR2 phosphorylation in failing EHT was difficult to perform due to low abundance of the RyR2, the PLB phospho-signature was extrapolated and it is assumed that S100A1 also has no effect on RyR2 phosphorylation in failing EHT. To test the effects of S100A1 overexpression on combined β-AR/Ca^{2+} stimulation, analysis in normal EHT were repeated with both stimulations. Again, there were no changes in RyR2 and PLB phosphorylation pattern after S100A1 overexpression, so these experiments were not repeated in failing EHT. In ACM, similar effects were seen with β-AR stimulation. According to this, S100A1 does not change PKA- and CamKII-mediated phosphorylation pattern in isolated cells.

In this study, the expression of phosphatases (eg. PP1 and PP2a) and their activity was not analyzed. So it remains unclear if S100A1 has a direct impact on their activity. However, as S100A1 overexpression did not change phosphorylation patterns of their targets it can be assumed that their activity did not change. In a very unlikely situation, phosphatase and kinase activity could both be regulated by S100A1; however net effects (phosphorylation pattern) would not change and therefore this more theoretical concept can be neglected.

Summarizing, these experiments indicate that S100A1's inotropic and anti-arrhythmic effects do not rely on PKA/CamKII signaling but that S100A1 acts independent on phospho-dependent changes. This challenges current anti-arrhythmic concepts, which assume normalized RyR2 phosphorylation as prerequisite for proper RyR2 function and anti-arrhythmic effects.

5.3.2 Regulating the RyR2 macrocomplex - S100A1/RyR2 interaction as key for anti-arrhythmic effects

As described before, the RyR2 is one of the largest ion channels that is tightly regulated not only by phosphorylation but also by the binding of accessory proteins. These are supposed to mediate channel opening and further regulate short- and long-term channel activity.[71, 200]

Currents concepts argue for a major role of **FKBP12.6** in the development of Ca^{2+} triggered arrhythmias. In combination with RyR2 Ser-2808 hyperphosphorylation, FKBP12.6 dissociation is supposed to increase the diastolic Ca^{2+} leak.[74, 75, 81, 83, 198, 201]
Supporting this notion, Vinet et al. demonstrated that transgenic overexpression of FKB12.6 protected against triggered ventricular tachycardia *in vivo*.[202] However, latest research by Galfré et al. (2012) and Zissimopoulos et al. provided evidence that not only FKBP12.6, but also its isoform FKBP regulates RyR2 channel opening and that their stoichiometry might be species dependent.[203, 204] This fact would also explain the differential outcome of *in vivo* and *in vitro* studies, using mice and isolated rat, sheep or pig sarcoplasmic reticulum vesicles respectively. In rat CMs, FKBP12.6 is supposed to be the predominant isoform.[204]
In this study, FKBP12.6 binding properties were analyzed in intact isolated rat ACM with the proximity ligation assay (PLA) technology, which has been demonstrated to be a reliable method to detect protein-protein interaction. Iso stimulation, which was shown to increases RyR Ser-2808 and Ser-2814 phosphorylation, was applied. Interestingly, FKBP12.6 binding did not change under β-AR stimulation nor after S100A1 overexpression. Thus, S100A1 overexpression has no effect on FKBP12.6 binding. So far, this study also does not support the hypothesis that RyR2 Ser-2808 phosphorylation is the major trigger for FKBP12.6 dissociation but that other factors might mediate this effect. It could also be that FKBP12.6/RyR2 interaction is not dynamic and that dissociation only occurs with chronic or long-term stimulation.

Sorcin is a general inhibitor of the RyR2, reducing Ca^{2+} transients and decreasing Ca^{2+} spark frequency.[97-99] Interestingly, this study revealed that sorcin binding to the RyR2 was slightly increased after β-AR stimulation; however, S100A1 overexpression had no impact on sorcin binding. Interestingly, Anthony et al. and Lokuta et al. provided evidence that sorcin can be phoyphorylated by both CamKII and PKA, thereby losing its inhibitory effect on the RyR2 despite persistent binding.[96, 205] Thus, it is rather speculating that activated CamKII and PKA (which has been demonstrated in this study by increased RyR Ser-2814 and Ser-2808 phosphorylation) phosphorylated sorcin. However, this does not explain the increased sorcin/RyR2 interaction after β-AR stimulation. As sorcin was reported to translocate quickly upon increasing $[Ca^{2+}]_i$, from the cytosol to the membrane, it might also be possible that increasing $[Ca^{2+}]$ rather increases sorcin binding to the RyR2, coordinating EC coupling.[97]

CaM binding to the RyR2 is supposed to occur rather static although CaM affinity is supposed to decline with decreasing [Ca^{2+}].[71, 92, 93] The binding site of CaM to cardiac as well as skeletal RyR is well defined, however shows distinct discrepancies: In skeletal muscle, CaM binding to RyR1 is Ca^{2+} dependent and apoCaM (Ca^{2+}-free CaM) and CaM show different affinities for the RyR1.[71, 206, 207] Additionally, structural studies suggest that S100A1 competes for the same binding site as CaM.[208] In cardiac muscle, CaM decreases RyR2 opening at all [Ca^{2+}].[71, 91, 92] Previous reports suggested that S100A1 binds to the same binding domain as CaM, however fluorescence resonance energy transfer (FRET) studies point towards differential binding sites of S100A1 and CaM (unpublished data).[209] This study indicates that S100A1 has no impact on CaM binding to the RyR2 neither under basal condition nor after β-AR stimulation. However, this must not necessarily mean that S100A1 and CaM have distinct binding sites but can have other reasons: 1) Comprehensive data suggests that CaM interacts with the RyR2 in 1:1 ratio, thus every RyR2 tetramer is loaded with 4 molecules CaM, although only 1 CaM/RyR2 is necessary for proper channel inhibition.[92] The ratio of S100A1:RyR2 remains elusive. However, these studies could overestimate the CaM/RyR2 ratio and it might be possible that only a subset of RyR2 is loaded with CaM. Assumed that only 20% of RyR2 are loaded with S100A1 and a 5-fold overexpression doubles S100A1/RyR2 interaction (40%), 60% of RyR2 might be loaded with CaM under physiological conditions. However, if the majority (50% or more) of RyR2 is loaded with S100A1, doubling this interactions would leave no space for CaM/RyR2 interaction. Thus, CaM/RyR2 needs to be lower than estimated if S100A1 competes for the same binding site or S100A1/RyR2 interaction needs to be extremely low. 2) S100A1 has a distinct binding site that is allosterically regulated by CaM. In this scenario, CaM and S100A1 binding would be dependent on each other but binding ratio would not interfere directly. However, a current work demonstrated that mutating one amino acid (aa) in the CaM binding site on the RyR2 distracts S100A1 effects on RyR2 P_o.[209] Still, there is no evidence about how this mutation affects channel structure and this might disturb S100A1/RyR2 interaction due to structural changes. Therefore, it will become quite interesting to identify the exact binding site of S100A1 on the RyR2 and to determine the exact binding stoichiometry.

In summary, S100A1 overexpression had no impact on the binding of accessory proteins to the RyR2 and thus changes in their binding properties do most likely not account for S100A1's effect. In line with this conclusion, a most recent study demonstrated that recombinant S100A1 reduced RyR P_o in lipid bilayers.[209] Thus, increased **S100A1/RyR2 interaction** might indeed reduce the diastolic Ca^{2+} leak and prevent Ca^{2+} triggered arrhythmias.

Expanding current theories for the regulation of RyR2, **redox-modifications** have come to fore as novel mediator of RyR2 activity.[87, 101, 102, 108, 109] However, analyzing their effects is not easy and it is important not only to consider one redox-modifications, but the whole spectrum as they are highly interactive and mostly dependent on each other.[210] In this study, quiescent cardiomyocytes were used and physiological amounts of Iso used for a short-term stimulation. This is not supposed to have

oxidative effects but rather increase cell activity in a physiological manner.[104] In failing CMs, the situation becomes more complex, as oxidation already takes place under basal conditions.[108] Still, S100A1 positive effects have also been seen in quiescent cells with physiological β-AR stimulation. Thus, effects seen in this state might also hold true in failing cells.

In this study, RyR2 s-nitrosylation (SNO) was analyzed with the PLA technology, which allows to specifically detect nitrosylated RyR2, as an unspecific nitro-antibody is linked to the RyR2-antibody. RyR2-SNO has been reported to increase RyR2 channel P_O in lipid bilayer recordings.[101, 107] In contrast, NOS1 knock-out mice demonstrated reduced RyR2-SNO and an increased diastolic Ca^{2+} leak.[102] However, oxidation of RyR2 was also increased in this study, which underlines the interaction of different redox-modifications. In failing hearts, reduced RyR2-SNO is also a results of increased oxidation, contributing to the diastolic Ca^{2+} leak.[103, 105, 108]

Here, β-AR increased RyR-SNO. As oxidation is supposed to reduce RyR2-SNO, Iso stimulation might not be oxidative in this setting.[104] Interestingly, S100A1 overexpression had no impact on RyR2-SNO under basal conditions, however, it blunted the increase in RyR2-SNO after Iso stimulation.

For the first time, this study demonstrates that S100A1 has an impact of protein modifications as RyR2-SNO. However, the reason for this effects might be pleiotropic and are beyond of the scope of this work.

5.4 Conclusion and Outlook

While the results presented in this work are far from providing a complete understanding of the mechanistic properties of S100A1's action in CM, they substantially extend our knowledge about S100A1's actions:

S100A1 anti-arrhythmic properties could be confirmed in a 3-dimensional tissue culture model and will most probably also account for anti-arrhythmic effects *in vivo*.

With regard to its mechanism, this study clearly demonstrated that S100A1 does not rely on phospho-dependent changes at the RyR2 nor on the differential binding of accessory proteins but that enhanced binding of S100A1 to the RyR2 will most probably account for its effects. This is contrary to the current understanding of the mechanism of anti-arrhythmic therapies, which assume normalization of phosphorylation-dependent changes at the RyR2 and restoration of complex formation with accessory proteins as prerequisite for anti-arrhythmic effects. However, this study also indicated that enhanced S100A1/RyR2 stoichiometry might furthermore be responsible for redox-dependent modifications of the RyR2.

Still, some questions from this study remain unanswered:

- Where is the binding site for S100A1 on the RyR2 and what is the binding ratio of S100A1:RyR2?
- How does S100A1 change RyR2 nitrosylation? Is this a direct effect and due to changes in redox-enzymes or is this due to general improved redox-balance in the cell?
- Are S100A1's effects dependent on its own redox-changes (e.g. changes in nitrosylation)?

Answering these questions will help us to even better understand S100A1's effect in cardiomyocytes, however they will be the goal of future studies.

6 References

1. (AHA), A.H.A., *Cardiovascular Disease Statistics.* 2010.
2. (WHO), W.H.O., *Fact Sheet No 317.* 2009.
3. Hunt, S.A., et al., *ACC/AHA guidelines for the evaluation and management of chronic heart failure in the adult: executive summary. A report of the American College of Cardiology/American Heart Association Task Force on Practice Guidelines (Committee to revise the 1995 Guidelines for the Evaluation and Management of Heart Failure).* J Am Coll Cardiol, 2001. **38**(7): p. 2101-13.
4. Ho, K.K., et al., *The epidemiology of heart failure: the Framingham Study.* J Am Coll Cardiol, 1993. **22**(4 Suppl A): p. 6A-13A.
5. Berridge, M.J., M.D. Bootman, and P. Lipp, *Calcium--a life and death signal.* Nature, 1998. **395**(6703): p. 645-8.
6. Berridge, M.J., P. Lipp, and M.D. Bootman, *The versatility and universality of calcium signalling.* Nat Rev Mol Cell Biol, 2000. **1**(1): p. 11-21.
7. Kretsinger, R.H., *Calcium-binding proteins.* Annu Rev Biochem, 1976. **45**: p. 239-66.
8. Berridge, M., P. Lipp, and M. Bootman, *Calcium signalling.* Curr Biol, 1999. **9**(5): p. R157-9.
9. Berridge, M.J., *Remodelling Ca2+ signalling systems and cardiac hypertrophy.* Biochem Soc Trans, 2006. **34**(Pt 2): p. 228-31.
10. Bootman, M.D., et al., *Calcium signalling--an overview.* Semin Cell Dev Biol, 2001. **12**(1): p. 3-10.
11. Berridge, M.J., *Calcium microdomains: organization and function.* Cell Calcium, 2006. **40**(5-6): p. 405-12.
12. Berridge, M.J., M.D. Bootman, and H.L. Roderick, *Calcium signalling: dynamics, homeostasis and remodelling.* Nat Rev Mol Cell Biol, 2003. **4**(7): p. 517-29.
13. Kretsinger, R.H., *Structure and evolution of calcium-modulated proteins.* CRC Crit Rev Biochem, 1980. **8**(2): p. 119-74.
14. Kretsinger, R.H., *Evolution and function of calcium-binding proteins.* Int Rev Cytol, 1976. **46**: p. 323-93.
15. Kretsinger, R.H., *The informational role of calcium in the cytosol.* Adv Cyclic Nucleotide Res, 1979. **11**: p. 1-26.
16. Kretsinger, R.H. and N.D. Moncrief, *Evolution of calcium modulated proteins.* Va Explor, 1989. **5**(5): p. 7-9.
17. Bers, D.M., *Excitation-Contraction Coupling and Cardiac Contractile Force.* Kluwer Academic Publishers, 2001. **Second Edition**: p. Chapter 1 Ultrastructure
18. Bers, D.M., *Cardiac excitation-contraction coupling.* Nature, 2002. **415**(6868): p. 198-205.

19. Lehnart, S.E., et al., *Stabilization of cardiac ryanodine receptor prevents intracellular calcium leak and arrhythmias.* Proc Natl Acad Sci U S A, 2006. **103**(20): p. 7906-10.
20. Lompre, A.M., M. Anger, and D. Levitsky, *Sarco(endo)plasmic reticulum calcium pumps in the cardiovascular system: function and gene expression.* J Mol Cell Cardiol, 1994. **26**(9): p. 1109-21.
21. Robertson, S.P., et al., *The effect of troponin I phosphorylation on the Ca2+-binding properties of the Ca2+-regulatory site of bovine cardiac troponin.* J Biol Chem, 1982. **257**(1): p. 260-3.
22. Wehrens, X.H., et al., *FKBP12.6 deficiency and defective calcium release channel (ryanodine receptor) function linked to exercise-induced sudden cardiac death.* Cell, 2003. **113**(7): p. 829-40.
23. Wehrens, X.H. and A.R. Marks, *Altered function and regulation of cardiac ryanodine receptors in cardiac disease.* Trends Biochem Sci, 2003. **28**(12): p. 671-8.
24. Fabiato, A. and F. Fabiato, *Contractions induced by a calcium-triggered release of calcium from the sarcoplasmic reticulum of single skinned cardiac cells.* J Physiol, 1975. **249**(3): p. 469-95.
25. Bers, D.M. and V.M. Stiffel, *Ratio of ryanodine to dihydropyridine receptors in cardiac and skeletal muscle and implications for E-C coupling.* Am J Physiol, 1993. **264**(6 Pt 1): p. C1587-93.
26. Cheng, H. and W.J. Lederer, *Calcium sparks.* Physiol Rev, 2008. **88**(4): p. 1491-545.
27. Marx, S.O., et al., *Coupled gating between cardiac calcium release channels (ryanodine receptors).* Circ Res, 2001. **88**(11): p. 1151-8.
28. Huxley, H.E., *Sliding filaments and molecular motile systems.* J Biol Chem, 1990. **265**(15): p. 8347-50.
29. Laver, D.R., et al., *Termination of calcium-induced calcium release by induction decay: an emergent property of stochastic channel gating and molecular scale architecture.* J Mol Cell Cardiol, 2013. **54**: p. 98-100.
30. Ruegg, J.C., *Towards a molecular understanding of contractility.* Cardioscience, 1990. **1**(3): p. 163-8.
31. Tada, M., et al., *Calcium transport by cardiac sarcoplasmic reticulum and phosphorylation of phospholamban.* Mol Cell Biochem, 1982. **46**(2): p. 73-95.
32. Delbridge, L.M., J.W. Bassani, and D.M. Bers, *Steady-state twitch Ca2+ fluxes and cytosolic Ca2+ buffering in rabbit ventricular myocytes.* Am J Physiol, 1996. **270**(1 Pt 1): p. C192-9.
33. Dibb, K.M., D.A. Eisner, and A.W. Trafford, *Regulation of systolic [Ca2+]i and cellular Ca2+ flux balance in rat ventricular myocytes by SR Ca2+, L-type Ca2+ current and diastolic [Ca2+]i.* J Physiol, 2007. **585**(Pt 2): p. 579-92.
34. Tada, M. and T. Toyofuku, *SR Ca(2+)-ATPase/phospholamban in cardiomyocyte function.* J Card Fail, 1996. **2**(4 Suppl): p. S77-85.

35. Sato, D. and D.M. Bers, *How does stochastic ryanodine receptor-mediated Ca leak fail to initiate a Ca spark?* Biophys J, 2011. **101**(10): p. 2370-9.
36. Ly, H., et al., *Gene therapy in the treatment of heart failure.* Physiology (Bethesda), 2007. **22**: p. 81-96.
37. Pogwizd, S.M., et al., *Arrhythmogenesis and contractile dysfunction in heart failure: Roles of sodium-calcium exchange, inward rectifier potassium current, and residual beta-adrenergic responsiveness.* Circ Res, 2001. **88**(11): p. 1159-67.
38. Knollmann, B.C. and D.M. Roden, *A genetic framework for improving arrhythmia therapy.* Nature, 2008. **451**(7181): p. 929-36.
39. Lehnart, S.E., et al., *Cardiac ryanodine receptor function and regulation in heart disease.* Ann N Y Acad Sci, 2004. **1015**: p. 144-59.
40. Dixit, S.S., et al., *Effects of CaMKII-mediated phosphorylation of ryanodine receptor type 2 on islet calcium handling, insulin secretion, and glucose tolerance.* PLoS One, 2013. **8**(3): p. e58655.
41. Mazzini, G.S., et al., *The ischemic rat heart releases S100B.* Life Sci, 2005. **77**(8): p. 882-9.
42. Kranias, E.G. and R.J. Solaro, *Phosphorylation of troponin I and phospholamban during catecholamine stimulation of rabbit heart.* Nature, 1982. **298**(5870): p. 182-4.
43. Witcher, D.R., et al., *Unique phosphorylation site on the cardiac ryanodine receptor regulates calcium channel activity.* J Biol Chem, 1991. **266**(17): p. 11144-52.
44. Marx, S.O., et al., *PKA phosphorylation dissociates FKBP12.6 from the calcium release channel (ryanodine receptor): defective regulation in failing hearts.* Cell, 2000. **101**(4): p. 365-76.
45. Bers, D.M. and E. Grandi, *Calcium/calmodulin-dependent kinase II regulation of cardiac ion channels.* J Cardiovasc Pharmacol, 2009. **54**(3): p. 180-7.
46. Wehrens, X.H., et al., *Ca2+/calmodulin-dependent protein kinase II phosphorylation regulates the cardiac ryanodine receptor.* Circ Res, 2004. **94**(6): p. e61-70.
47. Houser, S.R., V. Piacentino, 3rd, and J. Weisser, *Abnormalities of calcium cycling in the hypertrophied and failing heart.* J Mol Cell Cardiol, 2000. **32**(9): p. 1595-607.
48. Hobai, I.A. and B. O'Rourke, *Decreased sarcoplasmic reticulum calcium content is responsible for defective excitation-contraction coupling in canine heart failure.* Circulation, 2001. **103**(11): p. 1577-84.
49. Wasserstrom, J.A., et al., *Multiple defects in intracellular calcium cycling in whole failing rat heart.* Circ Heart Fail, 2009. **2**(3): p. 223-32.
50. Belevych, A., et al., *Enhanced ryanodine receptor-mediated calcium leak determines reduced sarcoplasmic reticulum calcium content in chronic canine heart failure.* Biophys J, 2007. **93**(11): p. 4083-92.

51. Piacentino, V., 3rd, et al., *Modulation of contractility in failing human myocytes by reverse-mode Na/Ca exchange.* Ann N Y Acad Sci, 2002. **976**: p. 466-71.
52. Hasenfuss, G. and B. Pieske, *Calcium cycling in congestive heart failure.* J Mol Cell Cardiol, 2002. **34**(8): p. 951-69.
53. Schwinger, R.H., et al., *Reduced Ca(2+)-sensitivity of SERCA 2a in failing human myocardium due to reduced serin-16 phospholamban phosphorylation.* J Mol Cell Cardiol, 1999. **31**(3): p. 479-91.
54. Hobai, I.A. and B. O'Rourke, *Enhanced Ca(2+)-activated Na(+)-Ca(2+) exchange activity in canine pacing-induced heart failure.* Circ Res, 2000. **87**(8): p. 690-8.
55. Marks, A.R., *Cardiac intracellular calcium release channels: role in heart failure.* Circ Res, 2000. **87**(1): p. 8-11.
56. Kilter, H. and M. Bohm, *[From hypertension to heart failure-a pathophysiological continuum].* Herz, 2004. **29**(3): p. 239-47.
57. Shannon, T.R., S.M. Pogwizd, and D.M. Bers, *Elevated sarcoplasmic reticulum Ca2+ leak in intact ventricular myocytes from rabbits in heart failure.* Circ Res, 2003. **93**(7): p. 592-4.
58. Venetucci, L.A., et al., *Reducing ryanodine receptor open probability as a means to abolish spontaneous Ca2+ release and increase Ca2+ transient amplitude in adult ventricular myocytes.* Circ Res, 2006. **98**(10): p. 1299-305.
59. Venetucci, L.A., A.W. Trafford, and D.A. Eisner, *Increasing ryanodine receptor open probability alone does not produce arrhythmogenic calcium waves: threshold sarcoplasmic reticulum calcium content is required.* Circ Res, 2007. **100**(1): p. 105-11.
60. Aistrup, G.L., et al., *Pacing-induced heterogeneities in intracellular Ca2+ signaling, cardiac alternans, and ventricular arrhythmias in intact rat heart.* Circ Res, 2006. **99**(7): p. e65-73.
61. Wasserstrom, J.A., et al., *Variability in timing of spontaneous calcium release in the intact rat heart is determined by the time course of sarcoplasmic reticulum calcium load.* Circ Res. **107**(9): p. 1117-26.
62. Brunello, L., et al., *Decreased RyR2 refractoriness determines myocardial synchronization of aberrant Ca2+ release in a genetic model of arrhythmia.* Proc Natl Acad Sci U S A, 2013. **110**(25): p. 10312-7.
63. Nattel, S., et al., *Arrhythmogenic ion-channel remodeling in the heart: heart failure, myocardial infarction, and atrial fibrillation.* Physiol Rev, 2007. **87**(2): p. 425-56.
64. Venetucci, L.A., et al., *Na/Ca exchange: regulator of intracellular calcium and source of arrhythmias in the heart.* Ann N Y Acad Sci, 2007. **1099**: p. 315-25.
65. Fujiwara, K., et al., *Burst emergence of intracellular Ca2+ waves evokes arrhythmogenic oscillatory depolarization via the Na+-Ca2+ exchanger: simultaneous confocal recording of membrane potential and intracellular Ca2+ in the heart.* Circ Res, 2008. **103**(5): p. 509-18.

66. Wang, Y. and J.A. Hill, *Electrophysiological remodeling in heart failure.* J Mol Cell Cardiol, 2010. **48**(4): p. 619-32.

67. Beuckelmann, D.J., M. Nabauer, and E. Erdmann, *Intracellular calcium handling in isolated ventricular myocytes from patients with terminal heart failure.* Circulation, 1992. **85**(3): p. 1046-55.

68. Houser, S.R., *Can novel therapies for arrhythmias caused by spontaneous sarcoplasmic reticulum Ca2+ release be developed using mouse models?* Circ Res, 2005. **96**(10): p. 1031-2.

69. Pogwizd, S.M., J.P. McKenzie, and M.E. Cain, *Mechanisms underlying spontaneous and induced ventricular arrhythmias in patients with idiopathic dilated cardiomyopathy.* Circulation, 1998. **98**(22): p. 2404-14.

70. Lanner, J.T., et al., *Ryanodine receptors: structure, expression, molecular details, and function in calcium release.* Cold Spring Harb Perspect Biol, 2010. **2**(11): p. a003996.

71. Bers, D.M., *Macromolecular complexes regulating cardiac ryanodine receptor function.* J Mol Cell Cardiol, 2004. **37**(2): p. 417-29.

72. Hohenegger, M. and J. Suko, *Phosphorylation of the purified cardiac ryanodine receptor by exogenous and endogenous protein kinases.* Biochem J, 1993. **296 (Pt 2)**: p. 303-8.

73. Yoshida, A., et al., *Phosphorylation of ryanodine receptors in rat myocytes during beta-adrenergic stimulation.* J Biochem, 1992. **111**(2): p. 186-90.

74. Shan, J., et al., *Role of chronic ryanodine receptor phosphorylation in heart failure and beta-adrenergic receptor blockade in mice.* J Clin Invest, 2010. **120**(12): p. 4375-87.

75. Shan, J., et al., *Phosphorylation of the ryanodine receptor mediates the cardiac fight or flight response in mice.* J Clin Invest, 2010. **120**(12): p. 4388-98.

76. Xiao, B., et al., *Characterization of a novel PKA phosphorylation site, serine-2030, reveals no PKA hyperphosphorylation of the cardiac ryanodine receptor in canine heart failure.* Circ Res, 2005. **96**(8): p. 847-55.

77. Huke, S. and D.M. Bers, *Ryanodine receptor phosphorylation at Serine 2030, 2808 and 2814 in rat cardiomyocytes.* Biochem Biophys Res Commun, 2008. **376**(1): p. 80-5.

78. Anderson, M.E., *Multiple downstream proarrhythmic targets for calmodulin kinase II: moving beyond an ion channel-centric focus.* Cardiovasc Res, 2007. **73**(4): p. 657-66.

79. Kohlhaas, M., et al., *Increased sarcoplasmic reticulum calcium leak but unaltered contractility by acute CaMKII overexpression in isolated rabbit cardiac myocytes.* Circ Res, 2006. **98**(2): p. 235-44.

80. Wehrens, X.H., et al., *Ryanodine receptor/calcium release channel PKA phosphorylation: a critical mediator of heart failure progression.* Proc Natl Acad Sci U S A, 2006. **103**(3): p. 511-8.

81. Wehrens, X.H., et al., *Protection from cardiac arrhythmia through ryanodine receptor-stabilizing protein calstabin2.* Science, 2004. **304**(5668): p. 292-6.

82. Lehnart, S.E., et al., *Sudden death in familial polymorphic ventricular tachycardia associated with calcium release channel (ryanodine receptor) leak.* Circulation, 2004. **109**(25): p. 3208-14.

83. Bers, D.M., *Ryanodine receptor S2808 phosphorylation in heart failure: smoking gun or red herring.* Circ Res, 2012. **110**(6): p. 796-9.

84. Belevych, A.E., et al., *Shortened Ca2+ signaling refractoriness underlies cellular arrhythmogenesis in a postinfarction model of sudden cardiac death.* Circ Res, 2012. **110**(4): p. 569-77.

85. Belevych, A.E., et al., *The relationship between arrhythmogenesis and impaired contractility in heart failure: role of altered ryanodine receptor function.* Cardiovasc Res, 2011. **90**(3): p. 493-502.

86. Curran, J., et al., *Beta-adrenergic enhancement of sarcoplasmic reticulum calcium leak in cardiac myocytes is mediated by calcium/calmodulin-dependent protein kinase.* Circ Res, 2007. **100**(3): p. 391-8.

87. Gonano, L.A., et al., *Calcium-calmodulin kinase II mediates digitalis-induced arrhythmias.* Circ Arrhythm Electrophysiol, 2011. **4**(6): p. 947-57.

88. Zhang, H., et al., *Hyperphosphorylation of the cardiac ryanodine receptor at serine 2808 is not involved in cardiac dysfunction after myocardial infarction.* Circ Res, 2012. **110**(6): p. 831-40.

89. Franzini-Armstrong, C., L.J. Kenney, and E. Varriano-Marston, *The structure of calsequestrin in triads of vertebrate skeletal muscle: a deep-etch study.* J Cell Biol, 1987. **105**(1): p. 49-56.

90. Zhang, L., et al., *Complex formation between junctin, triadin, calsequestrin, and the ryanodine receptor. Proteins of the cardiac junctional sarcoplasmic reticulum membrane.* J Biol Chem, 1997. **272**(37): p. 23389-97.

91. Yamaguchi, N., et al., *Molecular basis of calmodulin binding to cardiac muscle Ca(2+) release channel (ryanodine receptor).* J Biol Chem, 2003. **278**(26): p. 23480-6.

92. Balshaw, D.M., et al., *Calmodulin binding and inhibition of cardiac muscle calcium release channel (ryanodine receptor).* J Biol Chem, 2001. **276**(23): p. 20144-53.

93. Yamaguchi, N., et al., *Early cardiac hypertrophy in mice with impaired calmodulin regulation of cardiac muscle Ca release channel.* J Clin Invest, 2007. **117**(5): p. 1344-53.

94. Guo, T., et al., *Kinetics of FKBP12.6 binding to ryanodine receptors in permeabilized cardiac myocytes and effects on Ca sparks.* Circ Res, 2010. **106**(11): p. 1743-52.

95. Huang, F., et al., *Analysis of calstabin2 (FKBP12.6)-ryanodine receptor interactions: rescue of heart failure by calstabin2 in mice.* Proc Natl Acad Sci U S A, 2006. **103**(9): p. 3456-61.

96. Lokuta, A.J., et al., *Modulation of cardiac ryanodine receptors by sorcin.* J Biol Chem, 1997. **272**(40): p. 25333-8.

97. Farrell, E.F., et al., *Sorcin inhibits calcium release and modulates excitation-contraction coupling in the heart.* J Biol Chem, 2003. **278**(36): p. 34660-6.

98. Farrell, E.F., et al., *Regulation of cardiac excitation-contraction coupling by sorcin, a novel modulator of ryanodine receptors.* Biol Res, 2004. **37**(4): p. 609-12.

99. Seidler, T., et al., *Effects of adenovirus-mediated sorcin overexpression on excitation-contraction coupling in isolated rabbit cardiomyocytes.* Circ Res, 2003. **93**(2): p. 132-9.

100. Eager, K.R. and A.F. Dulhunty, *Cardiac ryanodine receptor activity is altered by oxidizing reagents in either the luminal or cytoplasmic solution.* J Membr Biol, 1999. **167**(3): p. 205-14.

101. Xu, L., et al., *Activation of the cardiac calcium release channel (ryanodine receptor) by poly-S-nitrosylation.* Science, 1998. **279**(5348): p. 234-7.

102. Gonzalez, D.R., et al., *Deficient ryanodine receptor S-nitrosylation increases sarcoplasmic reticulum calcium leak and arrhythmogenesis in cardiomyocytes.* Proc Natl Acad Sci U S A, 2007. **104**(51): p. 20612-7.

103. Gonzalez, D.R., et al., *Impaired S-nitrosylation of the ryanodine receptor caused by xanthine oxidase activity contributes to calcium leak in heart failure.* J Biol Chem, 2010. **285**(37): p. 28938-45.

104. Bovo, E., S.L. Lipsius, and A.V. Zima, *Reactive oxygen species contribute to the development of arrhythmogenic Ca(2)(+) waves during beta-adrenergic receptor stimulation in rabbit cardiomyocytes.* J Physiol, 2012. **590**(Pt 14): p. 3291-304.

105. Cutler, M.J., et al., *Aberrant S-nitrosylation mediates calcium-triggered ventricular arrhythmia in the intact heart.* Proc Natl Acad Sci U S A, 2012. **109**(44): p. 18186-91.

106. Donoso, P., et al., *Modulation of cardiac ryanodine receptor activity by ROS and RNS.* Front Biosci, 2011. **16**: p. 553-67.

107. Lim, G., et al., *Does nitric oxide modulate cardiac ryanodine receptor function? Implications for excitation-contraction coupling.* Cardiovasc Res, 2008. **77**(2): p. 256-64.

108. Terentyev, D., et al., *Redox modification of ryanodine receptors contributes to sarcoplasmic reticulum Ca2+ leak in chronic heart failure.* Circ Res, 2008. **103**(12): p. 1466-72.

109. Xie, H. and P.H. Zhu, *Biphasic modulation of ryanodine receptors by sulfhydryl oxidation in rat ventricular myocytes.* Biophys J, 2006. **91**(8): p. 2882-91.

110. Yano, M., *Ryanodine receptor as a new therapeutic target of heart failure and lethal arrhythmia.* Circ J, 2008. **72**(4): p. 509-14.

111. Mohler, P.J. and X.H. Wehrens, *Mechanisms of human arrhythmia syndromes: abnormal cardiac macromolecular interactions.* Physiology (Bethesda), 2007. **22**: p. 342-50.

112. Donato, R., *Functional roles of S100 proteins, calcium-binding proteins of the EF-hand type.* Biochim Biophys Acta, 1999. **1450**(3): p. 191-231.

113. Donato, R., *Intracellular and extracellular roles of S100 proteins.* Microsc Res Tech, 2003. **60**(6): p. 540-51.

114. Osterloh, D., V.V. Ivanenkov, and V. Gerke, *Hydrophobic residues in the C-terminal region of S100A1 are essential for target protein binding but not for dimerization.* Cell Calcium, 1998. **24**(2): p. 137-51.
115. Wright, N.T., et al., *S100A1: Structure, Function, and Therapeutic Potential.* Curr Chem Biol, 2009. **3**(2): p. 138-145.
116. Goch, G., et al., *Affinity of S100A1 protein for calcium increases dramatically upon glutathionylation.* FEBS J, 2005. **272**(10): p. 2557-65.
117. Zhukov, I., A. Ejchart, and A. Bierzynski, *Structural and motional changes induced in apo-S100A1 protein by the disulfide formation between its Cys 85 residue and beta-mercaptoethanol.* Biochemistry, 2008. **47**(2): p. 640-50.
118. Zhukova, L., et al., *Redox modifications of the C-terminal cysteine residue cause structural changes in S100A1 and S100B proteins.* Biochim Biophys Acta, 2004. **1742**(1-3): p. 191-201.
119. Lenarcic Zivkovic, M., et al., *Post-translational S-nitrosylation is an endogenous factor fine tuning the properties of human S100A1 protein.* J Biol Chem, 2012. **287**(48): p. 40457-70.
120. Haimoto, H. and K. Kato, *S100a0 (alpha alpha) protein in cardiac muscle. Isolation from human cardiac muscle and ultrastructural localization.* Eur J Biochem, 1988. **171**(1-2): p. 409-15.
121. Maco, B., et al., *Ultrastructural distribution of the S100A1 Ca2+-binding protein in the human heart.* Physiol Res, 2001. **50**(6): p. 567-74.
122. Kato, K. and S. Kimura, *S100ao (alpha alpha) protein is mainly located in the heart and striated muscles.* Biochim Biophys Acta, 1985. **842**(2-3): p. 146-50.
123. Kato, K., et al., *S100a0 (alpha alpha) protein: distribution in muscle tissues of various animals and purification from human pectoral muscle.* J Neurochem, 1986. **46**(5): p. 1555-60.
124. Pleger, S.T., et al., *Endothelial S100A1 modulates vascular function via nitric oxide.* Circ Res, 2008. **102**(7): p. 786-94.
125. Ritterhoff, J. and P. Most, *Targeting S100A1 in heart failure.* Gene Ther, 2012.
126. Boerries, M., et al., *Ca2+ -dependent interaction of S100A1 with F1-ATPase leads to an increased ATP content in cardiomyocytes.* Mol Cell Biol, 2007. **27**(12): p. 4365-73.
127. Brezova, A., C.W. Heizmann, and B. Uhrik, *Immunocytochemical localization of S100A1 in mitochondria on cryosections of the rat heart.* Gen Physiol Biophys, 2007. **26**(2): p. 143-9.
128. Heierhorst, J., et al., *Ca2+/S100 regulation of giant protein kinases.* Nature, 1996. **380**(6575): p. 636-9.
129. Heierhorst, J., R.J. Mann, and B.E. Kemp, *Interaction of the recombinant S100A1 protein with twitchin kinase, and comparison with other Ca2+-binding proteins.* Eur J Biochem, 1997. **249**(1): p. 127-33.
130. Hanson, J. and H.E. Huxley, *Structural basis of the cross-striations in muscle.* Nature, 1953. **172**(4377): p. 530-2.

131. Fukushima, H., C.S. Chung, and H. Granzier, *Titin-isoform dependence of titin-actin interaction and its regulation by S100A1/Ca2+ in skinned myocardium.* J Biomed Biotechnol. **2010**: p. 727239.

132. Gutierrez-Cruz, G., A.H. Van Heerden, and K. Wang, *Modular motif, structural folds and affinity profiles of the PEVK segment of human fetal skeletal muscle titin.* J Biol Chem, 2001. **276**(10): p. 7442-9.

133. Most, P., et al., *S100A1: a regulator of myocardial contractility.* Proc Natl Acad Sci U S A, 2001. **98**(24): p. 13889-94.

134. Most, P., et al., *Cardiac adenoviral S100A1 gene delivery rescues failing myocardium.* J Clin Invest, 2004. **114**(11): p. 1550-63.

135. Pleger, S.T., et al., *S100A1 gene therapy preserves in vivo cardiac function after myocardial infarction.* Molecular Therapy, 2005. **12**: p. 1120-1129.

136. Kettlewell, S., et al., *S100A1 increases the gain of excitation-contraction coupling in isolated rabbit ventricular cardiomyocytes.* J Mol Cell Cardiol, 2005. **39**: p. 900-910.

137. Remppis, A., et al., *The small EF-hand Ca2+ binding protein S100A1 increases contractility and Ca2+ cycling in rat cardiac myocytes.* Basic Res Cardiol, 2002. **97 Suppl 1**: p. I56-62.

138. Most, P., et al., *Cardiac S100A1 protein levels determine contractile performance and propensity toward heart failure after myocardial infarction.* Circulation, 2006. **114**(12): p. 1258-68.

139. Pleger, S.T., et al., *Stable myocardial-specific AAV6-S100A1 gene therapy results in chronic functional heart failure rescue.* Circulation, 2007. **115**(19): p. 2506-15.

140. Remppis, A., et al., *Altered expression of the Ca(2+)-binding protein S100A1 in human cardiomyopathy.* Biochim Biophys Acta, 1996. **1313**(3): p. 253-7.

141. Most, P., et al., *Transgenic overexpression of the Ca2+ binding protein S100A1 in the heart leads to increased in vivo myocardial contractile performance.* J Biol Chem., 2003. **278**(5): p. 33809-33817.

142. Desjardins, J.F., et al., *Lack of S100A1 in mice confers a gender-dependent hypertensive phenotype and increased mortality after myocardial infarction.* Am J Physiol Heart Circ Physiol, 2009. **296**(5): p. H1457-65.

143. Brinks, H., et al., *S100A1 genetically targeted therapy reverses dysfunction of human failing cardiomyocytes.* J Am Coll Cardiol, 2011. **58**(9): p. 966-73.

144. Most, P., et al., *Distinct subcellular location of the Ca2+-binding protein S100A1 differentially modulates Ca2+-cycling in ventricular rat cardiomyocytes.* J Cell Sci, 2005. **118**(Pt 2): p. 421-31.

145. Remppis, A., et al., *S100A1 gene transfer : A strategy to strenghten engineered cardiac grafts.* J Gene Medicine, 2004. **6**: p. 387-394.

146. Pleger ST, S.C., Kziencek J, Mueller O, Bekeredjian R, Remppis A et al. , *Retroinfusion-facilitated inotropic AAV9-S100A1 gene therapy restores global cardiac function in a clinically relevant pig heart failure model* Circulation, 2008. **118**: p. S_792.

147. Voekers M, W.C., Herzog N, Friedrich O, Fink RHA, Koch WJ et al. , *S100A1 prevents arrhythmogenic diastolic sarcoplasmic reticulum Calcium leak in ventricular cardiomyocytes.* Circulation, 2008. **118**: p. S_527.

148. Volkers, M., et al., *S100A1 decreases calcium spark frequency and alters their spatial characteristics in permeabilized adult ventricular cardiomyocytes.* Cell Calcium, 2007. **41**(2): p. 135-43.

149. Eisner, D.A., et al., *From the ryanodine receptor to cardiac arrhythmias.* Circ J, 2009. **73**(9): p. 1561-7.

150. Gyorke, S. and C. Carnes, *Dysregulated sarcoplasmic reticulum calcium release: potential pharmacological target in cardiac disease.* Pharmacol Ther, 2008. **119**(3): p. 340-54.

151. Zimmermann, W.H., et al., *Tissue engineering of a differentiated cardiac muscle construct.* Circ Res, 2002. **90**(2): p. 223-30.

152. Tiburcy, M., et al., *Terminal differentiation, advanced organotypic maturation, and modeling of hypertrophic growth in engineered heart tissue.* Circ Res. **109**(10): p. 1105-14.

153. Graham, F.L., et al., *Characteristics of a human cell line transformed by DNA from human adenovirus type 5.* J Gen Virol, 1977. **36**(1): p. 59-74.

154. Louch, W.E., K.A. Sheehan, and B.M. Wolska, *Methods in cardiomyocyte isolation, culture, and gene transfer.* J Mol Cell Cardiol, 2011. **51**(3): p. 288-98.

155. He, T.C., et al., *A simplified system for generating recombinant adenoviruses.* Proc Natl Acad Sci U S A, 1998. **95**(5): p. 2509-14.

156. Akhter, S.A., et al., *Restoration of beta-adrenergic signaling in failing cardiac ventricular myocytes via adenoviral-mediated gene transfer.* Proc Natl Acad Sci U S A, 1997. **94**(22): p. 12100-5.

157. Tollefson, A.E., et al., *Preparation and titration of CsCl-banded adenovirus stocks.* Methods Mol Med, 2007. **130**: p. 223-35.

158. Piper, H.M.V., A. ; Schwartz, P., *Adult Rat Heart Cells: Cell Culture*

Techniques in Heart and Vessel Research. Springer, 1990: p. S. 36-60.

159. Laemmli, U.K., *Cleavage of structural proteins during the assembly of the head of bacteriophage T4.* Nature, 1970. **227**(5259): p. 680-5.

160. Kyhse-Andersen, J., *Electroblotting of multiple gels: a simple apparatus without buffer tank for rapid transfer of proteins from polyacrylamide to nitrocellulose.* J Biochem Biophys Methods, 1984. **10**(3-4): p. 203-9.

161. Bioscience, O., http://www.olink.com, 2013.

162. Walker, J.S., X. Li, and P.M. Buttrick, *Analysing force-pCa curves.* J Muscle Res Cell Motil, 2010. **31**(1): p. 59-69.

163. Hirt, M.N., et al., *Increased afterload induces pathological cardiac hypertrophy: a new in vitro model.* Basic Res Cardiol, 2012. **107**(6): p. 307.

164. Hoshijima, M. and K.R. Chien, *Mixed signals in heart failure: cancer rules.* J Clin Invest, 2002. **109**(7): p. 849-55.

165. Gupta, V. and K.J. Grande-Allen, *Effects of static and cyclic loading in regulating extracellular matrix synthesis by cardiovascular cells.* Cardiovasc Res, 2006. **72**(3): p. 375-83.

166. Celik, S., et al., *Cardiac troponin T concentrations above the 99th percentile value as measured by a new high-sensitivity assay predict long-term prognosis in patients with acute coronary syndromes undergoing routine early invasive strategy.* Clin Res Cardiol, 2011. **100**(12): p. 1077-85.

167. Hessel, M.H., et al., *Release of cardiac troponin I from viable cardiomyocytes is mediated by integrin stimulation.* Pflugers Arch, 2008. **455**(6): p. 979-86.

168. Olivetti, G., et al., *Myocyte nuclear and possible cellular hyperplasia contribute to ventricular remodeling in the hypertrophic senescent heart in humans.* J Am Coll Cardiol, 1994. **24**(1): p. 140-9.

169. Zucchi, R. and S. Ronca-Testoni, *The sarcoplasmic reticulum Ca2+ channel/ryanodine receptor: modulation by endogenous effectors, drugs and disease states.* Pharmacol Rev, 1997. **49**(1): p. 1-51.

170. Jin, H., A.R. Lyon, and F.G. Akar, *Arrhythmia mechanisms in the failing heart.* Pacing Clin Electrophysiol, 2008. **31**(8): p. 1048-56.

171. Lampe, P.D. and A.F. Lau, *Regulation of gap junctions by phosphorylation of connexins.* Arch Biochem Biophys, 2000. **384**(2): p. 205-15.

172. Lampe, P.D. and A.F. Lau, *The effects of connexin phosphorylation on gap junctional communication.* Int J Biochem Cell Biol, 2004. **36**(7): p. 1171-86.

173. Charles, R., T. Jayawardhana, and P. Eaton, *Gel-based methods in redox proteomics.* Biochim Biophys Acta, 2013.

174. Rohde, D., et al., *S100A1 gene therapy for heart failure: a novel strategy on the verge of clinical trials.* J Mol Cell Cardiol, 2010. **50**(5): p. 777-84.

175. Pfeffer, M.A., et al., *Myocardial infarct size and ventricular function in rats.* Circ Res, 1979. **44**(4): p. 503-12.

176. Hasenfuss, G., *Animal models of human cardiovascular disease, heart failure and hypertrophy.* Cardiovasc Res, 1998. **39**(1): p. 60-76.

177. Klocke, R., et al., *Surgical animal models of heart failure related to coronary heart disease.* Cardiovasc Res, 2007. **74**(1): p. 29-38.

178. Simpson, P., *Norepinephrine-stimulated hypertrophy of cultured rat myocardial cells is an alpha 1 adrenergic response.* J Clin Invest, 1983. **72**(2): p. 732-8.
179. Yamazaki, T., et al., *Stretching the evidence in the case of cardiac growth.* Cardiovasc Res, 1996. **31**(4): p. 493-8.
180. Tung, L. and J. Cysyk, *Imaging fibrillation/defibrillation in a dish.* J Electrocardiol, 2007. **40**(6 Suppl): p. S62-5.
181. Chiesi, M., A. Wrzosek, and S. Grueninger, *The role of the sarcoplasmic reticulum in various types of cardiomyocytes.* Mol Cell Biochem, 1994. **130**(2): p. 159-71.
182. Naito, H., et al., *Optimizing engineered heart tissue for therapeutic applications as surrogate heart muscle.* Circulation, 2006. **114**(1 Suppl): p. I72-8.
183. Zimmermann, W.H., I. Melnychenko, and T. Eschenhagen, *Engineered heart tissue for regeneration of diseased hearts.* Biomaterials, 2004. **25**(9): p. 1639-47.
184. Zimmermann, W.H., et al., *Engineered heart tissue grafts improve systolic and diastolic function in infarcted rat hearts.* Nat Med, 2006. **12**(4): p. 452-8.
185. Katare, R.G., et al., *Engineered heart tissue: a novel tool to study the ischemic changes of the heart in vitro.* PLoS One, 2010. **5**(2): p. e9275.
186. Hansen, A., et al., *Development of a drug screening platform based on engineered heart tissue.* Circ Res, 2010. **107**(1): p. 35-44.
187. Schaaf, S., et al., *Human engineered heart tissue as a versatile tool in basic research and preclinical toxicology.* PLoS One, 2011. **6**(10): p. e26397.
188. Yildirim, Y., et al., *Development of a biological ventricular assist device: preliminary data from a small animal model.* Circulation, 2007. **116**(11 Suppl): p. I16-23.
189. Ito, H., et al., *Endothelin-1 induces hypertrophy with enhanced expression of muscle-specific genes in cultured neonatal rat cardiomyocytes.* Circ Res, 1991. **69**(1): p. 209-15.
190. van Hees, H.W., et al., *Levosimendan improves calcium sensitivity of diaphragm muscle fibres from a rat model of heart failure.* Br J Pharmacol, 2011. **162**(3): p. 566-73.
191. Du, X.J., et al., *Impaired cardiac contractility response to hemodynamic stress in S100A1-deficient mice.* Mol Cell Biol, 2002. **22**(8): p. 2821-9.
192. Tsoporis, J.N., et al., *The myocardial protein S100A1 plays a role in the maintenance of normal gene expression in the adult heart.* Mol Cell Biochem, 2003. **242**(1-2): p. 27-33.
193. Santiago, J.J., et al., *Cardiac fibroblast to myofibroblast differentiation in vivo and in vitro: expression of focal adhesion components in neonatal and adult rat ventricular myofibroblasts.* Dev Dyn, 2010. **239**(6): p. 1573-84.
194. Gullestad, L., et al., *Inflammatory cytokines in heart failure: mediators and markers.* Cardiology, 2012. **122**(1): p. 23-35.
195. Whelan, R.S., V. Kaplinskiy, and R.N. Kitsis, *Cell death in the pathogenesis of heart disease: mechanisms and significance.* Annu Rev Physiol, 2010. **72**: p. 19-44.

196. Chiong, M., et al., *Cardiomyocyte death: mechanisms and translational implications.* Cell Death Dis, 2011. **2**: p. e244.

197. Wang, S.Q., et al., *Imaging microdomain Ca2+ in muscle cells.* Circ Res, 2004. **94**(8): p. 1011-22.

198. Wehrens, X.H. and A.R. Marks, *Sudden unexplained death caused by cardiac ryanodine receptor (RyR2) mutations.* Mayo Clin Proc, 2004. **79**(11): p. 1367-71.

199. Bers, D.M., *Ryanodine receptor S2808 phosphorylation in heart failure: smoking gun or red herring.* Circ Res. **110**(6): p. 796-9.

200. Meissner, G., *Ryanodine receptor/Ca2+ release channels and their regulation by endogenous effectors.* Annu Rev Physiol, 1994. **56**: p. 485-508.

201. Lehnart, S.E., X.H. Wehrens, and A.R. Marks, *Calstabin deficiency, ryanodine receptors, and sudden cardiac death.* Biochem Biophys Res Commun, 2004. **322**(4): p. 1267-79.

202. Vinet, L., et al., *Cardiac FKBP12.6 overexpression protects against triggered ventricular tachycardia in pressure overloaded mouse hearts.* Basic Res Cardiol, 2012. **107**(2): p. 246.

203. Galfre, E., et al., *FKBP12 activates the cardiac ryanodine receptor Ca2+-release channel and is antagonised by FKBP12.6.* PLoS One, 2012. **7**(2): p. e31956.

204. Zissimopoulos, S., et al., *Disparities in the association of the ryanodine receptor and the FK506-binding proteins in mammalian heart.* J Cell Sci, 2012. **125**(Pt 7): p. 1759-69.

205. Anthony, D.F., et al., *Interaction of calcium/calmodulin-dependent protein kinase IIdeltaC with sorcin indirectly modulates ryanodine receptor function in cardiac myocytes.* J Mol Cell Cardiol, 2007. **43**(4): p. 492-503.

206. Boschek, C.B., et al., *Loss of the calmodulin-dependent inhibition of the RyR1 calcium release channel upon oxidation of methionines in calmodulin.* Biochemistry, 2008. **47**(1): p. 131-42.

207. Boschek, C.B., et al., *Calcium occupancy of N-terminal sites within calmodulin induces inhibition of the ryanodine receptor calcium release channel.* Biochemistry, 2007. **46**(37): p. 10621-8.

208. Wright, N.T., et al., *S100A1 and calmodulin compete for the same binding site on ryanodine receptor.* J Biol Chem, 2008. **283**(39): p. 26676-83.

209. Yamaguchi, N., et al., *Cardiac hypertrophy associated with impaired regulation of cardiac ryanodine receptor by calmodulin and S100A1.* Am J Physiol Heart Circ Physiol, 2013.

210. Fauconnier, J., et al., *Leaky RyR2 trigger ventricular arrhythmias in Duchenne muscular dystrophy.* Proc Natl Acad Sci U S A, 2010. **107**(4): p. 1559-64.

V. List of publications

2012 Most P, Lerchenmüller C, Rengo G, Mahlmann A, **Ritterhoff J**, Rohde D, Goodman C, Busch CJ, Laube F, Heissenberg J, Pleger ST, Weiss N, Katus HA, Koch WJ, Peppel K.
S100A1 Deficiency Impairs Post-Ischemic Angiogenesis via Compromised Proangiogenic Endothelial Cell Function and Nitric Oxide Synthase Regulation.
Circ Res. 2012 Oct 9.

Ritterhoff J, Most P.
Targeting S100A1 in heart failure.
Gene Ther. 2012 Jun;19(6):613-21.

2011 Raake PW, Tscheschner H, Reinkober J, **Ritterhoff J**, Katus HA, Koch WJ, Most P.
Gene therapy targets in heart failure: the path to translation.
ClinPharmacolTher. 2011 Oct;90(4):542-53.

Rohde D, Brinks H, **Ritterhoff J**, Qui G, Ren S, Most P.
S100A1 gene therapy for heart failure: a novel strategy on the verge of clinical trials.
Mol Cell Cardiol. 2011 May;50(5):777-84.

2010 Rohde D, **Ritterhoff J**, Voelkers M, Katus HA, Parker TG, Most P.
S100A1: a multifaceted therapeutic target in cardiovascular disease.
J CardiovascTransl Res. 2010 Oct;3(5):525-37.

V.I Poster presentation and talks

04/2013 79. Jahrestagung der Deutschen Gesellschaft für Kardiologie, Mannheim, Germany, oral presentation:
The positive inotropic S100A1 prevents arrhythmogenic sarcoplasmic reticulum Ca^{2+} leak and ventricular arrhythmias by modulating defective RyR2 function

11/2012 Scientific Sessions American Heart Association 2012, Los Angeles, USA, poster presentation:
S100A1 prevents SR Ca^{2+} leak and protects against arrhythmias in ventricular cardiomyocytes

06/2012 Gordon Research conference on Cardiac regulatory mechanisms, New London, USA; poster presentation:

S100A1 protects cardiomyocytes against pro-arrhythmogenic Ca^{2+} waves and after-contractions

04/2012 Frontiers in Cardiovascular Biology European Society of Cardiology, London, Great Britain; poster presentation:
S100A1 gene therapy protects cardiomyocytes against pro-arrhythmogenic Ca^{2+} waves and after-contractions

Acknowledgments

At this point, I would like to express my gratitude to all those, who contributed to the success of this work.

First of all, I am very grateful for the support of Prof. Dr. med. Patrick Most and for the opportunity to work in his group, for the trust he placed in me, the inspiring discussions, the great freedom that he has given me in carrying out this work and for his guidance, support and encouragement during my PhD.

I also want to thank the members of my thesis committee PD Dr. Martin Müller and PD Dr. Johannes Backs for their valuable advice on my project as well as Prof. Dr. Thomas Wieland and Prof. Dr. Hilmar Bading for agreeing to participate in the examination.

Further thanks go to Nicole and Jasmin for excellent technical support and to Tamara for exceptional help with any organizational issues.

I would also like to thank all my colleagues for the good working atmosphere, for the great time and their helpfulness. During this time I could not only learn a lot, I could also win great friends. Special thanks go to Sabine, Julia, Henni, Susi and Suzan.

Finally, I owe a very special thanks to Tobi. For his continuous support, his unfailing trust in me and my work and his tireless cheerfulness every morning.